LATVIAN JOURNAL of PHYSICS and TECHNICAL SCIENCES

ISSN 0868 - 8257

2

(Vol. 55)

2018

SATURS

ENERĢĒTIKAS FIZIKĀLĀS UN TEHNISKĀS PROBLĒMAS

LIETIŠĶĀ FIZIKA

CONTENTS

PHYSICAL AND TECHNICAL ENERGY PROBLEMS

APPLIED PHYSICS

СОДЕРЖАНИЕ

ФИЗИКО-ТЕХНИЧЕСКИЕ ПРОБЛЕМЫ ЭНЕРГЕТИКИ

ПРИКЛАДНАЯ ФИЗИКА

LATVIAN JOURNAL of PHYSICS and TECHNICAL SCIENCES

LATVIJAS FIZIKAS un TEHNISKO ZINĀTŅU ŽURNĀLS

ЛАТВИЙСКИЙ ФИЗИКО-ТЕХНИЧЕСКИЙ ЖУРНАЛ

Published six times a year since February 1964
Iznāk sešas reizes gadā kopš 1964. gada februāra
Выходит шесть раз в год с февраля 1964 года

2 (Vol. 55) • 2018

RĪGA

INDEKSĒTS (PUBLICĒTS) | INDEXED (PUBLISHED) IN

www.scopus.com
www.degruyter.com
EBSCO (Academic Search Complete, www.epnet.com), INSPEC (www.iee.org.com). VINITI (www.viniti.ru), Begell House Inc/ (EDC, www.edata-center.com).

Izdevējs: Fizikālās enerģētikas institūts
Reģistrācijas apliecība Nr. 0221
Redakcija: Krīvu iela 11, Rīga, LV-1006
Tel. 67551732, 67558694
e-pasts: ezerniec@edi.lv
Interneta adrese: www.fei-web.lv

LATVIAN JOURNAL OF PHYSICS AND TECHNICAL SCIENCES
2018, N 2

DOI: 10.2478/lpts-2018-0008

PHYSICAL AND TECHNICAL ENERGY PROBLEMS

APPLICATION OF SYNCHROPHASOR MEASUREMENTS FOR IMPROVING SITUATIONAL AWARENESS OF THE POWER SYSTEM

A. Obushevs, A. Mutule
Smart Grid Research Centre
Institute of Physical Energetics
11 Krivu Street, Riga, LV-1006, LATVIA
e-mail: amutule@edi.lv

The paper focuses on the application of synchrophasor measurements that present unprecedented benefits compared to SCADA systems in order to facilitate the successful transformation of the Nordic-Baltic-and-European electric power system to operate with large amounts of renewable energy sources and improve situational awareness of the power system. The article describes new functionalities of visualisation tools to estimate a grid inertia level in real time with monitoring results between Nordic and Baltic power systems.

Keywords: *dynamic parameter identification, phasor measurement, power system dynamics, wide-area monitoring*

1. INTRODUCTION

Power system operation is challenged by the "green shift", which is characterised by more extreme variations, faster and larger changes and uncertainty in generation and demand. Stable and secure operation of the next generation common Nordic-Baltic-and-European (NBE) power system will need new information tools for monitoring, more advanced automatic control systems and wide-area monitoring solutions that are adapted to the variability and complexity of the future electric power system.

The fundamental changes of the power system due to the increasing number of renewable energy sources, small-scale photovoltaic, feeding into networks at various voltage levels require radically new control schemes that strongly rely on the availability of adequate monitoring infrastructure [1], [2]. Phasor measurement units (PMUs) are crucial tools for the monitoring of the transmission networks [3] and are likely be used in the future in medium- and low-voltage distribution grids as well [4]. The deployment of PMUs could allow achieving a wide range of control objectives required for the future power system.

The paper presents part of the study under the SAMBA (Synchronized Area Monitoring for BAltic states) project, the purpose of which is to attempt a leverage of unpresented benefit of Synchrophasor Technology (PMU technology) at different voltage levels (i.e., including needs of both Transmission System Operators (TSOs), Distribution System Operators (DSOs) and other stakeholders in the electricity system). The overall project aim is to facilitate the successful transformation of the NBE electric power system to operate with large amounts of RES and to develop the NBE energy system as a supplier and carrier of RES, providing solutions to local and global challenges. Local challenges are as follows: 1) From an operational point of view, they are related to balancing, power quality and maintaining security of supply, especially considering the outlook for nuclear power in the region. 2) The transfer capacity could exceed current transmission capacity values if the synchrophasor technology is combined with other assets such as continuous PMU-based monitoring and alarming, and fast-controls on power-electronics assets such as SVC and HVDC. Global challenges are as follows: 1) The traditional assumption that grid inertia is sufficiently high with only small variations over time is thus not valid for power systems with high RES shares. Frequency dynamics are faster in power systems with low rotational inertia, making frequency control and power system operation more challenging. 2) Focus is shifting towards a more decentralised power system, which results in a greater emphasis on monitoring of power system in real time and new control algorithms to allow the power system to operate closer to its capacity while maintaining system security.

2. MONITORING AND ANALYSIS OF SYNCHROPHASOR SYSTEM DATA

Synchrophasor systems are considered to be one of the enablers of Smart Grids. They are able to scan the system from a large number of measuring points at a high scanning rate and report highly accurate and time-synchronized voltage and current phasors measurements together with frequency at a very high rate of 50/60 messages per second compared to SCADA systems (less than 1 measurement per second). The PMUs utilise the IEEE C37.118.2 standard to stream out synchronous phasor measurements. The development and implementation of Wide-Area Monitoring, Protection and Control Systems that exploit synchronised phasor measurement data to provide coherent real-time data for enhancing power system reliability has seen a significant increase in the past few years. A real-time approach based on wide-area PMU measurements is envisioned as a means of providing operators with information and tools in order to keep the power system in stable and secure operation. The system generates a large quantity of data, which has to be analysed promptly and monitored. The operator should be alerted of any abnormal situation so that they may take appropriate action to avoid escalation of an abnormal situation. Several tools have been developed to fulfil this need. Some of the tools in use today include SEL-5078-2 SynchroWAVe Central, OpenPDC Power System Outlook, Real Time Monitoring System – SMART, Real Time Dynamics Monitoring System – RTDMS and Phasor Grid Dynamic Analyser – PGDA. Some of the useful indicators of the "health" of the grid that can be monitored using this technology are as follows [5]: Performance Metrics; Transient Stability; Stability Metrics; Composite Indicator of

Reliability; Interconnections between areas (Tie-lines); Interconnected Grid – the entire grid that operates in synchronism, i.e., at the same system frequency, e.g., Belorussia, Russia, Estonia, Latvia and Lithuania (BRELL); Local Level or Area (Local Control Area) – an area covered by a single TSO; Wide-Area Visualisation – the ability to see the critical operating parameters from all locations in the entire control grid (Fig. 1 presents visualisation of phasor measurements among asynchronous areas).

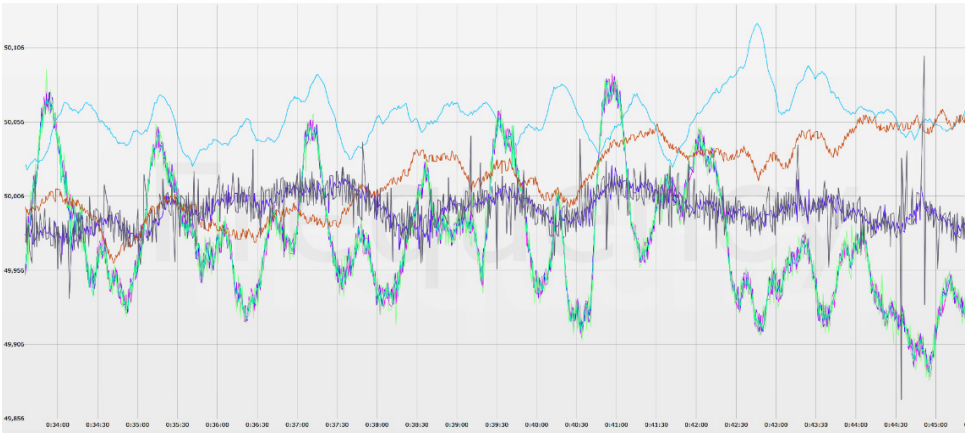

Fig. 1. Visualisation of frequency oscillations of four asynchronous areas by SEL-5078-2 SynchroWAVe.

In large interconnected power systems, wide-area situational awareness is critical to ensure reliable system operation. Synchrophasor visualisation tools provide wide-area situational awareness of the power system using geographic display of angle differences and colour-coded traffic light gauges for key metrics, including frequency, voltage, power flows and damping. This situational awareness overview of the entire interconnection and easy-to-use drill down menus enable operators to quickly pinpoint the location of a problem and better assist in formulating any corrective actions or mitigation measures.

It is envisaged to promote future development of synchrophasor analysis and visualisation tools with new functionalities for improving situational awareness of power systems, e.g., with dynamic line rating and grid inertia level estimations in real time.

3. INERTIA: RELATIONS WITH THE POWER SYSTEM

The energy stored in the power system and instantly available to be exchanged is stored as kinetic energy of the connected electric machines (synchronous and asynchronous generators and motors). Inertia is an inherent mechanical feature of rotating masses and it acts as an early intrinsic countermeasure against frequency deviation after perturbations due to load-generation imbalances. More precisely, the response of the present structure of the controlled power system to a sudden change in the active power balance can be divided into five stages [6], [7], the second of which is the Inertial Response (IR):

- First of all, the magnetic field of synchronous generators releases electromagnetic energy, for about 1/3 s, to contribute to maintaining synchronism;
- After the electromagnetic release, the IR acts, for a few seconds at most;
- Within a few seconds from the event, the primary frequency reserve is activated and stabilises frequency to a steady state;
- Within 15 minutes from the event, the secondary control reserve is deployed, to bring frequency back to its nominal value and free up the primary frequency reserve;
- The secondary control reserve is followed and supported by the tertiary control reserve.

When the active power balance in the power system undergoes large disturbance, both rotor angle and frequency stability have to be considered:

- IR is related to the rotor angle change in synchronous machines; namely, it contributes to keeping this angle within suitable bounds so that synchronism is preserved;
- IR is related to frequency stability because it affects both the ROCOF and the maximal frequency deviation: the former, in turn, influences the behaviour of protective relays.

Figure 2 reports the features of a typical frequency transient following power imbalance in the form of a large power step occurring at time $t=t_{pert}$.

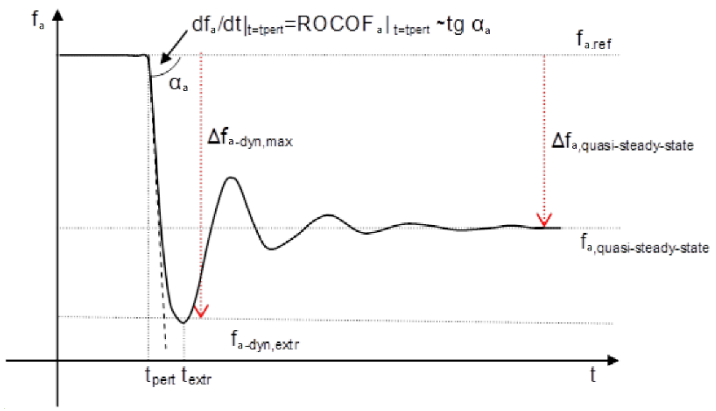

Fig. 2. A typical frequency transient due to a step power imbalance.

A set of quantities can preliminarily be envisaged as needed to study frequency stability in the power system [7], [8]: the (instantaneous) average frequency of each area, i.e., f_c (Hz); the rate of change $ROCOF_a$ (Hz/s) of the frequency of each area; the maximum deviation $|\Delta f_{a\text{-}dyn,max}|$ of the mentioned frequency due to a sudden and relevant change in power balance; the time interval t_{extr}-t_{pert}, where t_{extr} is the time instant for which $\Delta f_{a\text{-}dyn,extr}$ is attained; the maximal absolute value $|ROCOF_a|_{max}$ of the mentioned rate of change; the (quasi-)steady-state deviation of frequency $\Delta f_{a,quasi\text{-}steady\text{-}state}$ from its setpoint value $f_{a,ref}$, which can coincide with the frequency nominal value or be slightly different from it; the time interval, starting from t_{pert}, after which f_a reaches (quasi) steadily the value $f_{a,quasi\text{-}steady\text{-}state}$, namely after which

$|f_a - f_{a,quasi\text{-}steady\text{-}state}| < \varepsilon$, where the error value ε has to be quantified as well (10–20 mHz could be a starting point for the evaluation); the (physical) inertia constant H_i (s) of each synchronous generator in an area and "equivalent" inertia constant H_j (s) of each device that can be used to supply synthetic inertia; the overall inertia constant of each area, i.e., H_a (s) and the whole power system, i.e., H_{sys}; this could:

- be a combination, in terms of a suitable weighted average, of all physical and equivalent inertia constants of single machines and devices; in this combination, not only the individual H_i or H_j could be relevant, but also the electrical distance, or better impedance, of the lines connecting the machines or devices;
- be derived from area frequency measurement, assuming that the power system working point (in terms of active power injections and absorptions, inside the area and/or with respect to the neighbouring areas) is known and the perturbation is known, this measurement, in turn, can be made after a sudden and relevant change in power balance.

For inertia estimation the power system can be described in a simplified way by the following swing equation [9]:

$$M_{sys} \cdot \frac{df_{sys}}{dt} \simeq P_{m,sys} - P_{e,sys}\ [MW], \tag{1}$$

where $P_{m,\mathrm{sys}}$ is the power system mechanical power and $P_{e,\mathrm{sys}}$ – its electric power, M_{sys} – the power system mechanical inertia. In turn,

$$M_{sys} = \frac{2 \cdot H_{sys} \cdot S_{n,sys}}{f_n} = \sum_{i \in \alpha_G} \frac{2 \cdot H_i \cdot S_{n,i}}{f_n} \left[MW \cdot \frac{s}{Hz}\right], \quad H_i = \frac{J_i \cdot \omega_{n,i}^2}{2S_{n,i}}\ [s], \tag{2}$$

where $S_{n\,i}$ is the machine nominal apparent power, H_i – its inertia time constant, J_i – its moment of inertia, $\omega_{n,i}$ – its nominal rotational speed, f_n – the nominal frequency, α_G – a set of the Synchronous Generators connected to the network. To estimate the instantaneous ROCOF after power imbalance for the system:

$$\begin{aligned} ROCOF(t = pert^+) &= \frac{df_{sys}}{dt}(t = pert^+) \\ &\simeq \frac{P_{m,sys} - P_{e,sys}}{M_{sys}}\ [Hz/s] \end{aligned} \tag{3}$$

4. MONITORING APPLICATION AND OBSERVATION RESULTS

For situational awareness of power systems with grid inertia level estimation, the monitoring information from the Institute of Physical Energetics Smart Grid Research Centre has been used. After commissioning of NordBalt submarine power cable between Klaipeda in Lithuania and Nybro in Sweden at the end of 2015, connecting Nordic and IPS/UPS asynchronous areas by 700MW HVDC cable, ten sud-

den outages occured during 2016 and change power balances in Nordic and IPS/UPS power systems by 700MW. Figures 3–5 present a few power system frequency transients due to step power imbalances, where PMU measurements from both sides were used.

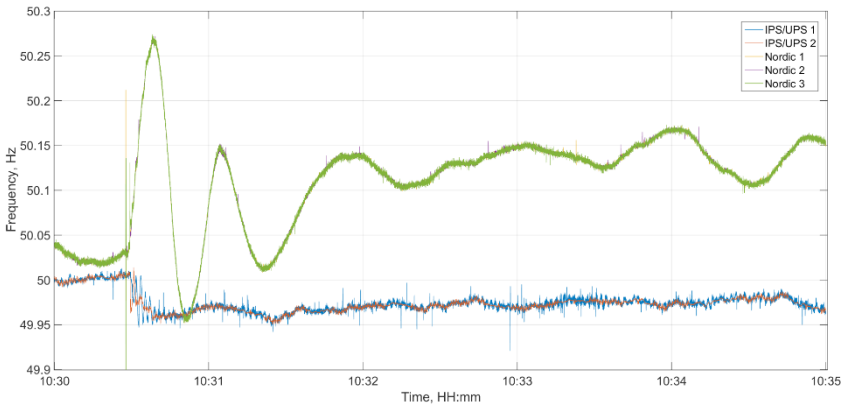

Fig. 3. NordBalt sudden outage – 700MW on Wednesday, 24/02/2016 at 10:30.

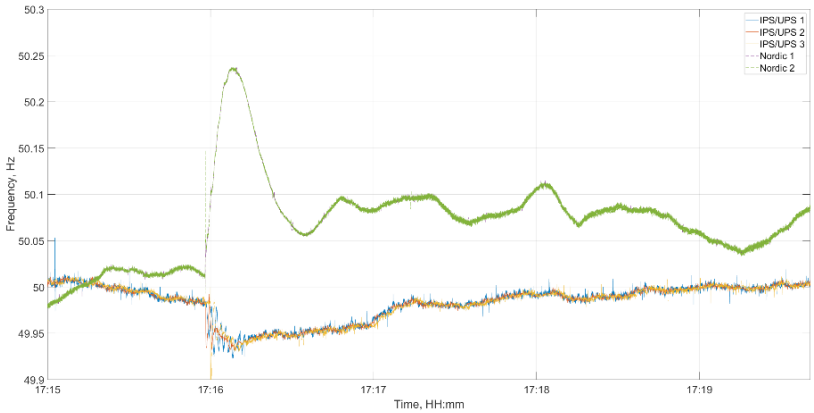

Fig. 4. NordBalt sudden outage – 700MW on Friday, 18/03/2016 at 17:16.

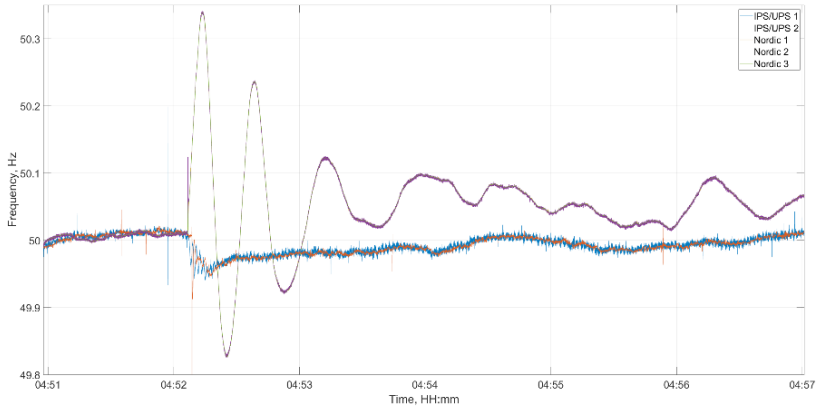

Fig. 5. NordBalt sudden outage – 700MW on Monday, 30/06/2016 at 4:52.

Table 1 presents the estimation of system mechanical inertia and inertia time constant based on eqs. 2 and 3, with derived information from frequency transients.

Table 1

Estimation of Power System Mechanical Inertia and Inertia Time Constant

Outage	NORDIC					IPS/UPS				
	$T_{,EXTR}$	$\Delta f_{a\text{-}dyn,extr}$	$ROCOF$	M_{SYS}	H_{SYS}	$T_{,EXTR}$	$\Delta f_{a\text{-}dyn,extr}$	$ROCOF$	M_{sys}	H_{sys}
24/02/2016 10:30	9	0.24	0.026	26250	9.94	1.4	0.035	0.025	28000	3.25
18/03/2016 17:16	10	0.23	0.023	30434	11.52	1	0.04	0.04	17500	2.03
30/06/2016 4:52	7	0.33	0.047	14848	5.62	1.3	0.05	0.038	18200	2.11

Due to incomplete information about power system states in the outage moment (production/consumption), inertia time constants have been estimated based on the assumption that Nordic power system has the total apparent power of 66 GW and IPS/UPS system – 215 GW. It can be seen that Nordic system inertia values fit the power system behaviour during the day, where inertia is higher during peak hours and lower at night. More precise initial information about the system is needed to estimate values more precisely. However, IPS/UPS system values seem unrealistic due to a reason that the system is approximately 3 times bigger than Nordic PS and outage of 700MW does not create significant disturbances for precise estimation.

5. CONCLUSIONS AND FURTHER RESEARCH

Application of synchrophasor measurements provides additional benefits to power system operators to quickly pinpoint the location of a problem and better assist in formulating any corrective actions or mitigation measures. It is envisaged to promote future development of synchrophasor analysis and visualisation tools with new functionalities for improving situational awareness of power systems, e.g., with dynamic line rating and grid inertia level estimations in real time.

Inertia can be foreseen to have a sort of “pervasive”, but also “tricky” role in the future power system; due to a decrease in physical inertia, machine or device inertial behaviour will have direct and indirect effects on phenomena related to different forms of stability.

New functionalities of visualisation tools to estimate a grid inertia level in real time should take into account external information about the power system state (production/consumption) to decrease inaccuracy in estimation and provide power system operators with new functionality and observability.

ACKNOWLEDGEMENTS

The research has been co-supported by the European Regional Development Fund for postdoctoral project “Synchronized Area Monitoring for BAltic States (SAMBA)” No. 1.1.1.2/VIAA/1/16/080 (project agreement No. 1.1.1.2/16/I/001).

REFERENCES

1. D'hulst, R., Fernandez, J. M., Rikos, E., Kolodziej, D., K. Heussen, D. … Caerts, C. (2015). Voltage and frequency control for future power systems: The ELECTRA IRP proposal. In *Proceedings of EDST'2015*. Vienna: IEEE.
2. Morch, A. Z., Jakobsen, S. H., Visscher, K., & Marinelli, M. (2015). Future control architecture and emerging observability needs. In *Proceedings of POWERENG'2015*. Riga: IEEE.
3. Phadke, A. G., & Thorp, J. S. (2018). *Synchronized phasor measurement and their applications.* New York: Springer.
4. Von Meier, A., Culler, D., & McEachern, A. (2014). Micro-synchrophasors for distribution systems. In *Proc. IEEE PES 5th Innov. Smart Grid Technol. (ISGT) Conf.* (pp. 1–5).
5. CIGRE WG C4.34. (2017). *Application of phasor measurements for monitoring power system dynamic performance*. Available at https://e-cigre.org/publication/702-application-of-phasor-measurement-units-for-monitoring-power-system-dynamic-performance
6. Knap, V., Sinha, R., Swierczynski, M., Stroe, D.-I., & Chaudhary, S. (2014). Grid inertial response with Lithium-ion battery energy storage systems. In *IEEE 23rd International Symposium on Industrial Electronics (ISIE)*, 1–4 June 2014 (pp.1817–1822).
7. Marinelli, M., Pertl, M., Rezkalla, M. N., Kosmecki, M., Sobczak, B., Jankowski, R. … Rossi, M. (2017). Functional description of the monitoring and observability detailed concepts for the Pan-European control schemes. *ELECTRA Deliverable D5.4. WP5: Increased Observability*.
8. Ørum, E., Kuivaniemi, M., Laasonen, M., Bruseth A. I., Jansson E. A., Danell A. … Modig N. (2015). *Future system inertia*. ENTSOE. Brussels.
9. Kundur, P. (1994). *Power system stability and control*. New York: McGraw-Hill.

FĀŽU VEKTORU MĒRĪŠANAS IEKĀRTU IZMANTOŠANA ENERGOSISTĒMU INFORMĒTĪBAS UZLABOŠANAI

A. Obuševs, A. Mutule

K o p s a v i l k u m s

Raksts veltīts fāžu vektoru mērīšanas iekārtu pielietošanai, kas salīdzinājumā ar esošām SCADA sistēmām sniedz papildus priekšrocības, lai sekmētu Ziemeļvalstu, Baltijas un Eiropas elektroenerģijas sistēmu veiksmīgu transformāciju, nodrošinot darbības ar liela skaita atjaunīgo enerģijas avotiem, uzlabojot izpratni par energosistēmu uzvedību reālā laikā. Rakstā aprakstītas jaunas vizualizācijas rīku funkcionalitātes, nodrošinot energosistēmu inerces līmeņa novērtēšanu reālā laikā, pateicoties novērojumu rezultātiem starp Ziemeļvalstu un Baltijas elektroenerģijas sistēmām.

21.03.2018.

LATVIAN JOURNAL OF PHYSICS AND TECHNICAL SCIENCES
2018, N 2

DOI: 10.2478/lpts-2018-0009

IMPACT OF FINANCING INSTRUMENTS AND STRATEGIES ON THE WIND POWER PRODUCTION COSTS: A CASE OF LITHUANIA

V. Bobinaite [1], I. Konstantinaviciute [1,2]
[1] Lithuanian Energy Institute,
3 Breslaujos Str., Kaunas, LT-44403, LITHUANIA
e-mail: viktorija.bobinaite@lei.lt
[2] Kaunas University of Technology,
48 Studentu Str., Kaunas, LT-51367, LITHUANIA

The paper aims at demonstrating the relevance of financing instruments, their terms and financing strategies in relation to the cost of wind power production and the ability of wind power plant (PP) to participate in the electricity market in Lithuania. The extended approach to the Levelized Cost of Energy (LCOE) is applied. The feature of the extended approach lies in considering the lifetime cost and revenue received from the support measures. The research results have substantiated the relevance of financing instruments, their terms and strategies in relation to their impact on the LCOE and competitiveness of wind PP. It has been found that financing of wind PP through the traditional financing instruments (simple shares and bank loans) makes use of venture capital and bonds coming even in the absence of any support. It has been estimated that strategies consisting of different proportions of hard and soft loans, bonds, own and venture capital result in the average LCOE of 5.1–5.7 EURct/kWh (2000 kW), when the expected electricity selling price is 5.4 EURct/kWh. The financing strategies with higher shares of equity could impact by around 6 % higher LCOE compared to the strategies encompassing higher shares of debt. However, seeking to motivate venture capitalists, bond holders or other new financiers entering the wind power sector, support measures (feed-in tariff or investment subsidy) are relevant in case of 250 kW wind PP. It has been estimated that under the unsupported financing strategies, the average LCOE of 250 kW wind PP will be 7.8–8.8 EURct/kWh, but it will reduce by around 50 % if feed-in tariff or 50 % investment subsidy is applied.

Keywords*: case study, financing instrument, financing strategy, levelized cost of energy, Lithuania, wind power*

1. INTRODUCTION

The Lithuanian National Energy Strategy is under debate [1]. There are a lot of open questions on how energy sectors should be developed and transformed in order to satisfy the increasing energy demand, achieve the target of greenhouse gas

emissions reduction, assure the sufficient level of energy supply security and improve the competitiveness of the country [2]. In this context, the question of the development of the competitive domestic power production capacities remains of high importance in Lithuania.

Following the European Commission's Energy Roadmap 2050 [3], it becomes evident that power producing systems would have to undergo structural changes in a way that the share of Electricity from Renewable Energy Sources (RES–E) reached 64 % under the high energy efficiency scenario and 97 % – under a high renewables scenario. This means that high fuel and operational cost fossil fuel-based power systems would have to be replaced by the renewable energy systems, whose functioning is based on high capital expenditure and low fuel cost.

Lithuania makes efforts to transform its power sector and increase the share of RES-E [4]. In 2016, the share of RES–E was 16.8 % in Lithuania [5]. Prior to the implementation of EU Directive 2009/28/EC on the Promotion of the Use of Energy from Renewable Sources [6] and the Law on Renewable Energy Sources [7], the share of RES–E did not exceed 6 % in the country. Lithuanian scientists [2] forecast that during 2020–2030 the share (from total) of RES–E could increase to 24–27 %. E. Norvaiša & A. Galinis [2] argue that in future renewable Power Plants (PP) could be constructed in Lithuania, since they would be competitive in the international electricity market. Furthermore, the results of modelling demonstrated that implementation of renewable energy technology would be a reasonable choice under any energy policy case.

However, it remains unclear, at which cost the renewable PPs could generate electricity in the long term in Lithuania. Moreover, there is little known, who should and could finance them, which financing instruments and strategies should be applied, under what financing terms the renewable PPs would be competitive in the international market and what additional terms (for example, support measures) should be requested to improve the competitive position of renewable PPs in the market. Knowing that renewable PPs are capital-intensive and requirements for high initial investment are set, this issue becomes relevant and worth being investigated. Thus, the present article deals with this issue.

The paper aims at substantiating the relevance of financing instruments, their terms and financing strategies in relation to the cost of wind power production and the ability of wind PP participating in the electricity market in Lithuania in the long-term perspective.

Wind PPs have been selected due to their increasing and meaningful role to Lithuanian power system [2]. In 2016, there were installed 509 MW of wind PPs (for comparison purposes, 423.7 MW in 2015 and 288 MW in 2014) in Lithuania [8], [9]. They produced 1135.9 GWh of electricity. This is 11.7 % of gross inland electricity consumption [9]. Lithuania committed itself to increase wind power production capacities to 500 MW till 2020 [7]. When 500 MW is installed, the government takes the responsibility of drawing up new procedures and targets for wind power sector development in relation to Lithuania's international commitments for reduction of greenhouse gas emissions and assurance of energy supply security [7]. However, the development plan for wind power is not foreseen so far in Lithuania. In [10], several

wind power sector development barriers are identified, including a lack of clarity for investment decisions, shortage of renewable energy policy continuity, insufficient conditions for construction of wind PPs in the farms, communities and for social business, as well as an irrelevant approach of the authorities regarding the connection of wind PP to the distribution grid. In relation to the barriers, identified in [10], particularly to the barrier of clarity for investment decision, the topic of the present research is relevant.

2. DATA AND METHODOLOGY

2.1. Data

Data relevant for the research have been collected from the databases of the Lithuanian Transmission System Operator [8], the National Control Commission for Energy and Prices [11], the Lithuanian Environmental Investment Fund [12], EU Structural Funds 2014–2020 [13], the Bank of Lithuania [14], publications in Lithuanian press and scientific papers.

2.2. Methodology

2.2.1. Method

The concept of the Levelized Cost of Energy (LCOE) is well presented by the International Renewable Energy Agency [15], "…the LCOE is the price of electricity required for a project where revenues would equal costs, including making a return on the capital invested equal to the discount rate. An electricity price above this would yield a greater return on capital, while a price below it would yield a lower return on capital, or even a loss…". M. Keith et al. [16] summarised the concept of LCOE by arguing that LCOE is the price at which energy could be sold over the lifetime of the technology. F. M. Ragnarsson et al. [17] and U.S. Energy Information Administration [18] defined the LCOE as a measure applied to estimate the energy technology costs and assess the competitiveness of various energy generating technologies.

The LCOE is measured by dividing the present value of all expected lifetime costs (including, construction, investment, O & M, fuel, taxes, etc.) by the present value of the expected volume of energy produced over the energy project's lifetime. In the present article, an extended approach to the LCOE is applied. The LCOE is computed as follows:

$$LCOE = \frac{\sum_{t=0}^{T} \frac{I_t + O\&M_t + F_t - SEP_t - IS_t}{(1+d)^t}}{\sum_{t=0}^{T} \frac{C_I \cdot 8760 \cdot LF}{(1+d)^t}}, \quad (1)$$

where $LCOE$ is the levelised cost of energy, EUR/kWh;
I_t is the investment cost at time step t, EUR;
$O\ \&\ M_t$ is the operation and maintenance cost at time step t, EUR;
F_t is the fuel cost at time step t, EUR;
SEP_t is the subsidy for energy production, EUR;
IS_t is the investment subsidy, EUR;
C_I is the installed capacity, kW;
LF is the load factor, %;
d is the discount rate, %;
t is the time period, years.

The subsidy for energy production is calculated as follows:

$$SEP_t = FiT_t - P_{F,t}, \tag{2}$$

where FiT_t is the feed-in tariff for a unit of electricity produced in time t, EURct/kWh;
$P_{F,t}$ is the forecasted electricity selling price in time t, EURct/kWh.

The feature of the extended approach to the LCOE is that it takes into account both lifetime cost and revenue from the support measures applied to foster the renewable energy sector development. The SEP t and IS t are included in the LCOE to demonstrate how the competitive position of wind power plant improves if support to electricity production or asset acquisition is available.

The approach used in the analysis is based on a discounted cash flow analysis. This approach of measuring electricity production cost is based on the discounting financial flows, taking into consideration the time value of money.

Three levels of the LCOE for wind power are modelled. The minimum $LCOE_{min}$ (i_{min}; t_{max}) is modelled taking into account that wind PP is financed through the financing strategy consisting of financing instruments, which have the softest financing terms, i.e., the lowest interest or coupon rate (i_{min}) and the longest investment period (t_{max}). The maximum $LCOE_{max}$ (i_{max}; t_{min}) is modelled considering the hardest financing terms, i.e., the highest interest or coupon rate (i_{max}) and the shortest investment period (t_{min}). Finally, the average $LCOE_{av}$ (i_{av}; t_{av}) is modelled taking into account the most possible values of interest or coupon rates and investment periods.

2.2.2. Technical and Economic Parameters

LCOE for wind power is calculated based on data presented in Table 1.

Table 1

Technical and Economic Parameters of Wind PPs [8], [19]–[27]

Variable More than 350 kW		The category of wind PP	
		10–350 kW	
Technical	Electric capacity, kW	2000	250
	Load factor, %	32	23
	Lifetime of WPP, years	25	20
Cost	Investment cost, EUR/kW	1350.0	1448.0
	Fixed cost, EUR/kW-yr	13.50	14.48
	Variable cost, EUR/MWh	0.29	0.29
	Fuel cost, EUR/MWh	0.00	0.00

2000 kW and 250 kW wind PPs are analysed; each is attributed to the respective category of wind PPs receiving support for electricity production. Actually, these are the most typical wind PPs installed and expected to be installed in future in Lithuania.

2.2.3. Support Measures

250 kW and 2000 kW WPP could be supported through the feed-in tariff or investment subsidies in Lithuania. Parameters of support measures are presented in Table 2.

Table 2

The Analysed Support Measures and Their Parameters [7], [28]–[30]

Parameters	Feed-in tariff	Investment subsidy
Provider / payer	Final electricity consumers	EU Structural Funds 2014–2020
Support level	5.6 EURct/kWh (2000 kW) 10.426 EURct/kWh (250 kW)	20 % of total investment cost (2000 kW) 30 % of total investment cost (250 kW)
Support period	12 years	

2.2.4. Financing Strategies

Single and mixed instrument financing strategies are analysed. They differ in financing instruments, proportions of financing instruments included in the strategy, investment period and required profitability. Besides, cash flows related to instrument specific financing are modelled differently.

When modelling LCOE, two points are taken into account. Initially, the LCOE is modelled considering the international statistics, which is justified with the theory of financing instruments and well reflects the long-term financing perspective in Lithuania. Later, the LCOE is modelled considering the regional or domestic statistics, which is short-term and significantly differs from international data. There is some doubt as to how long the regional / domestic statistics will be relevant in the longer perspective when the investors and owners of the wind PP have acquired greater experience.

Single instrument financing strategies include hard loan, corporate bond, equity and venture capital financing. V. Bobinaite & D. Tarvydas [31] discussed the peculiarities of single instrument financing. The parameters of single instrument financing based on the international and regional / domestic financing conditions are presented in Table 3 and Table 4, respectively.

Table 3

The Parameters of Single Instrument Financing Strategies Based on the International Financing Terms [34]–[37], [39]–[41]

	HLF: Hard loan financing	CBF: Corporate bond financing	EF: Equity financing	VCF: Venture capital financing
Instrument	Bank loan	Bonds	Simple shares	Simple shares
Required profitability	5.0 %, 5.25 % and 5.5 %	5.5 %, 5.75 % and 6.0 %	10 %, 12 %, 15 %	15 %, 17 %, 20 %
Investment period	8, 10 and 12 years	5, 7 and 8 years	Unlimited	6, 7 and 8 years

Table 4

The Parameters of Single Instrument Financing Strategies Based on the Regional / Domestic Financing Terms [14], [32], [33], [38], [39]

	SLF: Soft loan financing	HLFD: Hard loan domestic financing	GBF: Green bond financing	EF: Equity financing	VCF: Venture capital financing
Instrument	Soft loan	Bank loan	Green bonds	Simple shares	Simple shares
Interest rate, coupon rate	3.0%	2.782 %, 3.1 %, 3.4 %	1.9 %, 3.2 %, 4.5 %	10 %, 12 %, 15 %	15 %, 17 %, 20 %
Investment period	20 years	9 years	7 years	Unlimited	6, 7 and 8 years

Mixed instrument financing strategies include combinations of financing instruments with the parameters presented in Table 4 and Table 5. The analysed mixed instrument financing strategies are summarised in Table 5.

Table 5

The Mixed Instrument Financing Strategies*

Abbreviation of the strategy		Description of the strategy
International financing terms	Domestic / regional financing terms	
EF15_HLF85	EF15_HLFD85	15 % of equity financing; 85 % of hard loan financing
EF15_VCF10_HLF75	EF15_VCF10_ HLFD75	15 % of equity financing; 10 % of venture capital financing; 75 % of hard loan financing
EF15_VCF10_HLF60_ CBF15	EF15_VCF10_ HLFD60_GBF15	15 % of equity financing; 10 % of venture capital financing; 60 % of hard loan financing; 15 % of corporate / green bond financing
EF20_HLF40_SLF20_ CBF20	EF20_HLFD40_ SLF20_GBF20	15 % of equity financing; 40 % of hard loan financing; 30 % of soft loan financing; 15 % of corporate / green bond financing

* in case an investment subsidy is included as a support measure, the share of hard loan financing is reduced by 20 % (2000 kW) or 30 % (250 kW).

The proportions of financial instruments in the strategy are selected considering the observations for the wind power projects; usually the proportion of equity to loan is 20:80 or 15:85 in Lithuania [38].

2.2.5. Modelling Methods of Financing Instruments

Investment costs of wind PPs are financed through various financing instruments. The payments related to specific instrument financing are modelled based on the theory of financing instruments and approach of cash flows.

The zero-growth rate dividend valuation model is applied to model dividend payments, when simple shares as a financing instrument are used. Dividend payments are calculated as follows:

$$D = P_0 \cdot i \,, \tag{3}$$

where D is the dividend payment, EUR;
P_0 is the intrinsic value of equity, EUR;
i is the required rate of return, %.

Dividend payments related to the venture capital financing are modelled based on Eq. (3). However, it is considered that after the investment period ends, venture capitalist sells all his equity.

The bond financing related payments are modelled considering the fact that during the investment period the coupon payments are made and at the date of maturity the nominal value of bond is paid. Coupon payments are calculated as follows:

$$C = N_0 \cdot i\,, \tag{4}$$

where C is the coupon payment, EUR;
N_0 is the nominal value of bond, EUR;
i is the coupon rate, %.

The loan financing related payments are modelled considering the annuity payment method:

$$AP = L_0 \cdot \frac{i/m}{1-(1+i)^{-n\cdot m}}\,, \tag{5}$$

where AP is the annuity payment, EUR;
L_0 is the loan, EUR;
i is the annual interest rate, %;
n is the term of loan, years;
m is the number of times the annuity payments are made per year.

It is assumed that capital structure is fully formed at the end of wind PP construction period. Interest rate during construction is also computed.

2.2.6. Other Parameters

The discount rate is used to calculate the present value of future cost and revenue received from the support measures. Weighted Average Cost of Capital (WACC) is taken as a measure of the discount rate [42]. It is calculated by Eq. (6):

$$WACC_l = R_{E;l} \cdot \frac{E_l}{E_l + D_l} + R_{D;l} \cdot \frac{D_l}{E_l + D_l} \cdot (1 - T_{income}), \tag{6}$$

where $WACC_l$ is the weighted average cost of capital of the financing strategy l;
$RE;_l$ is the cost of equity, %;
E_l is the amount of equity financing, EUR;
D_l is the amount of debt financing, EUR;
$R_{D;l}$ is the cost of debt financing, %;
T_{income} is the income tax, %.

$WACC_i$ for wind PPs calculated by Eq. (6) and applied in the research is presented in Table 6.

Table 6

Ranges of the Estimated Discount Rates Subject to Different Financing Strategies and Financing Terms (made by the authors of the paper)

Financing strategy	2 MW wind PP		250 kW wind PP	
	Regional financing terms	International financing terms	Regional financing terms	International financing terms
EF15_HLF85 // EF15_HLFD85	3.5–5.2	5.1–6.6	3.5–5.5	5.1–6.8
EF15_VCF10_HLF75 // EF15_ VCF10_HLFD75	4.8–7.3	6.2–8.5	4.8–7.9	6.2–9.1
EF15_VCF10_HLF60_CBF15 // EF15_VCF10_HLFD60_GBF15	4.7–7.5	6.3–8.6	4.7–8.1	6.3–9.2
EF20_HLF40_SLF20_CBF20 // EF20_HLFD40_SLF20_GBF20	3.8–6.1	5.2–6.8	3.8–6.5	5.2–7.1

The Subsidy for Electricity Production (SEP) is calculated considering the forecasted long-term electricity price of 5.4 EURct/kWh. The price is the simulated price of Energinet.dk [43]. It corresponds to an average electricity price for Sweden, with which Lithuania has a 700 MW power link.

3. RESULTS

3.1. LCOE of 2000 kW Wind PP

3.1.1. Single Instrument Financing

The analysis of single instrument financing is performed seeking to identify the ranges of the highest and lowest LCOE of 2000 kW wind PP. Equity and hard loan financing strategies are applied to model the LCOE, respectively. The results of modelling are summarised in Fig. 1.

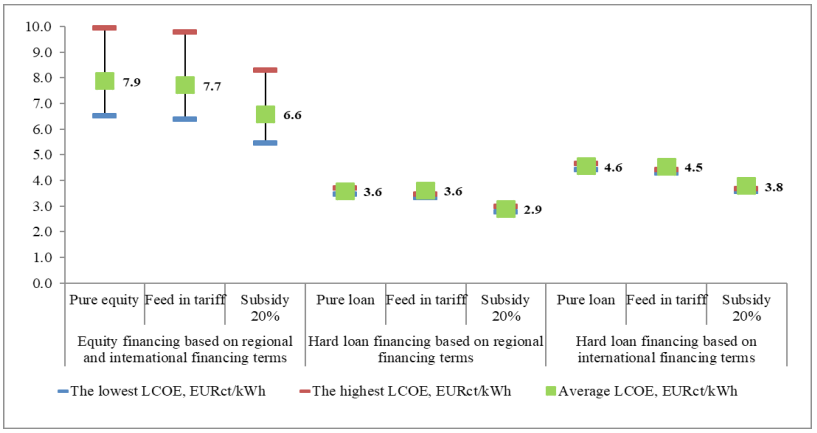

Fig. 1. LCOE for wind power (2000 kW) when single instrument financing is chosen (calculations are made by the authors of the paper)[1].

[1] In case an investment subsidy is included as a support measure, the share of hard loan financing is reduced by 20 %.

The results presented in Fig. 1 have shown that financing the acquisition of wind assets purely through the equity may cause the highest LCOE, with an average value of 7.9 EURct/kWh, if the desired return on equity is 12 % a year. If the rate of return on equity increased to 15 %, the LCOE could grow up by 27 % to 10.0 EURct/kWh, but could go down by 18 % to 6.5 EURct/kWh, if the rate of return on equity reduced to 10 %. Support measures – the feed-in tariff or 20 % investment subsidy – can decrease the average LCOE of equity financing by 2.0 % and 16.0 % to 7.7 EURct/kWh and 6.6 EURct/kWh, respectively, but the decrease is not sufficient to make a 2000 kW wind PP profitable today, when the electricity market price is 3.7 EURct/kWh or less, and in the future, when it is expected that the price will increase up to 5.4 EURct/kWh.

It is expected that if a 2000 kW wind PP is financed purely through the hard loan, an average LCOE is 3.6 EURct/kWh (the regional financing terms are considered) and 4.6 EURct/kWh (international financing terms are relevant). According to the strategy, the support measures are not critical, since the LCOE is modelled lower than the expected electricity selling price in future. This shows that a 2000 kW wind PP could be profitable under the hard loan financing in the near future or long-term perspective in the absence of the support.

3.1.2. Mixed Instrument Financing

Due to high investment costs and risks related to project implementation, the single instrument financing is not sufficient. A variety of financing instruments should be used and various types of investors / financiers should participate. Figures 2–3 summarise the LCOE strategies based on the mixed instrument financing.

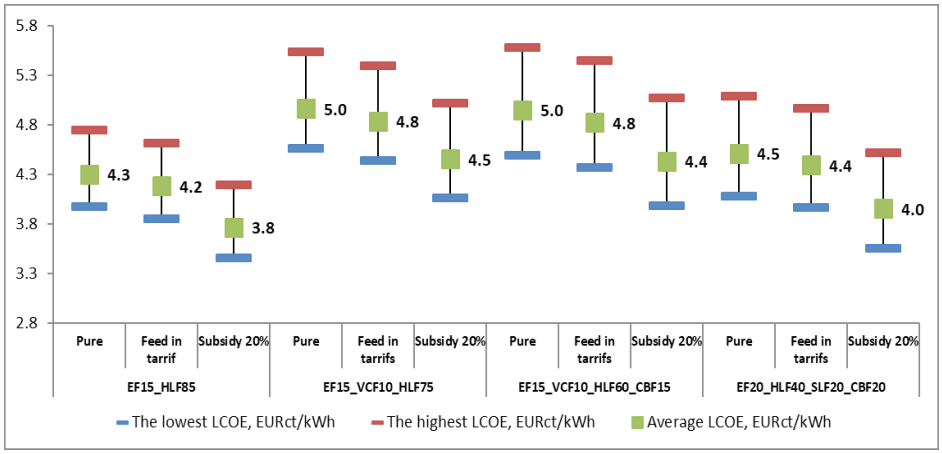

Fig. 2. LCOE for wind power (2000 kW) financed with the regional financing terms (calculations are made by the authors of the paper).

As it is shown in Fig. 2, in the absence of any support, the strategies of mixed instrument financing could cause an average LCOE vary in the range of 4.3–5.0 EURct/kWh. This shows that a 2000 kW wind PP could be profitable in the long term, when the expected electricity market price – 5.4 EURct/kWh, but nowadays at

a market price of 3.7 EURct/kWh the full cost recovery would not be available for this wind PP.

The feed-in tariff and investment subsidy could improve the profitability of 2000 kW wind PP, as the average LCOE could reduce by 2–12 %. The impact of 20 % investment subsidy on LCOE is more relevant than the effect of the feed-in tariff, since subject to 20 % investment subsidy the average LCOE is 3.8–4.5 EURct/kWh but 4.2–4.8 EURct/kWh in cases if the feed-in tariff is applied.

It has been found that the financing strategies with higher shares of equity (EF15_VCF10_HLFD75 and EF15_VCF10_HLFD60_GBF15) could affect higher LCOE compared to strategies encompassing higher shares of debt financing (EF15_HLD85 and EF20_HLFD40_SLF20_GBF20), i.e., 4.4–5.0 EURct/kWh vs. 3.8–4.5 EURct/kWh.

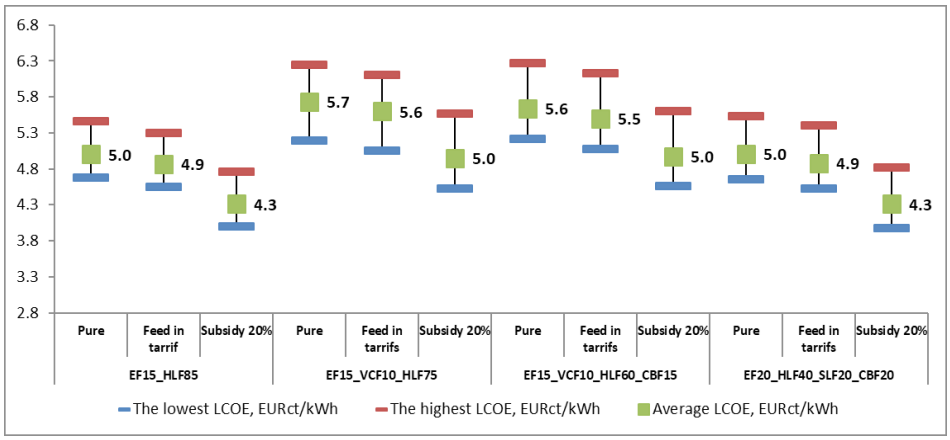

Fig. 3. LCOE for wind power (2000 kW) financed with international financing terms (calculations made by the authors of the paper).

As it is shown in Fig. 3, stricter and harder international financing terms increased the average LCOE by 9.1–16.3 % in comparison with regional terms. The pure (unsupported) strategies with higher shares of equity – EF15_VCF10_HLF75 and EF15_VCF10_HLF60_GBF15 – increased the average LCOE to 5.6–5.7 EURct/kWh, which remained higher than the expected electricity selling price in the long term (5.4 EURct/kWh). Higher LCOE could complicate the wind PP to fully recover its cost. Thus, the strategies could be used either with the investor's reduced requirements for profitability or through the use of support. However, the selected rate of the feed-in tariff would not be sufficient for the full cost recovery, since it causes the average LCOE drop to 5.5–5.6 EURct/kWh. However, 20 % investment subsidy could reduce the average LCOE to 5.0 EURct/kWh. Financing of 2000 kW wind PP with the resources acquired in the debt markets through the strategies EF15_HLF85 and EF20_HLF40_SLF20_GBF20 could assure that even without any support the full cost recovery would be possible, since the average LCOE would be 5.0 EURct/kWh. Support in a form of feed-in tariff or investment subsidy would create preconditions to trade wind power at low prices (4.3–4.9 EURct/kWh) and earn profit (before taxes).

3.2. LCOE of 250 kW Wind PP

3.2.1. Single Instrument Financing

Due to a lower load factor and higher investment costs per installed kW, the average LCOE of 250 kW wind PP was found higher than of 2000 kW wind PP. The estimated ranges of the LCOE for wind power of 250 kW in case of a single instrument financing are presented in Fig. 4.

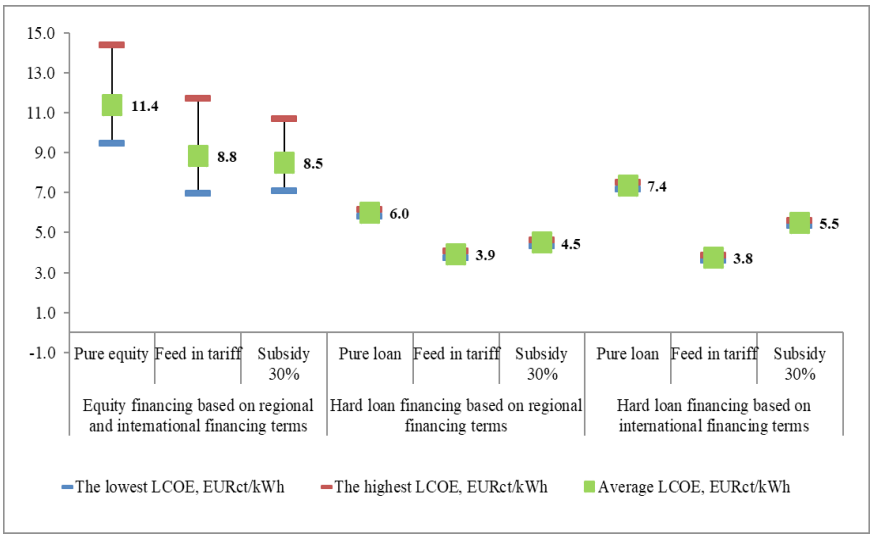

Fig. 4. LCOE for wind power (250 kW) when a single instrument financing is chosen (calculations made by the authors of the paper).

As it is seen in Fig. 4, the LCOE could be 9.5–14.4 EURct/kW, with an average value of 11.4 EURct/kW, if 250 kW wind PP were financed only through the pure equity strategy. The strategy of hard loan financing could cause the average LCOE dropping to 6.0 EURct/kWh (if regional financing terms were applied) and 7.4 EURct/kWh (if international financing terms were used). Seeking to finance wind PP through the hard loan financing, a feed-in tariff instead of investment subsidy should be chosen, since it creates possibilities to earn more profit before taxes.

3.2.2. Mixed Instrument Financing

Figures 5 and 6 present the LCOE for wind power of 250 kW when strategies of mixed instrument financing are applied.

As it is seen in Fig. 5, a feed-in tariff would be much more favourable than 30 % investment subsidy, if financial resources were received on the regional financing terms. The strategies of mixed instrument financing accompanied with a feed-in tariff would result in the average LCOE of 3.4–4.2 EURct/kWh. 30 % investment subsidy would not be sufficient, since it would cause an average LCOE of 5.5–6.5 EURct/kWh, which would exceed the electricity selling price of 5.4 EURct/kWh.

If support measures were not applied, the average LCOE would increase to 6.9–7.8 EURct/kWh. Seeking to promote 250 kW wind PP generator to use a variety of financing instruments and participate in debt and equity markets at a larger scale, a priority should be given to quite high feed-in tariff.

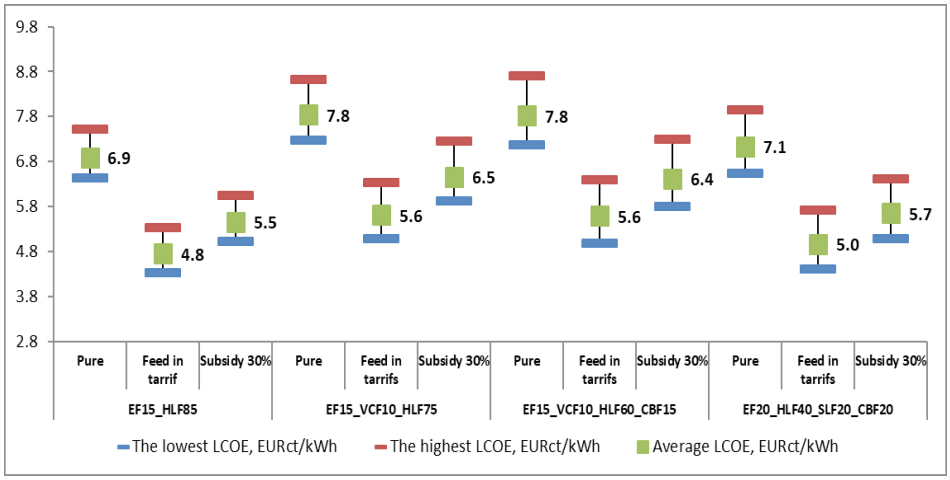

Fig. 5. LCOE for wind power (250 kW) financed with regional financing terms (calculations made by the authors of the paper).

Similar results were achieved if strategies were implemented on the international financing terms (Fig. 6).

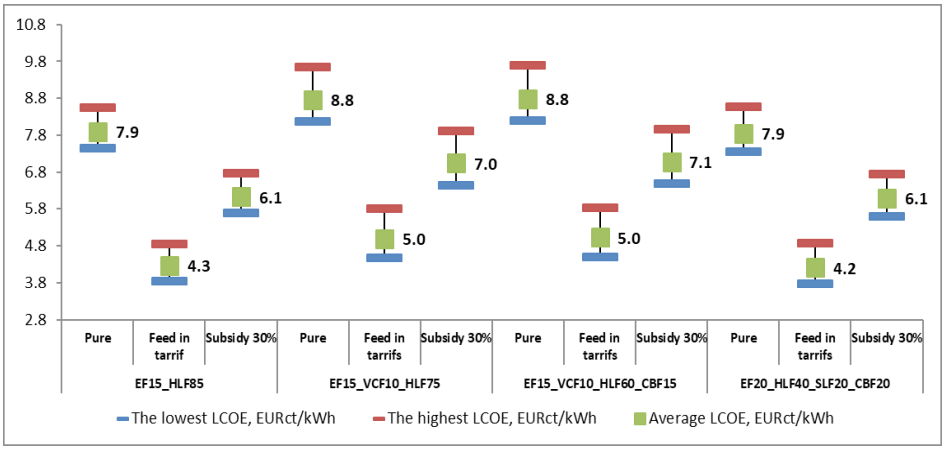

Fig. 6. LCOE for wind power (250 kW) financed with international financing terms (calculations made by the authors of the paper).

As it is shown in Fig. 6, the strategies of mixed instrument financing accompanied with a feed-in tariff could create preconditions for 250 kW wind PP to recover the total costs and earn profit before taxes in the long-term perspective, since LCOE could be 4.2–5.0 EURct/kWh.

4. CONCLUSIONS

The research has investigated the impact of financing instruments and strategies on the LCOE for wind power under the tight, average and soft financing terms based on regional and international statistics, which describe the development of financing terms in the near future and long-term perspective in Lithuania, respectively.

The research results obtained through the analysis of 2000 kW wind PP have shown that subject to the strategies of mixed instrument financing and the regional financing terms, the average LCOE for wind power would be 5.1–5.4 EURct/kWh. This shows that, although nowadays such a wind PP could not be competitive in the electricity market where the price is 3.7 EURct/kWh, its competitiveness would evidently improve in the future, when the price would increase to 5.4 EURct/kWh and even more. Subject to the strategies of mixed instrument financing and the international financing terms, support to 2000 kW wind PP should be provided to make the wind PP competitive in the market in the future. The feed-in tariff or investment subsidy could cause the average LCOE for wind power to decrease to 4.1–4.5 EURct/kWh.

The research results obtained through the analysis of 250 kW wind PP have demonstrated that despite the globally reducing investment cost (EUR/MW) and appearance of new financing instruments offering the alternative financing options, the investors to 250 kW wind PP will require additional support to produce electricity at competitive prices in the near future and long-term perspective. It has been estimated that the average LCOE for wind power can reduce to 4.4–4.6 EURct/kWh (if regional financing terms are applied) or 4.4–5.4 EURct/kWh (if international financing terms are used) due to the feed-in tariff.

The research results have shown that financing of 2000 kW wind PP with traditional financing instruments (equity and bank loan) makes use of venture capital and bond even in the absence of any support. The formation of 2000 kW wind PP's assets portfolio through a variety of instruments and in the absence of support could impact the average LCOE of 5.1–5.7 EURct/kWh depending on the financing terms. Availability of support measures could be a good motivating factor and attract various types of investors into 250 kW wind PP.

It has been found that a feed-in tariff or investment subsidy would be appropriate 2000 kW wind power support measures, but a priority to a feed-in tariff instead of 50% investment subsidy should be provided to increase the competitiveness of 250 kW wind PP in the market.

REFERENCES

1. Laboratory of Energy Systems Research at Lithuanian Energy Institute. (2015). *Draft of Lithuanian National Energy Strategy*. [Online]. Available at http://www.lei.lt/_img/_up/File/atvir/2016/NES/NES_projektas_(Versija_viesoms_diskusijoms)-2015.12.16.pdf.
2. Norvaiša, E., & Galinis, A. (2016). Future of Lithuanian energy system: Electricity import or local generation? *Energy Strategy Reviews*, *10*, 29–39.
3. European Commission. (2011). *Energy roadmap 2050*. [Online]. Available at http://eur-lex.europa.eu/legal-content/EN/TXT/PDF/?uri=CELEX:52011DC0885&from=EN.

4. Bobinaite, V., & Priedite, I. (2015). RES-E support policies in the Baltic States: Development aspect (part 1). *Latvian Journal of Physics and Technical Sciences*, *52*, 3–14.
5. Eurostat. (2016). *Database of Environment and Energy*. [Online]. Available at http://ec.europa.eu/eurostat/statistics-explained/index.php/File:Table_3-Share_of_electricity_from_renewable_sources_in_gross_electricity_consumption_2004-2016.png.
6. European Parliament and of the Council. (2009). *Directive 2009/28/EC on the promotion of the use of energy from renewable sources and amending and subsequently repealing directives 2001/77/EC and 2003/30/EC*. [Online]. Available at http://eur-lex.europa.eu/legal-content/EN/TXT/PDF/?uri=CELEX:32009L0028&from=EN.
7. Parliament of Lithuania. (2009). *Law on Renewable Energy Sources*. [Online]. Available at http://www3.lrs.lt/pls/inter3/dokpaieska.showdoc_l?p_id=478609.
8. Lithuanian Transmission System Operator. (2016). *Services*. [Online]. Available at http://www.litgrid.eu/index.php/paslaugos/paslaugos/511.
9. Lithuanian Statistics. (2018). *Consumption and production of renewable energy sources*. [Online]. Available at https://osp.stat.gov.lt/statistiniu-rodikliu-analize?theme=all#/.
10. Zailskaite, D. (2017). *Do we have enough wind power plants?* [Online]. Available at http://lsveikata.lt/sveika-visuomene/ar-vejo-jegainiu-turime-uztektinai-6012.
11. National Control Commission for Energy and Prices. (2018). *Renewable energy*. [Online]. Available at http://www.regula.lt/atsinaujinantys-istekliai/Puslapiai/default.aspx.
12. Lithuanian Environmental Investment Fund. (2016). *Support to business*. [Online]. Available at http://www.laaif.lt/lt/#.
13. EU Structural Funds 2014–2020. [Online]. Available at http://www.esinvesticijos.lt/.
14. Bank of Lithuania. (2017). *Database of interest rates*. [Online]. Available at http://www.lb.lt/pinigu_finansiniu_instituciju_paskolu_ir_indeliu_palukanu_normu_statistika.
15. International Renewable Energy Agency. (2012). Renewable Energy Technologies: Cost Analysis Series. 2012, 1 (5/5). [Online]. Available at https://www.irena.org/documentdownloads/publications/re_technologies_cost_analysis-wind_power.pdf.
16. Keith, M., Sunderland, K.M., Narayana, M., Putrus, G., Conlon, M.F., & McDonald, S. (2016). The cost of energy associated with micro wind generation: International case studies of rural and urban installations. *Energy*, *109*, 818–829.
17. Ragnarsson, B.F., Oddsson, G.V., Unnthorsson, R., & Hrafnkelsson, B. (2015). Levelized cost of energy analysis of a wind power generation system at Búrfellin Iceland. *Energies*, *8*, 9464–9485.
18. U.S. Energy Information Administration. (2015). *Levelized Cost and Levelized Avoided Cost of New Generation Resources in the Annual Energy Outlook 2015*. [Online]. Available at https://www.eia.gov/forecasts/aeo/pdf/electricity_generation.pdf.
19. Sagatauskas, A. (2014). *Vėjo energetika Lietuvoje pasiekė plėtros ribas?* [Online]. Available at http://www.delfi.lt/verslas/energetika/a-sagatauskas-vejo-energetika-lietuvoje-pasieke-pletros-ribas.d?id=65505856.
20. Investment into solar and wind power plants in Lithuania = Investicijos į saulės ir vėjo jėgaines Lietuvoje. 2010. [Online]. Available at https://roslekas.wordpress.com/category/vejo-energija-2/.
21. Misevičienė, R. (2010). *Vėjo elektrinių plėtrai daug stabdžių.* [Online]. Available at http://www.mokslasirtechnika.lt/mokslo-naujienos/v-jo-elektrini-pl-trai-yra-daug-stabdzi.html.
22. National Energy Forum. (2009). *Vėjas - neišsenkantis energijos* šaltinis. [Online]. Available at http://www.nefas.eu/news-cat-lt-1/188-vjas-neisenkantis-energijos-a.

23. Naujoji Ranga. (2009). *Calculator of investments into wind power plants.* [Online]. Available at http://www.jegaines.lt/index.php?lang=lt&page=skaiciuokle_komercines.
24. Vėjų spektras. (2012). *"Vėjų spektras" pradeda eksploatuoti naują vėjo elektrinių parką.* [Online]. Available at http://www.vejuspektras.lt/blog/2012/11/13/veju-spektras-pradeda-eksplotuoti-nauja-vejo-elektriniu-parka-2/#.
25. Jockus, A. (2015). *Vėjo jėgainės kelsis į Rytų Lietuvą*. [Online]. Available at http://lzinios.lt/lzinios/Ekonomika/vejo-parkai-kelsis-i-rytu-lietuva/210172.
26. Sabaliauskas, L. (2014). *"Renergos" vadovas Linas Sabaliauskas: vėjo jėgainė – patikimesnė už atominę elektrinę.* [Online]. Available at http://www.15min.lt/verslas/naujiena/energetika/dvejus-metus-jura-tiriancios-renergos-vadovas-dar-nezino-ar-statys-juriniu-vejo-jegainiu-parka-664-457074.
27. Global Wind Energy Council. (2014). *Global wind energy outlook 2014.* [Online]. Available at http://www.gwec.net/wp-content/uploads/2014/10/GWEO2014_WEB.pdf.
28. National Control Commission for Energy and Prices. (2017). *Archive of the auctions*. [Online]. Available at http://www.regula.lt/atsinaujinantys-istekliai/Puslapiai/aukcionai/aukcionu-archyvas.aspx.
29. Programme for Investment Actions of EU Funds during 2014–2020. 2014. [Online]. Available at file:///C:/Users/Viktorija/Downloads/2014-2020%20m.%20ES%20fondÅ³%20investicijÅ³%20veiksmÅ³%20programa_2%20(1).pdf.
30. Minister of Environment. (2016). *Regarding Approvement of Financial Plan for the Special Programme of Climate Change 2016*. [Online]. Available at http://www.laaif.lt/lt/klimato-kaitos-specialioji-programa/klimato-kaitos-specialiosios-programos-lesu-naudojimo-samatos/.
31. Bobinaite, V., & Tarvydas, D. (2014). Financing instruments and channels for the increasing production and consumption of renewable energy: Lithuanian case. *Renewable and Sustainable Energy Reviews*, 38, 259–276.
32. Orion Alternative Energy Fund. (2015). Documents of Orion Alternative Energy Fund. [Online]. Available at http://am.orion.lt/fund/orion-alternative-energy-fund/#viewThree.
33. Markevičienė, E. (2015). *Vėjo elektra kryžkelėje: ar reikia daugiau, ar jau užtenka*. [Online]. Available at http://vz.lt/archive/article/2015/4/6/vejo-elektra-kryzkeleje-ar-reikia-daugiau-ar-jau-uztenka.
34. Asia-Pacific Energy Sector Update: Financing Renewable Energy Projects. (2016). [Online]. Available at https://www.dlapiper.com/~/media/Files/Insights/Publications/2015/07/Financing%20renewable%20energy%20projects%2020%20July%202015.pdf.
35. Fried, R. (2015). *The World Bank's latest Green Bond is its biggest*. [Online]. Available at https://www.greenbiz.com/article/green-new-gold-world-banks-latest-green-bond-its-biggest.
36. Nasdaq Stock Exchanges in the Baltic States. Statistics of bonds. (2016). [Online]. Available athttp://www.nasdaqbaltic.com/market/?pg=details&instrument=LV0000801777&list=1&price=1.
37. Latvenergo. (2015). *Latvenergo – Green Bond Framework*. [Online]. Available at http://www.latvenergo.lv/files/news/Green%20Bond%20Framework_28.04.2015.pdf.
38. Bobinaite, V. (2015). Financial sustainability of wind electricity sectors in the Baltic States. *Renewable and Sustainable Energy Reviews*, 47, 794–815.
39. Noothout, P., de Jager, D., Tesnière, L., van Rooijen, S., Karypidis, N., Brückmann, … Resch, G. (2016). *The impact of risks in renewable energy investments and the role of smart policies*. [Online]. Available at http://www.diacore.eu/images/files2/WP3-Final%20Report/diacore-2016-impact-of-risk-in-res-investments.pdf.

40. Justice, S. (2009). *Private* financing *of renewable energy – A guide for policymakers*. [Online]. Available at http://sefi.unep.org/fileadmin/media/sefi/docs/publications/Finance_guide_F INAL-.pdf.
41. World Energy Council. (2013). *World energy perspective: Cost of energy technologies.* [Online]. Available at https://www.worldenergy.org/wp-content/uploads/2013/09/WEC_J1143_CostofTECHNOLOGIES_021013_WEB_Final.pdf.
42. Short, W., Packey, D.J., & Holt, T. (1995). *A Manual for the Economic Evaluation of Energy Efficiency and Renewable Energy Technologies.* [Online]. Available at http://www.nrel.gov/docs/legosti/old/5173.pdf.
43. Energinet.dk (2013). *Energinet.dk's analysis assumptions 2013–2035.* [Online]. Available at https://www.energinet.dk/SiteCollectionDocuments/Engelske%20dokumenter/El/Energinet%20dk's%20analysis%20assumptions%202014-2035%20-%20September%202014.pdf.

FINANSĒŠANAS INSTRUMENTU UN STRATĒĢIJU IETEKME UZ VĒJA ENERĢIJAS RAŽOŠANAS IZMAKSĀM: LIETUVAS PIEREDZE

V. Bobinaite, I. Konstantinavičiūte

K o p s a v i l k u m s

Raksta mērķis ir parādīt finansēšanas instrumentu, to nosacījumu un finansēšanas stratēģiju atbilstību vēja enerģijas ražošanas izmaksām un vēja elektrostacijas spējai piedalīties elektroenerģijas tirgū Lietuvā. Pētījumā izmantota paplašinātā pieeja izlīdzinātajām elektrības izmaksām (LCOE).

Paplašināto pieeju raksturo tas, ka tiek ievērotas visa ekspluatācijas perioda izmaksas un ieņēmumi, kas saņemti no atbalsta pasākumiem.

Pētījuma rezultāti apstiprināja, ka finansēšanas instrumenti, to nosacījumi un stratēģijas ietekmē LCOE un vēja elektrostacijas konkurētspēju.

Tika konstatēts, ka vēja elektrostacijas finansēšana, izmantojot tradicionālos finanšu instrumentus (akcijas un banku aizdevumi), ir saistīta ar riska kapitālu un obligācijām pat bez jebkāda atbalsta. Tika aprēķināts, ka izmantojot stratēģijas, kas iekļauj nelabvēlīgos aizdevumus un atvieglojumus, obligācijas, pašu kapitālu un riska kapitālu, vidējās izlīdzinātās elektrības izmaksas sastāda 5,1–5,7 EURct / kWh (2000 kW), kad paredzamā elektroenerģijas pārdošanas cena ir 5,4 EURct / kWh. Finansēšanas stratēģijas ar lielāku pašu kapitāla daļu varētu paaugstināt izlīdzinātās elektrības izmaksas par 6 %, salīdzinot ar stratēģijām, kas paredz lielākas parādsaistības. Tomēr, cenšoties motivēt riska kapitālistus, obligāciju turētājus vai citus jaunus finansētājus, kas ienāk vēja enerģētikas nozarē, atbalsta pasākumiem (ieguldījumu tarifi vai ieguldījumu subsīdijas) ir būtiska loma 250 kW vēja elektrostacijas gadījumā. Tika aprēķināts, ka, izmantojot neatbalstītās finansēšanas stratēģijas, vidējās izlīdzinātās elektrības izmaksas sastādīs 7,8–8,8 EURct / kWh 250 kW vēja elektrostacijā, bet tās samazināsies par aptuveni 50 %, ja tiks piemēroti ieguldījumu tarifi vai 50 % ieguldījumu subsīdijas.

02.05.2017.

LATVIAN JOURNAL OF PHYSICS AND TECHNICAL SCIENCES
2018, N 2

DOI: 10.2478/lpts-2018-0010

THE CONTROL PRINCIPLES OF THE WIND ENERGY BASED DC MICROGRID

G. Zaleskis, I. Rankis
Riga Technical University, Faculty of Power and Electrical Engineering, Institute of Industrial Electronics and Electrical Engineering,
12-1 Azenes Str., Riga, LV-1048, LATVIA
e-mail: genadijs.zaleskis@rtu.lv

According to the strategical objectives of the use of the renewable energy sources, it is important to minimise energy consumption of conventional power grid by effective use of the renewable energy sources and providing stable operation of the consumers. The main aim of research is to develop technical solutions that can provide effective operation of the wind generators in the small power DC microgrids, which also means wind energy conversion at as wider generator speed range as possible.

Keywords: *energy resources, renewable energy sources, wind energy*

1. INTRODUCTION

The strategic objectives of the use of renewable energy sources can be reached by integration of the renewable energy sources, e.g., wind turbines. This way, the appropriate laws and regulations on the use of renewable resources and energy efficiency in buildings will be implemented. Political and ecological factors stimulate the development of the renewable energy. The main aim of the present research is to develop technical solutions that can provide effective operation of the wind generators in the small power microgrids, which means stable operation of the consumers and wind energy conversion at as wider generator speed range as possible.

According to the strategical objectives of the use of the renewable energy sources, it is important to minimise power consumption of conventional power grid by effective use of the renewable energy sources and providing stable operation of the consumers. This task can be decided by the use of the DC microgrid, which can operate synchronously with the conventional network and autonomously, ensuring energy supply to the decentralised consumers or in the emergency case.

According to the defined aim of the research, it is of special significance to provide an operative coordination of the main partners of wind energy based system – wind generator itself, the conventional three-phase network and an energy storage system for providing supply of consumers when wind power and energy of conventional network both are not available for some reasons. The energy storage system is

an optional part and is not included in the present research. Solution of the defined tasks should be provided taking into account static and dynamic parameters of the systems involved considering its controllability.

The defined tasks are very topical for investigators of wind power based systems and some of their aspects are investigated in the papers [1]–[4], which propose applications of different approaches to solve the task of maximum wind power extraction. Therefore, it can be stated that the problem is topical and asks for efficient solutions.

2. PRINCIPLES OF THE DEVELOPMENT OF WIND ENERGY BASED DC MICROGRID

There are three main groups of microgrids depending on the bus voltage: DC based microgrid; AC based microgrid; DC and AC based microgrid [5]. The DC based microgrid topology is discussed in the present research. This choice is determined by the most efficient use of the renewables, which is achieved by reducing the conversion losses, and the ability to provide uninterrupted power supply [5]–[12]. The possibility of using the recuperated braking energy of the electrical drives is also taken into account. Due to this option, DC microgrid becomes popular in the industry sector [13]. All generating object and energy storages are connected to common DC bus in the DC based microgrid topology through the relevant converters [5]. It is appropriate to use a variable speed wind turbine with permanent magnet synchronous generator (PMSG) and full power electronics conversion in the DC based microgrid [14]. The energy storage system is not studied in the present research, so the principal scheme of the wind energy based DC microgrid with connection to the conventional AC grid is presented in Fig. 1.

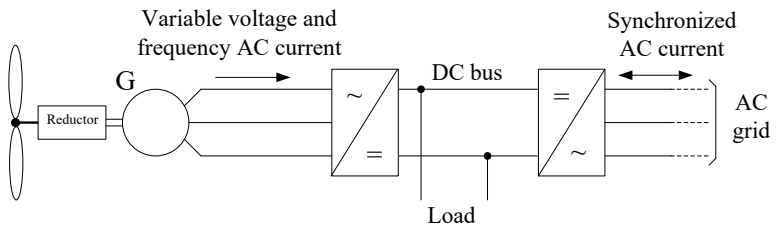

Fig. 1. The wind energy based DC microgrid with connection to the conventional AC grid.

Taking into account the power grid standard of the Republic of Latvia on 230/400 V and household connection types, there is a possibility to connect a microgrid to one- or three-phase AC grid. The connection to three-phase power grid is discussed in the present research. It can be implemented by the use of the active rectifier (active front-end) [15]; in this case, DC bus minimum voltage must be equal to rectified AC voltage peak value [16], which is equal to AC line voltage amplitude:

$$V_{d,\min} = V_l \cdot \sqrt{2} = 565\text{V}, \tag{1}$$

where $V_l = 400$ V – line voltage r.m.s., V.

According to standard LVS EN 60038 [17], the rated DC bus voltage $V_{d,r}$ was accepted equal to 600 V.

3. PERMANENT MAGNET SYNCHRONOUS GENERATOR CONNECTION TO THE DC BUS

In accordance with the generator parameters, the use of non-inverting buck-boost DC/DC converter was prompted [1], [18], [19]. The control system of the converter is based on setting the wind generator optimal power curve and directly adjusting the DC/DC converter duty cycle [2]–[4]. The block diagram of the proposed system and principal scheme of the converter are shown in Fig. 2. The DC bus voltage is equal to:

$$V_d = V_{g,dc} \cdot \frac{D1}{1 - D2}, \text{V}, \tag{2}$$

where $D1$ – the duty cycle of the switch VT1;
$D2$ – the duty cycle of the switch VT2;
$V_{g,dc}$ – the output DC voltage of the generator.

Accepting the maximum value of $D2$ equal to 0.9, the generator output voltage is:

$$V_{g,dc}^{1} = 0.1 \cdot V_d, \text{V}. \tag{3}$$

At this generator voltage generator, output direct current must be:

$$I_{g,dc}^{1} = \frac{k_{dc} \cdot n}{R_g} - \frac{0.1 \cdot V_d}{R_g}, \text{A}. \tag{4}$$

At a low generator speed range, generator converter output current is:

$$I_1^1 = 0.1 \cdot I_{g,dc}^{1} = \frac{0.1 \cdot k_{dc} \cdot n}{R_g} - \frac{0.01 \cdot V_d}{R_g}, \text{A}. \tag{5}$$

The resistance R_g characterises the internal resistance of the generator and the impact of commutation:

$$R_g = \frac{V_{g,dc,0}}{I_{g,dc,\max}} - \frac{P_{ref}}{I_{g,dc,\max}^2}, \Omega. \tag{6}$$

At $I_1 = 0$, generator speed is:

$$n_0 = \frac{0.1 \cdot V_d}{k_{dc}}, \text{rpm}. \tag{7}$$

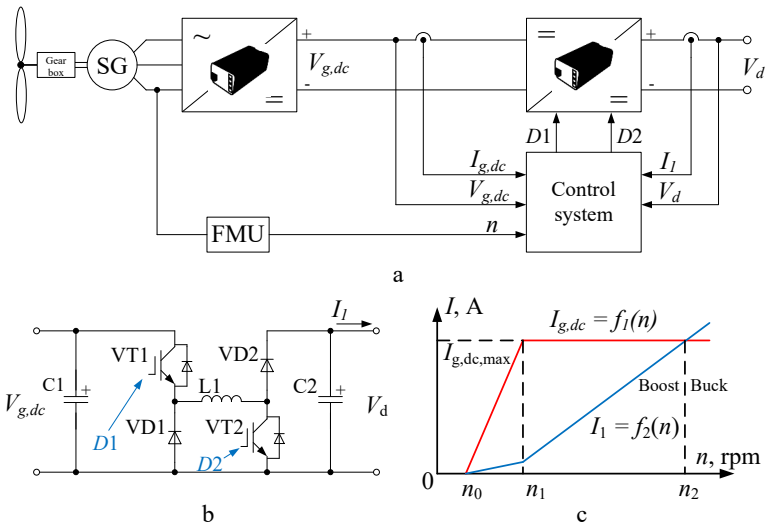

Fig. 2. The block diagram of the proposed system (a); the principal scheme (b) of the DC/DC converter and the wind turbine circuit current as a function of generator speed (c): SG – a synchronous generator; FMU – a frequency measurement unit.

Generator current reaches the maximum value $I_{g,dc,max}$ when speed is equal to n_1 (Fig. 3); in this case converter current is:

$$I_1^1 = 0.1 \cdot I_{g,dc,\max}, \text{A}. \tag{8}$$

The maximum current of the discussed generator GL-PMG-5000 is $I_{g,dc,max}$ = 10 A. If DC bus rated voltage is 600 V, the speed n_0 is equal to 18.5 rpm, but n_1 is approximately 65 rpm (Fig. 3). Between n_0 and n_1 generator, DC voltage is equal to 60 V according to (3). At n_2, converter current I_1 is equal to $I_{g,dc,max}$, and operation mode of the converter changes to step-down. At $n > n_2$ converter operates in step-down mode.

4. THE CONTROL PRINCIPLES OF THE ACTIVE FRONT-END IN THE DC MICROGRID

When $I_{g,dc} = I_{g,dc,max}$ = 10 A and $V_d = V_{d,r}$ = 600 V, generator converter current is equal to:

$$I_1 = \frac{I_{g,dc} \cdot V_{g,dc}}{V_d} = \frac{V_{g,dc}}{60} = \frac{k_{dc} \cdot n - R_g \cdot I_{g,dc}}{60}, \text{A}. \tag{9}$$

At the same time, converter current must be equal to:

$$I_1 = \frac{k_{dc} \cdot n}{60 + \dfrac{R_g \cdot D1}{(1 - D2)}}, \text{A}. \tag{10}$$

The DC microgrid connection to the 3-phase AC grid through the active front-end is studied in the present research [15], [20], so the front-end output current I_2 (Fig. 4) is equal to:

$$I_2 = I_{load} - I_1, \text{A}, \tag{11}$$

where I_{load} – load current, A.

If I_2 is with "-" sign, the current is transferred into the AC grid. The calculation of the reference current $I_{2,ref}$ of the active rectifier is shown in block diagram (Fig. 3.a). AC grid phase current amplitude is:

$$I_{ph,a} = \frac{2 \cdot I_2}{\sqrt{3}}, \text{A}. \tag{12}$$

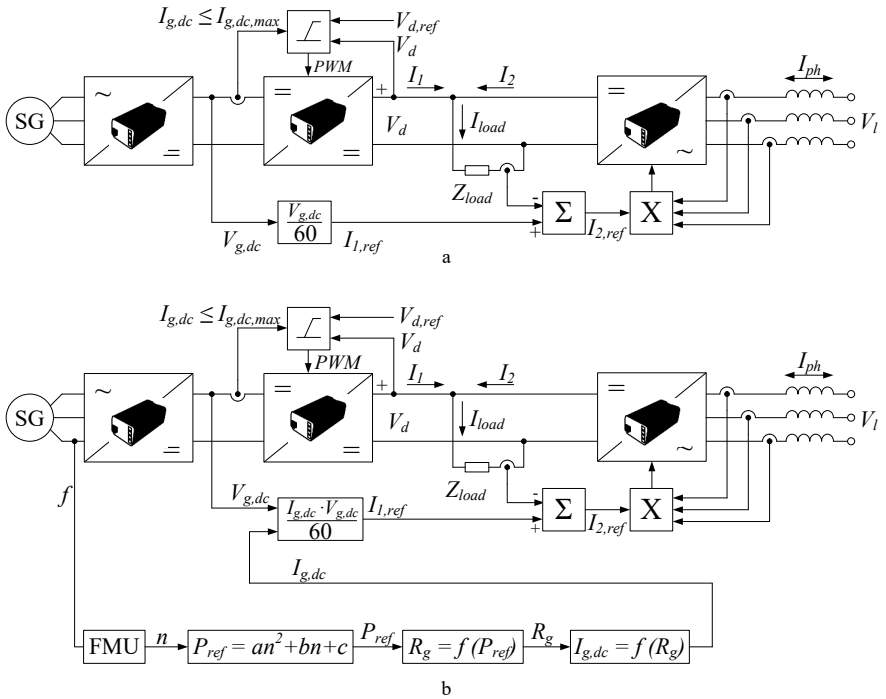

Fig. 3. The calculation of the reference current of the active rectifier at generator speed $n > n_1$ (a) and at generator speed $n \le n_1$ (b): $V_{g,dc}$ – wind generator output DC voltage; V_d – DC bus voltage; V_l – AC grid line voltage; Z_{load} – load impedance; $I_{g,dc}$ – wind generator output DC current; I_1 – wind generator converter output current; I_{ph} – AC grid phase current; I_2 – active rectifier output current; I_{load} – load current.

If generator speed is $n \le n_1$, the calculation of the generator output current $I_{g,dc}$ is needed. For this purpose, the reference power of the generator is calculated [20]. In case of the generator GL-PMG-5000 it is:

$$P_{ref} = 0.0988 \cdot n^2 + 5.3682 \cdot n - 109.02. \quad (13)$$

The current of the generator DC-DC converter is calculated as in (4). The principle of the estimation of the $I_{g,dc}$ and I_1 values is presented in Fig. 3.b. According to Fig. 2.c, the mentioned currents were calculated for the generator GL-PMG-5000 (Fig. 4).

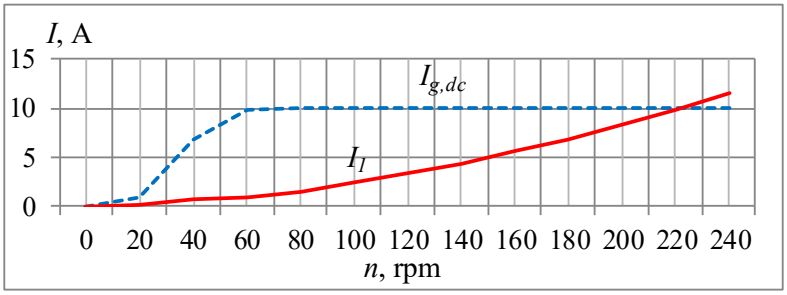

Fig. 4. The calculated currents for the circuit of the wind turbine: $I_{g,dc}$ – wind generator output direct current; I_1 – wind generator converter output current.

5. SIMULATION RESULTS

The proposed control method was confirmed by the PSIM simulation. The current distribution (Fig. 5) is presented at the load resistance 200 Ω and the DC bus rated voltage 600 V. The speed n_2 of the discussed PMSG is equal to 222 rpm in the case of generator rated current 10 A.

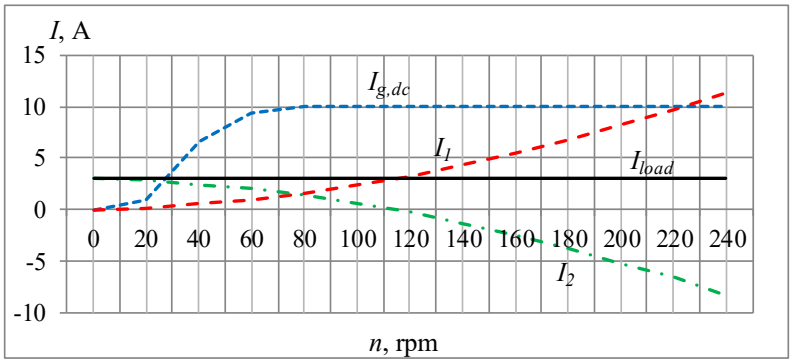

Fig. 5. Simulation diagrams of the wind energy based DC microgrid connected to the conventional AC power grid: $I_{g,dc}$ – wind generator output direct current; I_1 – wind generator converter output current; I_2 – active rectifier current; I_{load} – load current.

The received generator power, conventional grid power and load power are presented in Fig. 6. When n > 118 rpm and a load is 200 Ω, the generator starts to transfer produced energy to a conventional power grid; therefore, I_2 and P_{grid} values are negative in this speed range.

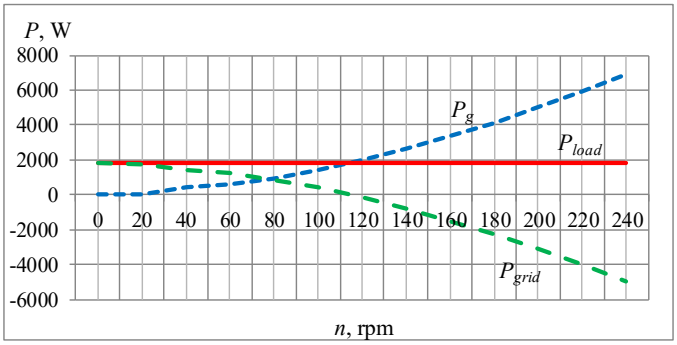

Fig. 6. Simulation diagrams of the wind energy based DC microgrid connected to the conventional AC power grid: P_g – wind generator power; P_{grid} – conventional grid power; P_{load} – load power.

In case of DC microgrid connection to the conventional AC grid, the power quality must be taken into account. The simulation presents that the proposed system can provide implementation of this condition. At positive I_2 values (the energy is consumed from the AC grid), the AC grid voltage and current are the same phase (Fig. 7).

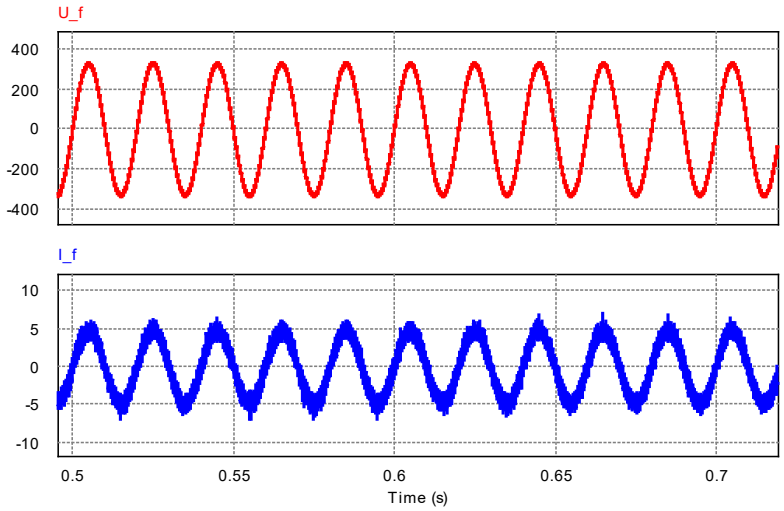

Fig. 7. The simulation diagram of the DC microgrid operation with conventional AC grid at generator speed of 200 rpm and load of 50 Ω: U_f – AC grid phase voltage; I_f – AC grid phase current.

6. CONCLUSIONS

The DC based microgrid topology is discussed in the present research. Firstly, this choice is determined by the most efficient use of the renewables and the ability to provide uninterrupted power supply. Secondly, the possibility to recuperate the braking energy of the electrical drives and the rest of the generated energy is taken into account. The synchronous generator with full power electronics conversion as a basic energy source of the microgrid has been chosen. In accordance with the national standards and features of the DC bus cooperation with a three-phase power

grid, the microgrid rated voltage value of 600 V has been selected, but the allowed minimum voltage has been accepted equal to 565 V.

Synchronous generator interconnection with DC bus is ensured by the use of the buck-boost DC/DC converter, which has been chosen because of the generator technical parameters. The converter control system is based on setting the wind generator optimal current and directly adjusting the DC/DC converter duty cycle. The minimum necessary speed of the discussed generator is 18.5 rpm.

The proposed system is based on the active rectifier, whose control is implemented by determination of the difference between the maximally allowed wind generator DC-DC converter current and load current. This method provides bidirectional energy transmission between DC microgrid and conventional power grid. According to the proposed control principle, the optimum current curve of the discussed permanent magnet synchronous generator has been calculated and recognised by the computer model. The theoretical analysis and computer modelling show the correct operation of the control principles. The proposed method allows using all wind turbine generated energy in a wide range of speeds. Surplus wind energy can be transmitted to the conventional power grid and, if necessary, energy flow from the conventional grid can support the needs of consumers.

ACKNOWLEDGEMENTS

The present research has been supported by the Latvian National Research programme "The Next Generation of Information and Communication Technologies (NexIT)".

REFERENCES

1. Suskis, P., & Rankis, I. (2012). Buck-boost DC-DC converter for wind and hydrogen based autonomous energy supply system. *Biennial Baltic Electronics Conference (BEC) 2012*, 215–218.
2. Koutroulis, E., & Kalaitzakis, K. (2006). Design of a maximum power tracking system for wind-energy-conversion applications. *IEEE Transactions on Industrial Electronics, 53*(2), 486–494.
3. Eltamaly, A.M., Alolah, A.I., & Farh, H.M. (2013). Maximum power extraction from utility-interfaced wind turbines. New Developments in Renewable Energy. *InTech*, 159–192.
4. Wang, Q., & Chang, L. (2004). An intelligent maximum power extraction algorithm for inverter-based variable speed wind turbine systems. *IEEE Transactions on Power Electronics, 19*(5), 1242–1249.
5. Graillot, A. (2009). Hybrid micro grids for rural electrification: Developing appropriate technology. *AIE Event*, *41*.
6. Karlsson, P. (2002). *DC distributed power systems*. Lund University, 148.
7. Laudani, G.A., & Mitcheson, P.D. *Comparison of cost and efficiency of DC versus AC in office buildings*. Transformation of the Top and Tail of Energy Networks, London.
8. Deaconu, D., Chirila, A., Albu, M., & Toma, L. (2007). Studies on a LV DC network. *European Conference on Power Electronics and Applications*, 1–7.

9. Sannino, A., Postiglione, G., & Bollen, M. H. J. (2003). Feasibility of a DC network for commercial facilities. *IEEE Transactions on Industry Applications, 39*(5), 1499–1507.
10. Hammerstrom, D. J. (2007). AC versus DC distribution systems-did we get it right? *IEEE Power Engineering Society General Meeting*, 1–5.
11. Kwasinski, A. (2012). *Micro-grids architectures, stability and protections*. Available at http://users.ece.utexas.edu/~kwasinski/EE394J10_DG_stability%20architecture%20comp.ppt
12. Zaleskis, G., Steiks, I., Pumpurs, A., & Krievs, O. (2015). DC-AC Converter for Load Supply in Autonomous Wind-Hydrogen Power System. In *56th International Scientific Conference on Power and Electrical Engineering of Riga Technical University (RTUCON)*, 14 October 2015 (pp. 169–173). Riga: RTU Press.
13. Pellicciari, M., Avotins, A., Bengtsson, K., & Meike, D. (2015). AREUS – Innovative hardware and software for sustainable industrial robotics. *IEEE Conference on Automation Science and Engineering*, *2015*, 1325–1332.
14. Camm, E.H., Behnke, M.R., Bolado, O., Walling, R. (2009). *Characteristics of wind turbine generators for wind power plants*. University of Tennessee, 1–5.
15. Rashid, M.H. (2001). *Power electronics handbook*. San Diego, California: Academic Press.
16. Meike, D. (2013). *Increasing energy efficiency of robotized production systems in automobile manufacturing*. Ph.D. Thesis. Riga: Riga Technical University.
17. Latvian National standardisation institution "Latvijas Standarts". (2012). LVS EN 60038:2012 "CENELEC standard voltages".
18. Suskis, P., & Rankis, I. (2012). Performance of a voltage step-up/step-down transformerless dc/dc converter: Analytical model. *Latvian Journal of Physics and Technical Sciences*, *49*(4), 29–40.
19. Suskis, P. (2013). DC/DC voltage h-bridge converter for autonomous hydrogen system with fuzzy logic. *The 54th International Scientific Conference of Riga Technical University*, 1–4.
20. Zaleskis, G. (2017). *Research of the automation tasks of the wind generators in the low-power microgrids*. Ph.D. Thesis (in Latvian). Riga: Riga Technical University.

UZ VĒJA ENERĢIJAS BALSTĪTA LĪDZSTRĀVAS MIKROTĪKLA VADĪBAS PRINCIPI

G. Zaļeskis, I. Raņķis

Kopsavilkums

Saskaņā ar atjaunojamo enerģijas resursu pielietošanas stratēģiskiem mērķiem, ir svarīgi minimizēt enerģijas patēriņu no centralizētā elektroapgādes tīkla, efektīvi izmantojot atjaunojamos enerģijas resursus un nodrošinot patērētāju stabilo darbību. Pētījuma mērķis ir izveidot tehniskos risinājumus, kas var nodrošināt vēja ģeneratoru efektīvu darbību mazās jaudas līdzstrāvas mikrotīklos, kas nozīme arī vēja enerģijas pārveidošanu pēc iespējas plašākā vēja ģeneratora ātrumu diapazonā.

21.11.2017.

LATVIAN JOURNAL OF PHYSICS AND TECHNICAL SCIENCES
2018, N 2

DOI: 10.2478/lpts-2018-0011

MODELLING OF TWO-STAGE METHANE DIGESTION WITH PRETREATMENT OF BIOMASS

A. Dychko[1], N. Remez[1], I. Opolinskyi[1], S. Kraychuk[2],
N. Ostapchuk[2], L. Yevtieieva[1]
[1] Institute of Energy Saving and Energy Management, National Technical University of Ukraine "Igor Sikorsky Kyiv Polytechnic Institute"
37 Peremohy Ave., Kyiv, 03056, UKRAINE
[2] Department of Economic Cybernetics, Rivne State University of Humanities
12 Stepana Bandery Str., Rivne, 33000, UKRAINE

Systems of anaerobic digestion should be used for processing of organic waste. Managing the process of anaerobic recycling of organic waste requires reliable predicting of biogas production. Development of mathematical model of process of organic waste digestion allows determining the rate of biogas output at the two-stage process of anaerobic digestion considering the first stage. Verification of Konto's model, based on the studied anaerobic processing of organic waste, is implemented. The dependencies of biogas output and its rate from time are set and may be used to predict the process of anaerobic processing of organic waste.

Keywords*: biogas, digestion, intensification, modelling, organic waste*

1. INTRODUCTION

Nowadays more than 50 billion tons of waste from energetic, industrial, agricultural enterprises and domestic sector are received by the atmosphere, water and soil in the world annually, including more than 150 million tons of waste from industrial enterprises [1].

With an increase in the amounts of organic waste, the methods of their processing should be studied. Today about 140 thousand hectares of land area in Ukraine are occupied by landfills, which hold more than 38 billion tons of solid waste. Only 3 % of such waste is utilised or processed [2].

Most of the existing landfills have already exceeded their designed lifetime of exploitation. Lack of monitoring systems almost at all landfills increases their environmental hazards.

The main pollutant emissions from landfills are formed from the decomposition of organic waste. A major contributor to environmental pollution is organic waste that remains after sewage treatment. During the storage of organic waste,

methane and carbon dioxide are generated and released to the atmosphere out of control.

For processing of organic waste, the method of anaerobic digestion is advisable to use, which produces an additional source of energy, reduces the level of technogenic load and increases the level of environmental safety in general.

Use of anaerobic technology of organic waste processing allows getting rid of manure of different types (including bird droppings), recycling plant remains (overwintered silage, foliage of food crops, etc.) and utilising organic waste of poultry factories and poultry slaughterhouses, as well as wastewater treatment products. Waste treatment is, first of all, a system that is cost-effective and that increases the environmental safety of the country.

One person produces 0.5–3 kg of household and industrial waste per day, from which 0.00125–0.5 m^3 of biogas may be received. Amount of the produced biogas depends on the type of waste and recycling technologies [2].

Our own experimental studies confirm the environmental and economic feasibility of anaerobic organic waste processing technologies [3], [4].

To improve the management of organic waste treatment, it is necessary to create a mathematical model of predicting biogas production, which optimises the fermentation process.

The existing mathematical models of biogas produce differ in a set of state variables that are taken into account during their calculation and in the type and order of equations on which they are based [5], [7], [9], [12]. The simplest models are based on algebraic equations that allow predicting the dynamics of methane producing. However, these simple models do not always give an adequate prediction because their equations are based on empirical relationships under specific conditions. Model prediction becomes meaningless outside of these conditions.

More complex models are based on Cauchy problems for systems of ordinary differential equations and on initial-boundary value problems for differential equations in partial derivatives. The latter describe not only the dynamics of the number of substances but also their spatial distribution. These complex models are based on fundamental studies of biochemical reactions and contain more state variables, so their forecast is adequate in wide limits of changing conditions of the process. However, despite their universality, the application field of complex models is limited. This is due to the fact that the problem of their identification is very complex and is solved only under laboratory conditions, so the mentioned models require to be updated for modelling industrial processes characterised by significant uncertainty [5].

The usual forms of describing of anaerobic processes of biomass digestion are discrete dynamic models based on Mono's equations and their numerous modifications. One of the possible variants is modelling based on Chen and Hashimoto equation that describes the intensity of process of anaerobic digestion and biogas producing [6].

Andrews and Graef (1971) published a mathematical model, which is general and does not imply any particular type of organic substrate. pH of environment should be from 6 to 8, fixed temperature – 38 °C, while the stage of hydrolysis is not included. The model describes only one type of microorganisms [7].

The model of Hill and Barth (1977), which describes the process of methane fermentation of animal waste, includes the stage of hydrolysis and its parameters are expressed as the Arrhenius equation.

Hill (1983) predicts anaerobic process of recycling of waste from poultry, beef, dairy or pigs with two parameters – biorecycling stable and constant of acidity. Temperature range is 20 °C…60 °C; the hydrolysis step is not included.

Husain model (1998) is based on the model of Hill, but includes a large number of chemical reactions.

The model of Batstone (2002) is known as ADM1 (Anaerobic Digestion Model No. 1). It describes biochemical and physical-chemical processes and includes the stage of dissolution, extracellular hydrolysis, methanogenesis and acidogenesis [8]. ADM1 is described by 32 ordinary differential equations, 12 of which describe the dynamic behaviour of particles and biomass, 10 – dissolved components, 2 – inorganic nitrogen and carbon, 2 – cation/anion balance of fluids, 6 – acid-base reactions to determine the pH [9].

Zaher (2009) describes the process of anaerobic digestion of dairy waste, which includes hydrolysis acidogenesis, methanogenesis. The model is presented for periodic processes with continuous mixing at 35 °C [8].

The analysed models differ in a set of state variables that is taken into account during their building and in the type and order of equations on which they are based.

The key factors influencing the flow of methanogenesis under conditions of substrate mixing and constant temperature are the period of process, concentrations of bacteria and of nutrients of substrate. That is why bacteria growth may be modelled using the equation of Kobozev.

The growth of bacteria populations is also described by the model of Mono considering the dying process (the equation of Kolpykov).

One of the main parameters characterising the intensity of process of anaerobic digestion is the volume of biogas output. The equation of Chen and Hashimoto is used to determine the rate of biogas output.

Modern biogas plants are based on the use of heated reactors, since energy should be constantly spent on methanogenesis realisation. Efficient production of biogas is only possible when the total energy of the gas is significantly bigger than the energy consumed for its production. Conditions of marketable biogas production may be represented mathematically considering the heat balance of bioreactor. Material balance of substrate, biogas and biomass is a biokinetic model of bioreactor.

To describe kinetic processes of methane tank with mixing for anaerobic digestion of wastewater, it is possible to use the mathematical model developed by Andrews and Graef [7].

Growth and development of biomass, degradation of substrate and formation of products of bioreaction are inseparably interrelated and their description is a complete model of transformation processes of organic pollutants of substrate into biogas.

This way, depending on the set parameters, conditions of anaerobic digestion and the origin of biomass, the process can be described by various models. Expedi-

ent choice of models makes it possible to project and operate efficiently with anaerobic digestion of biomass.

The models above have certain disadvantages: the simplest models, based on algebraic equations, allow predicting the dynamics of methane formation, but they do not always provide an adequate forecast. Equations of the models are based on empirical correlations for specific conditions. Complex models are based on Cauchy problem for systems of ordinary differential equations and on initial and boundary value problems for differential equations in partial derivatives, but the range of their applications is limited.

For example, the model of Andrews and Graef (1971) operates only at a fixed temperature and contains one type of microorganisms; the model of Batstone (2002) is complex and described by 32 ordinary differential equations characterised by cumbersome calculations; the model of Zaher (2009) is reliable only at a fixed temperature of periodic processes [13], [14].

The existing mathematical models of biogas output [10]–[12] are based on microbiological processes in the digester and biogas plant compound, and do not include the initial phase of fermentation and compound of loaded biomass.

To eliminate these disadvantages, the authors of the research propose using modelling for predicting biogas output at the two-stage process of anaerobic digestion of biomass. The aim of the research is to develop a mathematical model of digestion process of organic waste by Konto's model verification.

2. EXPERIMENTAL MODELLING

To describe complex systems of anaerobic treatment of organic waste, wastewater and biomass, equations based on dependencies of Mono and Michaelis-Menten are used:

$$-\frac{dS}{dt}=\frac{K_m \cdot S_x}{K_S + S}\ ; \tag{1}$$

$$-\frac{dx}{dt}=\gamma\left(-\frac{dS}{dt}\right)-b_0 x\ , \tag{2}$$

where $\frac{dS}{dt}$ – the rate of conversion of organic substrate, kg/(m^3·per day); K_m – the maximum specific rate of substrate utilization, kg / (kg per day); K_s – Mono's constant, which is equal to substrate concentration at $\mu = 0.5 \cdot \mu_m$, kg/m^3 (μ – the specific growth rate of biomass per day); μ_m – the maximum specific rate of biomass growth per day); x – the concentration of biomass, kg/m^3; $\frac{dx}{dt}$ – the rate of growth of biomass, kg/(m^3·per day); γ – the increase of biomass at utilisation of substrate, kg/kg; b – the rate of inactivation of biomass, a day^{-1}.

The equation below is obtained by substituting equation (1) with equation (2) and dividing by x:

$$\left(-\frac{dx}{dt}\right)\Big/ x = \mu = \frac{\gamma \cdot K_m \cdot S}{K_S + S} - b_0 \ , \tag{3}$$

where the specific growth rate of biomass μ is associated with substrate utilisation. The value changes depend on specific characteristics of microorganisms and biomass.

For further simulation, the model of Konto is used to describe the process of anaerobic digestion of organic waste mathematically:

$$b/\tau = B\left(S/\tau\right) \cdot \left(1 - \frac{K}{\mu_m \cdot \tau^{-1+k}}\right), \tag{4}$$

where b/τ – the rate of methane forming, m^3·per day; $\overline{B}$ – the limit of methane output per unit of mass of organic matter loaded in the digester under the condition of infinitely long duration of process, m^3/kg; S – the concentration of organic matter at the loaded substrate, kg/m^3; τ – the duration of fermentation, days; $K = f(S)$ – the kinetic parameter of process.

From equations (1) and (4), it is clearly that at a certain load $b = \frac{S}{\tau}$ the rate of biogas output b/τ depends on the maximum possible formation of methane $\overline{B}$, the time of stay of fermented biomass in the digester and kinetic parameters μ_m and K.

Limit output of methane $\overline{B}$ depends on factors that determine the chemical compound of biomass.

3. RESULTS AND DISCUSSION

Dependences of productivity of biogas output b/τ on the digestion time τ are obtained on the basis of experimental research [3], [4], [15] (Fig. 1).

Dependence of rate of biogas output on the fermentation duration is obtained by using equation (4) – the model of Konto and values of the dependences (Fig. 1).

The dependence of biogas output b/τ on the fermentation time demonstrates that the optimal duration of fermentation substrate is 4–6 days. After the 7th–8th day, a decrease in productivity takes place so the fermentation process becomes inappropriate.

Using the obtained dependences, the authors of the research implemented the verification of Konto's model. The following dependence is obtained:

$$\frac{b}{\tau} = 0.13 \cdot e^{(-0{,}05 \cdot \tau)} \ . \tag{5}$$

The coefficient of determination for this function R^2 is equal to 0.99. However, as it is seen from the graph, curve *2*, based on the experimental data and model of Konto, describes only a decline in the function of biogas output rate.

To complete the description of the process, using the experimental data curve *1* is obtained with the equation below:

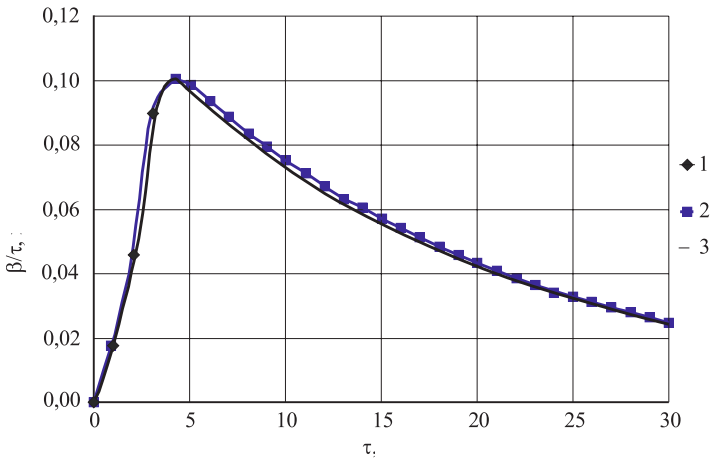

Fig. 1. Dependence of biogas productivity b/τ on the time of digestion τ:
1 – the experimental data; 2 – the model of Konto;
3 – the approximation curve of process of primary digestion of substrate.

$$\frac{b}{\tau} = 0.019 \cdot \tau^{1,3} \ . \tag{6}$$

The coefficient of determination for this function R^2 is equal to 0.98. Equation (6) describes the growth of function of biogas output rate. It is important for the description of the whole process of fermentation and the further optimisation of the digestion process.

The interpolation using the Lagrange polynomial of the 4th degree allowed obtaining the expression below:

$$b/\tau = 0.2095 \cdot \tau^4 - 2.1958 \cdot \tau^3 + 6.9904 \cdot \tau^2 - 6.4541 \cdot \tau + 1.96 \ . \tag{7}$$

Using equation (7) allows predicting the anaerobic processing of organic waste by considering the rate of biogas output and the intensification of the digestion process.

4. CONCLUSIONS

Depending on the set parameters, the conditions of anaerobic digestion and the nature of biomass origin, the process can be described by various models. Expedient choice of models makes it possible to project and operate with anaerobic processing of biomass efficiently.

The obtained dependency is valid only for the studied input substrate, since biogas output depends on the compound, state and properties of the substrate.

The verified model of Konto is proposed to be used in order to predict the rate of biogas output for a given compound of the substrate. To complete the prediction, the equation that takes into account the specifics of anaerobic treatment of waste of various types should be used.

Further research should be directed to create a mathematical model of two-stage digestion of organic waste considering the compound of substrate, which predicts the quality and quantity of biogas.

REFERENCES

1. Ignatenko, A.P. (2003). Economic and ecological aspects of solid wastes recycling. *Ecology and Resources*, *4,* 115–120.
2. Efimov, N.N., Fedorova, N.V., Mirgorodsky, A.I., & Kolomiytseva, A.M. (2007). Gasification of organic fuels and biomass. *Successes of Modern Natural Science*, *1*, 15–21.
3. Dychko, A., Opolinskyi, I., & Yevtieieva, L. (2016). Waste and wastewater treatment bottleneck management. *Ecological Safety*, *21*(1), 123–126.
4. Dychko, A., Opolinskyi, I., & Yevtieieva, L. (2015). The intensification of the process of transformation of biomass into biogas. *Managing the Development of Complex Systems, 22*(1), 193–198.
5. Martsenyuk, E.O., Divak, M.P., Pigovsky, J.R., & Divak, J.R. (2010). Identification of discrete dynamic process models with interval uncertainty in biogas plants processing organic waste. *Proceedings of DonNTU. Series "Informatics, Cybernetics and Computer Science"*,*11*, 181–187.
6. Kushchev, L.A., Suslov, D.Yu., & Alifanova, A.I. (2014). Theoretical aspects of the process of obtaining biogas during anaerobic fermentation of organic waste. *Science Time*, *10*, 258–262.
7. Andrews, J.F., & Graef, S.P. (1971). Dynamic modeling and simulation of the anaerobic digestion process. *Advances in Chemistry Series (Am. Chem. Soc.)*, *105*, 126.
8. Haugen, F., Bakke, R., & Lie, B. (2013). Adapting dynamic mathematical models to a pilot anaerobic digestion reactor. *Modeling, Identification and Control, 34*, 35–54.
9. Dewil, R., & Lauwers, J. (2011). Anaerobic digestion of biomass and waste: Current trends in mathematical modeling. *IFAC Proceedings Volumes*, *44*, 5024–5033.
10. Presura, A., Robescu, L., & Panaitescu, I. (2010). Modeling and simulation of biological anaerobic treatment of sludge resulted from wastewater treatment. *Recent Advances in Energy, Environment, Economics and Technological Innovation*, *1*, 55–60.
11. Gunter, L., & Goldfarb, L. (1991). *Methane tanks*. Moscow: Stroyizdat.
12. Borovska, T.N., & Severilov, P.V. (2009). Simulation and optimization of manure gas production systems. *Proceedings of VNTU*, *2*, 138–147.
13. Fedailaine, M., & Moussi, K. (2015). Modeling of the anaerobic digestion of organic waste for biogas production. *Procedia Computer Science, 52*, 730–737. https://doi.org/10.1016/j.procs.2015.05.086.
14. Ruzhinskaya, L.I., & Fomenkova, A.A. (2014). Mathematical modeling of the process of anaerobic digestion of organic substrate. Review. *Scientific Journal "ScienceRise"*, *2*, 63–69.
15. Vorobiev, V., Dychko, A., & Opolinskiy, I. (2016). Improving the efficiency of biotransformation of hazardous pollutants in wastewater biogas. *Proceedings of the National Technical University of Ukraine "Kyiv Polytechnic Institute". Series "Mining"*, *30*, 153–159.

DIVPOSMU METĀNA FERMENTĀCIJAS MODELĒŠANA AR BIOMASAS PIRMAPSTRĀDI

A. Dičko, N. Remezs, I. Opoļinskis,
S. Kraičuks, N. Ostapčuks, L. Jevtijeva

K o p s a v i l k u m s

Organisko atkritumu pārstrādei nepieciešams izmantot anaerobās fermentācijas sistēmas. Organisko atkritumu anaerobās pārstrādes procesa vadīšanā jāveic precīza biogāzes ražošanas prognozēšana. Organisko atkritumu fermentācijas procesa matemātiskā modeļa izstrāde ļauj noteikt biogāzes izvades ātrumu anaerobās fermentācijas divposmu procesā, ņemot vērā pirmo posmu. Pētījumā pārbaudīts Konto modelis, izmantojot organisko atkritumu anaerobo apstrādi. Biogāzes izvades un ātruma atkarība no laika ir noteikta un to var izmantot, lai prognozētu organisko atkritumu anaerobās apstrādes procesu.

08.11.2017.

LATVIAN JOURNAL OF PHYSICS AND TECHNICAL SCIENCES
2018, N 2

DOI: 10.2478/lpts-2018-0012

APPLICATION OF COAL THERMAL TREATMENT TECHNOLOGY FOR OIL-FREE FIRING OF BOILERS

B. Aliyarov, A. Mergalimova, U. Zhalmagambetova
Almaty University of Power Engineering and Telecommunications
126 Baitursynov Str., Almati, 050013, KAZAKHSTAN
e-mail:kazresearch@mail.ru

The theoretical and practical introduction of this kind of firing boiler units in coal thermal power plants is considered in the article. The results of an experimental study of three types of coals are presented in order to obtain the required gaseous fuel.

The aim of the study is to develop a new, economically and ecologically more acceptable method for firing boilers at thermal power plants, which is able to exclude the use of expensive and inconvenient fuel oil.

The tasks of the experiment are to develop a technological scheme of kindling of boilers at thermal power plants, using as a type of ignition fuel volatile combustible substances released during the heating of coal, and to investigate three types of coal for the suitability of obtaining gaseous fuels, in sufficient volume and with the required heat of combustion.

The research methods include the analysis of technical and scientific-methodological literature on the problem of the present study, the study of the experience of scientists of other countries, the full-scale experiment on the production of volatile combustible substances.

During the full-scale experiment, the coal of 3 fields of Kazakhstan has been studied: Shubarkul, Maikuben and Saryadyr. The analysis has been performed and the choice of the most convenient technology for boiler kindling and maintenance of steady burning of the torch has been made according to the proposed method, as well as the corresponding technological scheme has been developed.

As a result of the experiment, it can be stated that from coal in the process of its heating (without access to oxygen), it is possible to obtain a sufficient amount of combustible volatile substances. The released gaseous fuel has the necessary parameters and is quite capable of replacing an expensive fuel oil. The resulting gaseous fuel is quite convenient to use and environmentally cleaner. The piloting scheme developed as a result of the experiment can be introduced in pulverized-coal thermal power plants, as a result of which they become single-fuel.

Keywords: *boiler, coal, fuel oil, gas, ignition fuel, thermal power plants, volatile combustibles*

1. INTRODUCTION

The coal industry is one of the leading branches of the fuel and energy complex in many countries. Coal is used as a technological raw material (in the form of coke) in ferrous metallurgy and chemical industry (coke oven gas) for the production of mineral fertilizers and plastics, and coal is the energy source for electricity production at TPPs and for heating of dwellings. As a result of using coal, approximately 44 % of the world's electricity is produced. In Kazakhstan, this figure is approximately 72 % [1], [2].

As it is known, coal is much inferior to natural gas and oil for its own needs and especially for environmental performance. However, according to the estimates of the International Energy Agency [3], at the current consumption rates, the explored oil reserves will be depleted in 30 years, and gas – in the next 50 years (however, Kazakhstan has a more favourable prospect [4]), while coal reserves, with the most intensive use, will be sufficient for 200 years [5]. No one doubts today the need for the development of coal technologies. The remaining fuel resources will be enough for a much shorter period, and at the same time their cost is much higher.

According to the World Coal Institute [6], coal accounts for about 90 % of the energy potential of all organic minerals suitable for the development of minerals. Prospects for the development of the world energy industry significantly depend on its resource availability. In this respect, the coal industry is in a much better position than the oil and gas industry, and therefore, in the long term, it is a more promising sector of the fuel and energy sector. For today's Kazakhstan, coal is the main fuel resource. The coal industry of Kazakhstan is one of the largest branches of the country's economy [7]. In terms of coal reserves, Kazakhstan is second only to China, the United States, Russia, Australia, South Africa and Ukraine. The state balance of Kazakhstan takes into account the reserves of 49 deposits amounting to 33.6 billion tons, including 21.5 billion tons of coal, and 12.1 billion tons of brown coal [8]. Most of the coal deposits are concentrated in the Central (Karaganda and Ekibastuz coal basins, as well as the Shubarkol field) and Northern Kazakhstan (Turgai coal basin), in southern Kazakhstan – Lenger and Nizh-Ili coals [5].

Among the CIS countries, Kazakhstan ranks second in terms of reserves and pre-bogs of coal, and takes the first place in terms of coal production per caput. The greatest volume of coal production in the republic falls on the Central (Karaganda) and North-Eastern (Pavlodar) regions – 96.2 %. Kazakhstan's coal exports in 2003 amounted to 25.7 million tons with a total production volume of over 89 million tons [2]. At present, Kazakhstan is among the ten largest coal producers on the world market, as well as the top ten largest exporters. The republic gives about 3 % of the world's coal exports. It should be noted that the need for coal will grow every year not only in Kazakhstan but also in the world as a whole. According to some data, in some developing countries the demand for coal will increase by 6 % per year. The growth in the consumption of coal is caused by the need for numerous thermal power plants, which generate more and more electrical and thermal energy. Consequently, coal mining and development of new coal deposits will intensively increase.

2. THEORETICAL FRAMEWORK

During the course of the research, the analysis of available sources (scientific literature and Internet resources) has been performed. The analysis has shown that the problem of replacing ignition fuel for another way is being investigated in many countries, including studies performed by scientists of the Republic of Kazakhstan, in particular on the use of plasma technologies for kindling of boiler units.

2.1. Literature Review

At the moment, all thermal power plants (TPPs) and large boiler plants that use natural gas and / or coal as the main fuel provide emergency and ignition fuel. As a rule, this fuel is fuel oil. Fuel oil, as fuel, has a number of unquestionable qualities: a high calorific value of 9500 kcal / kg, a low ash content of 0.3–0.5 %, the possibility of obtaining a glowing flame (providing high radiation heat exchange in the furnace space), the possibility of organising certain conditions of burning in small (in size) furnaces. However, fuel oil, as fuel, has a number of serious shortcomings. Co-combustion of coal with fuel oil worsens the ecological and economic parameters of the boilers: the mechanical underfunding of fuel increases and the gross efficiency reduces (due to the increase in costs for own needs), the specific fuel consumption for the released electric energy increases, the high-temperature corrosion of the convective heating surfaces increases, the output of nitrogen oxides and sulfur (in the case of a higher sulfur content in fuel oil), there are emissions of carcinogenic vanadium pentoxide [7], [13]. The most significant drawback of fuel oil as a backup and pilot fuel is the inconvenience associated with its operation, caused by the multistage in the preparation of fuel oil for use [6]. Loading into tanks and subsequent unloading from tanks require its heating up to a state with acceptable fluidity, which, as a rule, is achieved through the use of water vapour. This means that at the points of loading and unloading of fuel oil it is necessary to have a source of steam with the required temperature. In addition to heating and mixing in tanks, it is also necessary to maintain the circulation of fuel oil throughout the entire path of its movement, from the storage to the injector, to provide, if necessary, the possibility of supplying fuel oil to the furnace. Therefore, the preparation of fuel oil for combustion is a complex and time-consuming process, in which it is necessary to ensure: a low (up to 3 %) water content in fuel oil, deep mixing of water with fuel oil, and necessary heating temperatures for fuel oil. Another important aspect is price; fuel oil is an expensive energy fuel.

All of the above-mentioned factors make the very urgent task of modern heat power engineering – the development of new technologies of oil-free firing of boilers at coal-fired TPPs.

One way of oil-free ignition of a coal torch at a TPP is to use plasma technologies. In [7]–[10], various technologies of fuel oil replacement at coal plants are considered, including methods of using plasma pilot burners for ignition of low-grade fuels and anthracite. Plasma torches consist of a longitudinal chamber through which a dust-air mixture is fed into the boiler. Along the chamber, there are two rod

electrodes, between which a powerful electric arc is excited by means of a movable plasmatron-igniter, which heats the incoming fuel-air mixture. The temperature of the gas jet at the exit from the plasma torch is 3500–5400 °C. At this temperature, the thermal decomposition of coal and the inflammation of volatile substances take place rapidly, and, accordingly, the coke base ignites. When such a "prepared" mixture is supplied to the combustion chamber, a steady burning of the flame is ensured. However, the high temperature causes rapid wear of the rod electrodes, and frequent replacement is required. For the operation of a plasma torch, a water and air supply system is required, and a rather complex system of converting electrical energy into thermal energy is required. This complicates the design of the device and significantly increases the cost of installation.

Research [9] describes the development by the employees of the Institute of Combustion Problems (Almaty) and the Industry Centre for Plasma Energy Technologies of RAE UES of Russia. The research focuses on a new plasma-fuel system (PFS) for oil-free firing of boilers and for stabilising the combustion of a coal flare while reducing the amount of mechanical fuel burn-up and reducing the level of oxide formation nitrogen.

PFS technology is based on plasma thermo-chemical preparation of coal for combustion. It consists in heating the air mixture (coal dust and air) by electric arc plasma (at a temperature above 3000 °C). Due to gasification of fuel, a two-component mixture of combustible gases and coke is formed, which is easily ignited when it mixes with secondary air and stably burns without additional illumination with fuel oil. It is based on the technology of electrothermal-chemical fuel preparation (ETCPF). The essence of ETCPF (for low-reactive coal) consists in heating the air mixture to the temperature at which the most complete liberation of volatile $V^{г}$% from coal dust is achieved and partial gasification of the coke residue is carried out in order to obtain a combustible mixture at the level of volatile, highly reactive coal. To reduce the energy consumption for processing, the flow of the air mixture entering the burner is divided into two unequal parts, with the heating of the smaller of them (15 %–20 %), to the temperature of the complete release of volatile fuels (in the arc-plasma zone) and partial gasification of the coke residue. As a result, a high potential ignition agent is formed that can initiate ignition and stabilise the combustion of a pulverized torch.

However, the way in which plasma technologies are used to kindle boiler units has a number of significant drawbacks that limit its use: high cost, limited plasmatron operating life, and energy costs.

It is suggested in [13] that natural gas (compressed or liquefied) is to be used to kindle boilers. Gas, as a fuel, has a number of advantages over fuel oil: an essentially simple technology of preparation for combustion and supply to the furnace (with sufficient heat of combustion), which significantly reduces the cost of own needs. But natural gas has relatively limited reserves compared to coal, and is not available in all regions of the country. The shortage of natural gas causes the development of solid fuel processing technologies to produce gaseous fuel, a natural gas substitute.

3. RESEARCH DESCRIPTION

The Utility Model patent [14] shows the efficient, ecologically and economically more acceptable method of oil-free firing of the boiler units developed by the authors of the present research and the stabilisation of the flame burning. This technology is based on the use of gaseous fuels obtained from the thermal processing of coal. Figure 1 shows a possible technological scheme of oil-free ignition of the boiler, using combustible volatile substances as a fuel.

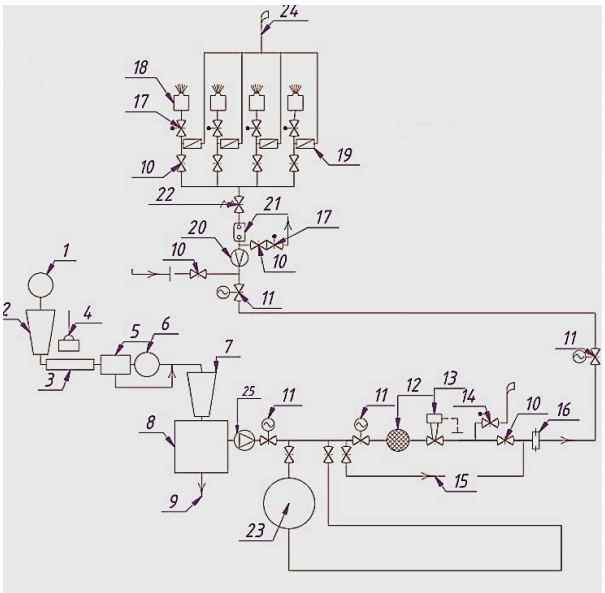

Fig. 1. Diagram of the technology of boiler firing with the use of combustible volatile substances. 1 – a car dumper, 2 – a receiving hopper, 3 – a belt conveyor, 4 – an electromagnetic separator, 5 – a vibrating screen, 6 – a hammer crusher, 7 – a raw coal bunker, 8 – a furnace for coal heating, 9 – an output of enriched coal mass, 10 – a gas stop valve, 11 – a gate valve with electric drive, 12 – a mechanical filter, 13 – a gas pressure regulator, 14 – a safety valve, 15 – a bypass line, 16, 20 – a flow meter, 17 – a gas regulating valve, 18 – a gas burner, 19 – a cork valve, 21 – a high-speed gas valve, 22 – an asbestos damper regulator, 23 – a gas storage-receiver, 24 – safety candles, 25 – a fan.

The release of combustible volatiles is carried out in a special device (8), in which, without access to oxygen, the coal layer is heated. As a carrier of the initial thermal energy necessary for heating coal, steam can be used, in the presence of a working boiler; electricity or other medium of thermal energy. The combustible volatile substances released after heating (CO, H_2, CH_4 and others) in the case of kindling are directly fed to the boiler burners (18), after ignition they can accumulate in a special gas storage tank (23), at a certain pressure and in the future used to stabilise the combustion of the torch.

This process of obtaining volatile fuels from coal is not a process of coal gasification. Gasification technologies [15]–[18] are more complex and expensive. However, the process in question differs from the processes of high-temperature pyrolysis [14] and gasification in that the heating is carried out only up to the

temperatures required for the release of combustible volatile substances in the required volume and with sufficient heat of combustion, which depends on the charcoal characteristics.

In order to produce gaseous fuels capable of replacing fuel oil at pulverized coal plants, we have experimentally investigated three types of solid fuels, whose deposits are located in Kazakhstan: brown coal Maikubenskoe, brown coal Shubarkulskoye and brown coal Saryadyrskoye. The composition of the samples of the coal [1], [11] (on the working mass) and the value of analytical moisture are presented in Table 1.

Table 1

Composition and Analytical Moisture of Coal Samples

Element	Element content in mass %		
	Black coal Shubarkulskoe	Brown coal Maikubenskoe	Brown coal Saryardyrskoe
C	76.9	73.52	40.71
H	5.35	5.0	2.66
N	1.48	1.0	0.39
O	15.3	6.3	6.56
S	0.5	0.67	0.27
A	9.27	13.51	46.47
Analytical moisture content, %	14.25	7.11	2.94

Experimental studies of the process of obtaining combustible gaseous substances from coal have been carried out on a hardware complex, the structural diagram of which is shown in Fig. 2.

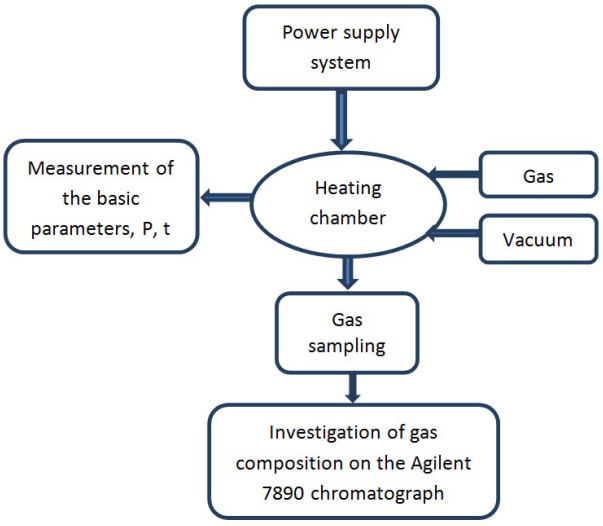

Fig. 2. Structural diagram of installation.

A pre-treated coal sample (a particle of about 5 mm in size) has been placed on a substrate in an experimental chamber (Fig. 3). Then a smooth increase in voltage has been carried out. As a result of voltage increase and temperature increase, the process of thermal destruction of the sample begins, thereby initiating the sublimation of volatile compounds, after which heating is continued while maintaining a constant voltage level, by adjusting the current.

Fig. 3. Experimental installation chamber.

The experiments have been carried out in a nitrogen atmosphere at a given pressure not exceeding the permissible maximum chamber pressure.

In the course of the experiment, the temperature dynamics at certain points of the sample are measured to construct patterns of the dynamics of the thermal field. During and after the completion of the experiment, gas samples from the chamber are sampled and analysed. Sampling of gas is made directly from the chamber and through polymer pneumatic hose is fed to the filter regulator LFR-1/4-D-5M-MINI. This device allows taking a gas sample without affecting the pressure in the chamber, and also removes the aerosol phase and dust particles from the gas. After the filter regulator, the gas flows to the Agilent 7890 chromatograph, which analyses the resulting gas.

The duration of the experiment has been limited to reaching a set maximum temperature of 600 °C.

Tables 2 and 3 demonstrate the results of experimental studies to determine the quantitative composition of the gas obtained from the coal samples of the various deposits presented above.

Figure 4 shows the dependence of the yields of the main combustible gas components (CO, H_2, CH_4) on the temperature in the range of 300–600 °C, and Table 2 demonstrates their total yields.

Table 2

The Total Yield of Combustible Gas Components (CO, H_2, CH_4) in the Temperature Range of 300 °C–600 °C

The deposit of coal samples	Total yield **CO, H_2**, CH_4 (%) depending on the heating temperature , **°C**			
	300	400	500	600
Shubarkul	1.2	4.56	12.32	18.71
Maikuben	0.9	3.22	8.41	10.85
Saryadyr	0.5	2.13	5.2	6.70

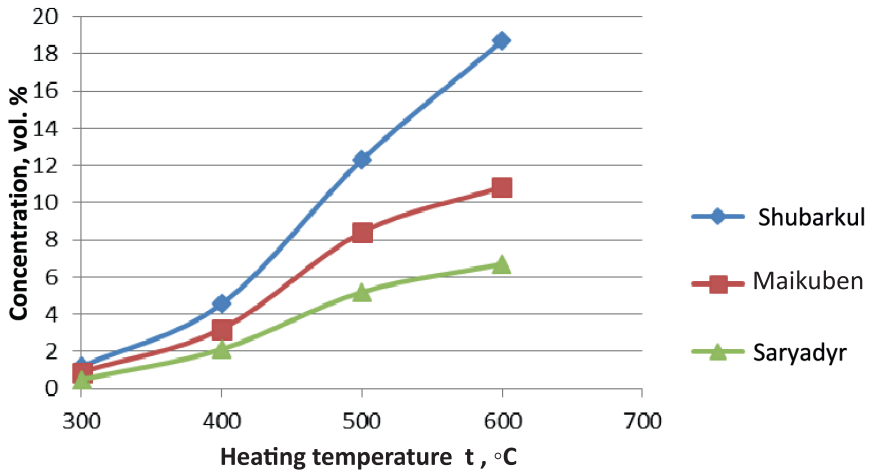

Fig. 4. Dependence of the output of combustible gas components (CO, H2, CH4) on the heating temperature.

Based on the results of the experiments performed, it is evident that with increasing temperature of heating of coal samples in the range of 300 °C–600 °C, volumetric concentrations of combustible gas components increase. The composition of the gas also changes significantly with an increase in temperature. Table 3 shows the composition of the gas obtained from the Shubarkul stone long-flame coal.

Table 3

Composition of Gases from the Shubarkul Long-flame Coal

Heating temperature t, °C	CO_2+H_2S	CO	C_mH_n	CH_4 and homology	C_2H_6	H_2	N_2
300	18.2	9.0	11.3	21.2	30.1	6.3	3.9
400	14.4	8.4	9.6	31.6	21.2	10.4	4.4
500	6.2	6.2	4.6	40.3	14.4	24.8	5.7
600	5.0	5.2	2.2	41.4	6.8	34.3	6.2

Based on the results of determining the quantitative composition of the gas presented in Table 3, it can be concluded that with an increase in the heating temperature, the yield of carbon dioxide CO_2 decreases, which favourably affects the heat of combustion of the gas, and the yield of CH_4 increases. An increase in the yield of resinous substances is also observed, especially in the coal of the Shubarkul field, which is long-flame.

The results of calculating the heat of combustion, the produced gas from the presented samples of coal at different heating temperatures have shown that with increasing temperature of heating, the heat of combustion of combustible gases obtained from coal samples also increases. In all considered coal samples, the maximum value of the heat of combustion can be traced at a heating temperature of 600 °C. The greatest value is observed in the coal of the Shubarkul field – 29.1 MJ / m3, and the minimum value for brown coal of the Saryadyr field is 13.5 MJ / m3.

Based on the results of experimental studies, it is possible to conclude that from the three samples of coal presented for the production of combustible gas, the coal of the Shubarkul and the coal of the Maikuben deposits are most suitable. For use in the boiler as a pilot fuel, it is sufficient to heat the coal to temperatures of 350–450 °C. The resulting flammable gas, at relatively low heating temperatures, is released in the required volume and has a sufficient heat of combustion to be used in the process of firing boiler units, thereby replacing the expensive and difficult fuel oil.

4. CONCLUSION

The analysis of the results of this stage of the study has shown that the issue of replacing ignition fuel at pulverized coal plants is relevant. Based on the results of experimental studies, the authors of the present research can conclude that it is possible to obtain gaseous fuel from coal, with the necessary parameters for combustion in boilers.

The next stage of the research is the analysis of the influence of the fuel replacement technology on the emissions of sulfur, nitrogen, and vanadium dioxide oxides released during the combustion of fuel oil. On the basis of this technology for the production of volatile combustible substances, the further research will also be devoted to the investigation of the possibility of using them in small boilers designed to supply thermal energy to small settlements. In this case, it is possible to supply this settlement with three types of energy: electric, heat and gas fuel for domestic needs.

As a result of the research, it can be stated that the proposed method of oil-free firing of boiler units with combustible volatile substances allows excluding the use of fuel oil or natural gas to kindle the boiler and maintain a stable ignition of the pulverized flame, while operating the boiler with reduced loads. This gives a significant reduction in financial costs associated with the high cost of fuel oil. Energy costs for the plant's own needs are also reduced, due to the multi-stage preparation of fuel oil for incineration. The efficiency of boiler units is improved.

REFERENCES

1. Dukenbayev, K.D. (1995). *Energetics of Kazakhstan* (vol. 1). Almaty: Gylym.
2. Aliyarov, B.K., & Aliyarova, M.B. (2010). *Kazakhstan: Energetic security, energetic efficiency and energy development stability*. Almaty: Gylym.
3. International Energy Agency (1994). *World Energy Outlook*. Available at http://www.worldenergyoutlook.org/media/weowebsite/2008-1994/weo1994.pdf
4. Nadirov, N.K. (1995). *Oil and gas of Kazakhstan*. Almaty: Gylym.
5. Chokin, Sh.Ch., Sartayev, T.S., & Shkret, A.F. (1985). *Energetics and electrification of Kazakhstan* (vol. 1). Almaty: Nauka.
6. Aliyarov, A.B., Aliyarov, B.K., & Aliayrova, M.B. (2016). *Supply of thermal energy in Kazakhstan (features, experience, problems)*. Almaty: LEM.
7. Karpenko, E.I., Messerle, V.E., & Konokhov, N.M. (2010). Plasma-Energy technologies of coal use for effective replacement of fuel oil and natural gas in the fuel balance of TPPs. *Thermal Energy*, *10*, 53–60.
8. Messerle, A. V., Messerle, E., & Ustimenko, A. B. (2017). Plasma thermochemical preparation for combustion of pulverized coal. *High Temperature*, *55*(3), 352–360.
9. Messerle, V., Ustimenko, A., & Lavrichshev, O. (2016). Arc plasma thermochemical preparation of coal to effective combustion in thermal power plants. *International Journal of Energy and Power Engineering, 3*(11).
10. Dubrovsky, V.A., & Zubova, M.V. (2012). *Energy-saving systems of kindling and lighting of a torch of combustion chamber of boilers*. Krasnoyarsk: Siberian Federal University.
11. Verbovetsky, E.H., & Kotler, V.R. (1984). Replacement of fuel oil with coal at the kindling and illumination of a torch in pulverized-coal boilers. *Energo-Economy Abroad*, *1*, 16–17.
12. Yermagambet, B.T., & Kasenov, B.K. (2013). *Clean coal technologies: Theory and practice.* Karaganda: TENGRI Ltd.
13. Aliyarov, B.K., & Mergalimova, A.K. (2017). On the advantages of using gas to kindle boiler units. *Proceedings of the 1st International Scientific and Practical Conference "Modern Trends in Boiler Building"*, Barnaul.
14. Aliyarov, B.K., & Mergalimova, A.K. (2017). *The method of oil-free firing of boiler units*. Patent for Utility Model No. 2450. State Register of Utility Models of the Republic of Kazakhstan.
15. Zhang, D. Thermal Decomposition of Coal. *Coal, Oil Shale, Natural Bitumen, Heavy Oil and Peat*, *1*. Encyclopaedia of Life. Available at http://www.eolss.net/sample-chapters/c08/E3-04-03-02.pdf
16. Messerlea, V.E., & Ustimenko, A.B. (2016). Plasma gasification of coal with the extraction of valuable components of the mineral mass. *Engineering & Technologies*, *9*(8), 1311–1313.
17. Zhao, Y., & Wang, S. (2017). Analysis of thermoelectric generation characteristics of flue gas waste heat from natural gas boiler. *Energy Conversion and Management, 148*, 820–829
18. Reid, D., Cabe, J.E., & Bearden, M.D. (2010). *PNNL coal gasification research*. Richland, WA: Pacific Northwest National Laboratory.

AKMEŅOGĻU TERMISKĀS APSTRĀDES TEHNOLOĢIJAS PIELIETOŠANA APKURES KATLOS BEZ ŠĶIDRĀ KURINĀMĀ IZMANTOŠANAS

B. Alijarovs, A. Mergalimova,
U. Žalmagambetova

K o p s a v i l k u m s

Šajā rakstā aplūkota teorētiska un praktiska apkures katlu agregātu ieviešana akmeņogļu termoelektrostacijās. Eksperimentālā pētījuma rezultāti par trīs veidu oglēm ir paredzēti, lai iegūtu vajadzīgo gāzveida kurināmo.

Pētījuma mērķis ir izstrādāt jaunu, ekonomiski un ekoloģiski pieņemamāku metodi apkures katlu izmantošanai termoelektrostacijās, lai nebūtu jāizmanto dārgās un neērtās degvieleļļas.

Eksperimenta uzdevums ir izstrādāt katlu sildīšanas tehnoloģisko shēmu termoelektrostacijās, izmantojot ogļu sildīšanas laikā izdalītās degošās vielas. Izpētītas trīs veidu ogles, lai iegūtu pietiekamu daudzumu gāzveida kurināmā, un ar vajadzīgo sadegšanas siltumu.

Pētījuma metodes iekļauj tehniskās un zinātniski-metodiskās literatūras analīzi par pētījuma problēmu, citu valstu zinātnieku darba pieredzes analīzi; gaistošu degošu vielu pilna apjoma ražošanas eksperimentu.

Eksperimenta laikā tika pētītas Kazahstānas ogles trīs dažādās ieguves vietās: Šubarkuļā, Maikubenā un Sariadirā. Tika veikta analīze un izvēlēta visērtākā tehnoloģija katlu uzkarsēšanai un degļa vienmērīgas degšanas uzturēšanai saskaņā ar izstrādāto metodi, kā arī piedāvāta atbilstoša tehnoloģiskā shēma.

Eksperimenta rezultātā var secināt, ka no oglēm to sildīšanas procesā (bez pieejas skābeklim) ir iespējams iegūt pietiekamu daudzumu degošu gaistošu vielu. Atbrīvotajai gāzveida degvielai piemīt nepieciešamie parametri, un tā var aizstāt dārgo mazutu. Iegūtā gāzveida degviela ir ļoti ērta lietošanā un videi draudzīgāka. Eksperimenta rezultātā izstrādāto pilotprojektu var ieviest pulverizētās ogles termoelektrostacijās, kā rezultātā tās izmanto vienu degvielas veidu.

06.03.2018

LATVIAN JOURNAL OF PHYSICS AND TECHNICAL SCIENCES
2018, N 2

DOI: 10.2478/lpts-2018-0013

APPLIED PHYSICS

ADDITIVE MANUFACTURING AND CASTING TECHNOLOGY COMPARISON: MECHANICAL PROPERTIES, PRODUCTIVITY AND COST BENCHMARK

A. Vevers, A. Kromanis, E. Gerins, J. Ozolins
Institute of Mechanical Engineering
Riga Technical University
36a Viskalu Str., Riga, LV-1006, LATVIA
e-mail: artursvevers@gmail.com

The casting technology is one of the oldest production technologies in the world but in the recent years metal additive manufacturing also known as metal 3D printing has been evolving with huge steps. Both technologies have capabilities to produce parts with internal holes and at first glance surface roughness is similar for both technologies, which means that for precise dimensions parts have to be machined in places where precise fit is necessary. Benchmark tests have been made to find out if parts which are produced with metal additive manufacturing can be used to replace parts which are produced with casting technology. Most of the comparative tests have been made with GJS-400-15 grade which is one of the most popular cast iron grades. To compare mechanical properties samples have been produced using additive manufacturing and tested for tensile strength, hardness, surface roughness and microstructure and then the results have been compared with the samples produced with casting technology. In addition, both technologies have been compared in terms of the production time and production costs to see if additive manufacturing is competitive with the casting technology. The original paper has been written in the Latvian language as part of the Master Thesis within the framework of the production technology study programme at Riga Technical University.

Keywords: *additive manufacturing, casting, 3D printing, hardness, surface roughness, tensile strength*

1. INTRODUCTION

In recent years a new technology has been evolving very fast, which is called metal Additive Manufacturing or metal 3D printing. The principle of additive manufacturing (AM) operation is that you use 3D object (CAD part) which is sliced into 2D sections and part is produced layer by layer from bottom to top. For metal additive manufacturing there are many technology types and names for each method. Most common ones are Selective Laser Melting (SLM) and Direct Metal Laser Sintering (DMLS). Metal additive manufacturing machine in the SLM method applies a thin

layer of metal powder (usually 20-50 μm) on a build platform then based on sliced 2D data generates a laser scan pattern and with CNC controlled laser melts powder only in places where the part is located. Then the next powder layer is applied and melted together with the previous layer. The process is repeated layer by layer till the part is finished. DMLS method works based on the same 3D object slicing principle but it uses a different powder supply principle. In the DMLS method powder is injected straight in a laser beam. This method works faster because it saves time for powder recoating process but parts that are produced using this method have a worse surface quality. Additive manufacturing opens new possibilities for complex part production and can change the way the parts are designed and produced in the future [1].

Casting technology is one of the oldest production technologies in the world. Due to its simplicity, the basic principles of technology have not changed for many years. Casting technology and Additive Manufacturing are completely different technologies by the principles how they work, but it is possible to find many similarities in the parts that can be produced with technologies: complex internal channels, surface roughness, and dimensional accuracy for both technologies are in very close tolerances [2].

The main disadvantage of the casting technology is start-up costs for a new project because it is time consuming and expensive to produce a new pattern. It takes many hours to redesign a 3D model with all necessary draft angles according to the split line so it can be used for pattern design which means that in reality your part will not be the same as planned in the beginning. On the other hand, additive manufacturing does not have these design limitations which means that you can start to produce parts straight from a 3D file and gain time on redesign and pattern manufacturing.

Since additive manufacturing is a new technology, which develops very rapidly, a decision has been made to compare this technology with the casting technology and the objective of the research is to determine whether it is possible to produce parts using metal additive manufacturing to replace the cast parts.

2. MATERIALS AND METHODS

To benchmark additive manufacturing to casting technology a decision has been made to compare tensile strength, hardness, surface roughness, microstructure and chemical composition tests for samples produced using both technologies. In addition, technologies have been compared to each other to determine production time and approximate costs. All the tests have been made with iron powder, which corresponds to GJS-400-15 material grade for castings. It is not common to use iron for additive manufacturing but as one of the authors' works in the iron casting foundry, it gives access to the data about this metal grade as well as equipment to accurately compare the samples. GJS-400-12 metal grade has been used because this ductile iron grade is one of the most widely used grades for cast iron parts. Samples have been produced on 3D systems ProX DMP 300 machine. Machine is equipped with single 500 w laser and the build platform for this machine is 250x250x325 mm. Casting samples have been produced of GJS-400-15 grade in the foundry which uses a green sand technology for moulding [2].

2.1. CHEMICAL COMPOSITION AND MICROSTRUCTURE

The first test has been done to compare chemical composition. Both samples have been compared using Thermo Fischer 3480 OES thermal analyser. AM iron powder by manufacturer's specification corresponds to GJS-400-15 metal grade and the results have also approved it. Chemical composition is very close to parts, which are cast with only some minor deviations. Since cast iron grades do not have specified element values (only suggested), it means that this powder can be used in parts to replace castings.

In addition, the samples have been compared for microstructure. The samples have been polished and surfaces prepared with etching. Microstructure of AM sample and that of cast sample are very similar. Both samples have shown the same ductile iron microstructure with spherical graphite nodules.

2.2. TENSILE STRENGTH TESTS

To compare mechanical properties for both technologies, test specimens have been made using both technologies. For AM, test specimens have been produced using the SLM technology with 30 μm layer thickness. Samples using AM have been made of iron powder, which corresponds to GJS-400-15 iron grade. Samples have been made with machining allowances and machined according to ISO6892-1:2009 tensile strength standard for casting samples. Testing has been done on Hegewald & Pesche Inspekt 250 tensile strength testing machine [3].

For GJS-400-15 grade standard, a tensile strength minimal value should be 400 MPa and elongation should be at least 15 %. Average values of AM sample tests are 440 MPa and elongation -16.78 %. Testing has shown very stable results: a tensile strength value has changed +- 20 MPa and elongation changed +- 1 %. It is possible to see that breaking surface for both technologies looks almost the same (Fig. 1). Tensile strength results have shown that AM can produce the same quality parts as the casting technology and can maintain necessary values for specific material grade standard. During research it has been found that there are some other experiments which have been done with other materials with also very successful results. With other materials, additive manufacturing shows even better tensile strength results compared to casting technology [4].

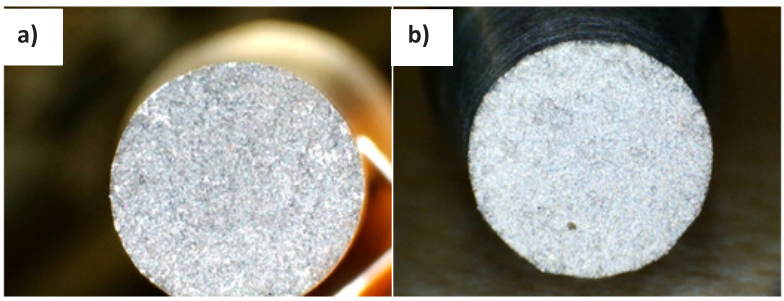

Fig. 1. Comparing breaking surface of tensile strength tests: a) AM sample, b) casting sample.

2.3. HARDNESS

Test for hardness has been made according to EN ISO 6506-1:2005 standard. It has shown average values between 160-175 HB. By standard for GJS-400-15, it should be in the range of 135-180 HB. The results have shown that AM part results are in the range and closer to upper values. In hardness tests it has been observed that using AM it is possible to get very close hardness values for whole part even if the wall thicknesses are different. For the casting technology it is impossible because it will show higher values for thinner sections and lower for thicker because cooling time is different. For additive manufacturing, layer thickness is relatively small compared to part size and cools down very fast and it is almost the same for all layers. Additive manufacturing in the SLM method allows for easy control and maintaining of cooling time by increasing powder recoating time between the layers, for example, when producing part with big wall thickness it is possible to increase wait time and let the part cool down more between layers [5].

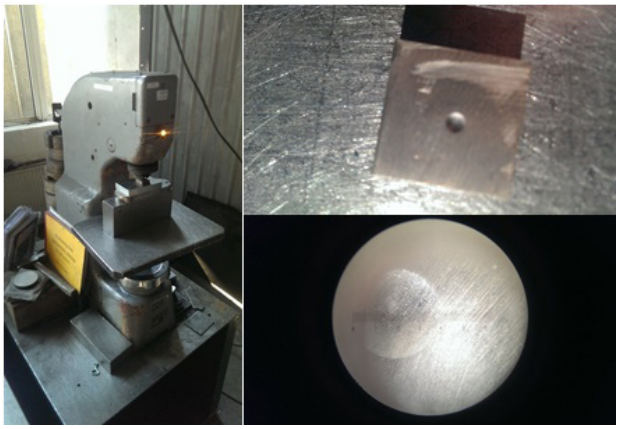

Fig. 2. Hardness measuring.

2.4. SURFACE ROUGHNESS

To compare surface roughness Taylor Hobson profiler has been used. AM samples and cast samples have been compared to determine if AM surface quality is equivalent to parts, which are cast in greensand. By evaluating the measured values it is possible to see that AM surface quality is better. Maximal surface waviness for AM parts is 60 µm but for cast parts it is 80 µm. Average surface roughness calculated by ISO standard is Ra 11 µm for AM parts and Ra 13.5 µm for cast parts.

Fig.3. Surface roughness measuring process.

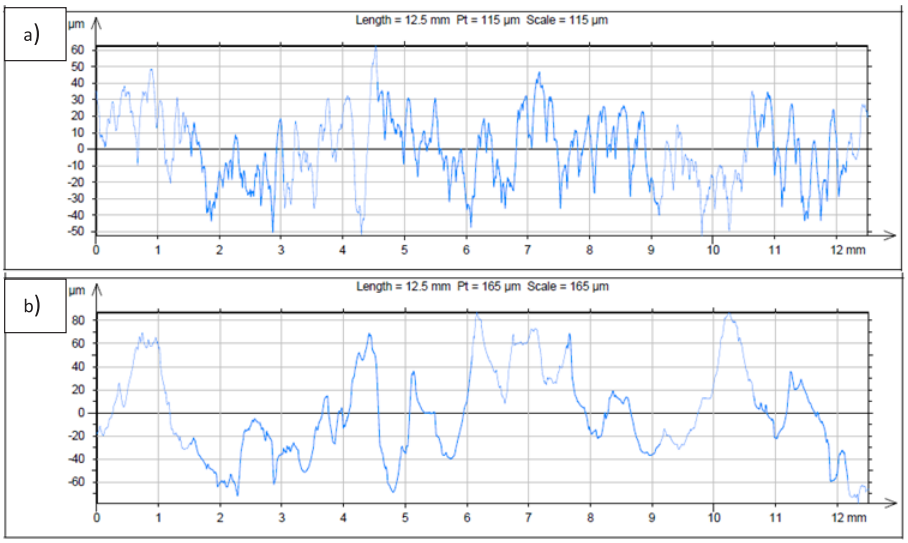

Fig. 4. Surface roughness graphics: a) graphic shows AM sample, b) graphic for casting.

2.5 PRODUCTION TIME

To compare production time it is not possible to make a small sample and then compare with the casting technology by volume or weight. Decision is to compare both technologies on one part, which is typical geometry for the casting industry. It weights around 1 kg and to make such kind of part it would be necessary to use 2 cores to make this part using the casting technology. Production time and costs have been compared for 1 and for 10 parts by values obtained by choosing each technology and buying the outsourcing service.

Part, which has been used for comparison purposes, is of average complexity for the casting technology. To cast such kind of part, it would be necessary to use 2 cores, which means two additional core boxes for pattern equipment. Production time has been calculated from time when company receives 3D CAD geometry from a customer. For casting technology it would be necessary to have around 3 days to redesign a 3D model with all necessary draft angles and prepare 3D pattern geometries. Then it would be necessary to have around 2 weeks from 3D geometries to a ready pattern - this includes CNC machining for negatives, CNC machining for core boxes and copying epoxy models and making the gating system. When pattern equipment is finished it would take additional time for core production and forming. For the casting technology an additional benefit is that usually in one mould there is more than 1 part and in one casting process it is possible to produce 10 parts. Next step would be the moulding and casting process, which takes around half an hour. When the casting process is finished the mould should cool down around 4 hours. In the end, when the mould is cooled down, parts can be taken out for post processing - grinding, shot blasting etc.

All these steps are not needed in the AM process. It would be necessary to have around 2 - 4 hours to prepare a program in slicer to start producing the part.

For AM most time is spent on the printing process. With 30 μm layer thickness, for this part one layer printing time is around 0.5 - 1 min. The total printing time for this part would be 72 hours. After printing usually parts have to go through the heat treatment process for stress relief. It takes additional 2 hours. The last step for AM is post-processing where parts are cut of the build plate, separated of support structures and polished.

In Table 1, it is possible to see typical values or both production technologies for 1 and for 10 parts side by side. There are steps which are only for AM or the casting technology and there are steps which are common to both technologies. It is clearly visible that AM has advantages during the first steps. If it is necessary to produce only 1 - 4 parts it will be more convenient to use the AM technology, but for series production for this part the casting technology is more suitable. At the moment, AM is suitable for products which are not possible to produce with other technologies or in the cases where time is a limiting factor, for example, production companies, that have equipment, which has broken down, cannot afford to stop production but spare part delivery takes too much time.

Table 1

Production Time Comparison for Both Technologies for 1 and 10 Parts

	1 part		10 parts	
Task	Production time for AM (h)	Production time for casting (h)	Production time for AM (h)	Production time for casting (h)
CAD modelling	0	24	0	24
Pattern equipment production	0	310	0	315
Core production	0	1	0	1
Setup forming	0	0.5	0	0.5
Preparing program for AM	2	0	2	0
Casting, Cooling time	0	8	0	8
AM process	72		960	
Post-processing	4	2	22	20
Total	82	351	982	346

3. COSTS

To compare costs, the same comparison principle has been used as for production time. The same part has been used, and costs have been compared for 1 and 10 parts. 3D geometry has been sent to a few casting companies and a few companies that provide the AM service. Average price received from casting companies is 4000 EUR for pattern equipment and 14.50 EUR - for each part. For the casting technology, there are high start-up costs because it is necessary to cover pattern equipment costs. For one and also for ten parts, the price is very high because the casting technology is suitable for series production. In case if it is necessary to produce 5000 parts then the pattern cost is divided and one part costs only 15.30 EUR.

On the other hand, the AM technology does not have start-up costs, but printing time is very slow. Price for 1 part, which is produced with additive manufacturing, is 3650 EUR and the price is almost the same for producing 1 part or 10 parts. At the moment, an average price for metal AM varies from 40 to 100 EUR/h and iron powder costs are in the range of 30 - 50 EUR.

Cost comparison has shown similar results to production time. For small number of part, the AM technology is cheaper because for the casting technology project start-up costs are higher due to pattern costs. AM has almost a constant price for one part regardless of quantity, especially if the AM machine build size volume allows printing only one part at the same time.

4. CONCLUSIONS

The comparison test results have shown that additive manufacturing can be used to produce parts in order to replace the cast parts. All tests for mechanical properties have proven that parts, which are produced using metal additive manufacturing, can provide the same parameters compared to the cast parts and in most of them the results have been even better.

At the moment, the only disadvantages for AM are price and production speed. Price and production time are competitive for small parts and for 1 - 5 qty. because at the moment AM machines are very expensive. The price of one AM machine starts at 250 000 EUR till many millions of EUR. In the nearest future, AM machine prices should go down because most of the patents, which protected this technology, ended at the end of 2016 and are not valid anymore. This should also make influence on the metal AM service price, so it is expected to a rapid growth of additive manufacturing in the nearest time.

At the same time, there is already a market niche for AM and it can be used to produce parts for industries where there is no need for series production and part technological possibilities are more important than product price, for example, auto/motorsport, aviation and prosthetics.

REFERENCES

1. Gibson I., David W., Rosen D. & Stucker B. (2006). *Additive Manufacturing Technologies: 3D Printing, Rapid Prototyping, and Direct digital manufacturing.* New York: Springer.
2. Campbell J. (2002) *"Castings"* Butterworth-Heinemann.
3. Verdins G. & Dukulis I., (2008). *"Material science"* – Riga, LLU.
4. Karnati, S., Axelsen, I., Liou, F. F., & Newkirk, J. W. (2016). Investigation of tensile properties of bulk and SLM fabricated 304L stainless steel using various gage length specimens. *Proceedings of the 27th Annual International Solid Freeform Fabrication Symposium – An Additive Manufacturing Conference* (pp. 592–604). Laboratory for Freeform Fabrication and University of Texas at Austin.
5. Gu, D. (2015). *Laser additive manufacturing of high-performance materials.* Berlin: Springer.

6. Kamath, C., & El-dasher, B. (2013). *Density of Additively-Manufactured, 316L SS Parts Using Laser Powder-Bed Fusion at Powers Up to 400W.* Lawrence Livermore National Laboratory.

ADITĪVĀS RAŽOŠANAS UN LIEŠANAS TEHNOLOĢIJU SALĪDZINĀJUMS - MEHĀNISKO ĪPAŠĪBU, PRODUKTIVITĀTES UN IZMAKSU NOVĒRTĒJUMS

A. Vēvers, A. Kromanis, Ē. Geriņš, J. Ozoliņš

Kopsavilkums

Liešanas tehnoloģija ir viena no vecākajām ražošanas tehnoloģijām pasaulē bet pēdējos gados ļoti strauji attīstās metāla aditīvā ražošana jeb metāla 3D printēšana. Abas tehnoloģijas paver iespējas ražot sarežģītas detaļas ar iekšējiem dobumiem, kā arī, detaļām, kuras ir ražotas ar abām tehnoloģijām, ir līdzīgs virsmas raupjums, kas nozīmē, ka, lai iegūtu precīzus izmērus vai urbumus, detaļām būtu nepieciešama virsmu apstrāde. Lai noskaidrotu vai detaļas, kas ražotas ar aditīvo ražošanu varētu aizstāt detaļas, kas iepriekš tikušas ražotas ar liešanas tehnoloģiju, tika veikti salīdzinošie testi. Autors strādā ķeta liešanas uzņēmumā, tāpēc, lai būtu objektīvs salīdzinājums tika izvēlēts testus veikt ar GJS-400-15 ķeta lējuma marku, kas ir viena no populārākajām augstas stiprības ķeta markām. Ar abām tehnoloģijām tika izgatavoti paraugi un salīdzinātas to stiepes, cietības un virsmas raupjuma īpašības. Papildus abu tehnoloģiju salīdzināšanai tika salīdzināti detaļu izgatavošanas laiki un detaļu izgatavošanas izmaksas. Pētījums tika izstrādāts maģistra darba ietvaros Rīgas Tehniskajā universitātē ražošanas tehnoloģiju programmā.

28.02.2018.

LATVIAN JOURNAL OF PHYSICS AND TECHNICAL SCIENCES
2018, N 2

DOI: 10.2478/lpts-2018-0014

NON-WOVENS AS SOUND REDUCERS

D. Belakova[1], A. Seile[1], S. Kukle[1], T. Plamus[2]
[1] Institute of Design Technologies, Riga Technical University,
3/7 Paula Valdena Str., Riga, LV-1048, LATVIA
[2] Tallinn University of Technology, Department of Materials and Environmental Technology, Laboratory of Polymers and Textile Technology,
5 Ehitajate Str., Tallinn, 19086, ESTONIA

Within the present study, the effect of hemp (40 wt%) and polyactide (60 wt%), non-woven surface density, thickness and number of fibre web layers on the sound absorption coefficient and the sound transmission loss in the frequency range from 50 to 5000 Hz is analysed. The sound insulation properties of the experimental samples have been determined, compared to the ones in practical use, and the possible use of material has been defined. Non-woven materials are ideally suited for use in acoustic insulation products because the arrangement of fibres produces a porous material structure, which leads to a greater interaction between sound waves and fibre structure. Of all the tested samples (A, B and D), the non-woven variant B exceeded the surface density of sample A by 1.22 times and 1.15 times that of sample D. By placing non-wovens one above the other in 2 layers, it is possible to increase the absorption coefficient of the material, which depending on the frequency corresponds to C, D, and E sound absorption classes. Sample A demonstrates the best sound absorption of all the three samples in the frequency range from 250 to 2000 Hz. In the test frequency range from 50 to 5000 Hz, the sound transmission loss varies from 0.76 (Sample D at 63 Hz) to 3.90 (Sample B at 5000 Hz).

Keywords*: non-woven, sound absorption, sound transmission*

1. INTRODUCTION

1.1. Noise Control

A typical noise control application involves a combination of absorption of sound and transmission of sound energy by a variety of airborne and structure-borne paths [1].

There are two important noise-related quantities of a material: 1) the ability to absorb acoustic energy characterised by absorption coefficient α; 2) the ability to

reflect or block sound energy characterised by sound transmission loss (STL) measured in decibels, or τ – the transmission coefficient, which is a frequency-dependent physical property of the material:

$$\tau = I_{transmitted} / I_{incident}. \quad (1)$$

Sound Transmission Loss:

$$STL = 10 \log I/\tau. \quad (2)$$

Sound absorption is the incident sound that strikes a material and is not reflected back. Performance of sound absorbers is determined by their ability to dissipate sound energy at various sound frequencies. Fibre-based materials are the best sound absorbers. When a sound wave strikes an acoustic material, the sound wave causes the fibres of the absorbing material vibrate. This vibration causes tiny amounts of heat due to friction and, thus, sound absorption is accomplished by energy to heat conversion. The more fibrous a material is, the better the absorption; conversely less absorptive materials have a higher density. The sound absorbing characteristics of acoustic materials vary significantly with frequency. In general, low frequency sounds are very difficult to absorb because of their long wavelength. On the other hand, humans are less susceptible to the low frequency sounds, which can be beneficial in many cases. For a vast majority of conventional acoustic materials, the material thickness has the greatest impact on the sound absorption qualities. While the inherent composition of the acoustic material determines the material acoustic performance, other factors can be applied to bear, improve or influence the acoustic performance. For example, incorporation of air space behind an acoustic surface often serves to improve low frequency performance.

Good absorbing materials allow sound pressure fluctuations to enter their surface and dissipate energy by air friction. They are generally porous and lightweight, such as fibres, open-cell foam, or acoustic ceiling tiles. Good barrier materials reflect sound, and are dense and non-porous (concrete, lead, steel, brick, glass, and gypsum board). In general, a single homogeneous material will not be both a good absorber and a barrier. It is common to laminate an absorbing layer to a barrier material [2].

1.2. Noise Emission of Passenger Vehicles

The permissible noise emission of a passenger vehicle has decreased from 82 dB (1978) to 74 dB (1996). A new EU regulation was introduced in July 2016 [3], which would phase in stricter noise limits over 10 years, together with a revised, more representative test procedure. By 2026 the limit for most new passenger cars will be 68 dB [3].

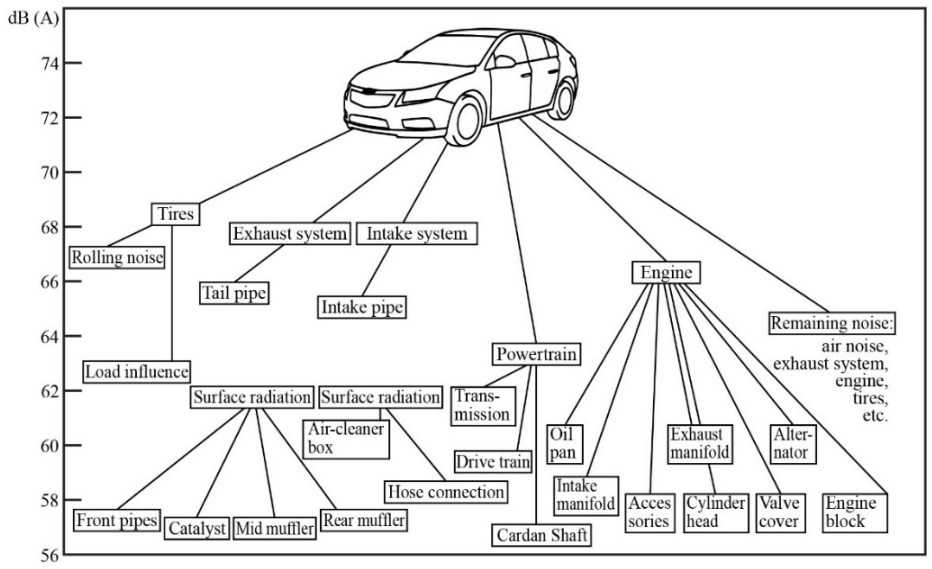

Fig. 1. Noise source ranking for a vehicle during the pass-by noise test [5].

The four major noise sources that contribute significantly to the noise level created by cars are the engine, the intake system, the exhaust system and the tyre/road system [4]. Pressure pulsations at the intake and exhaust valves of the engine are the main excitation source for the intake and the exhaust system noise. Gas flow in their piping systems is the source for flow noise, which occurs as broadband noise in the mid-frequency range. At the exhaust outlet, the mixing of hot exhaust gas and still ambient air is the cause of jet noise. Tyre/road interaction noise is caused by the impact, adhesion and air-displacement mechanisms between the tyre and the road [4].

Figure 1 [5] presents a ranking of the noise sources with the highest contributions to pass-by noise in the following order: tyres, exhaust system, intake system, and engine. Analysis of the frequency content of noise helps us to understand noise source characteristics. However, detailed testing of each major noise source is required in order to identify and reduce critical noise contributions. There are no specific resonance frequencies, but the increased amplitude components in the frequency range between 500 Hz and 2 kHz are caused by tyre/road noise. Dominant frequencies are around 1000 Hz. The frequency range below 500 Hz is dominated by the engine movement, which is related to the sound radiation of the engine, intake and exhaust system [4].

The so-called flow noise is caused by turbulence and vortices of the high speed mass flow around sharp edges, small bends and free jets [6]. Opinions about its characteristic vary. According to [6], flow noise is of a broadband character between 1 kHz and 3 kHz. In contrast, it is described in [7] as being a rather tonal character with low and high frequency components. Therefore, noise of frequency range from 125 Hz to 500 Hz and 500 Hz to 3 kHz needs to be reduced by car interior elements to ensure user comfort.

1.3. Noise Insulation Materials Used in Transport

In contrast to the sound insulation materials used in buildings, the soundproofing materials used in vehicles are relatively thin (< 50 mm). A material provides absorption best if its thickness is between ¼ to ½ of the sound wave length acting on the material.

Up until 2005, the weight of textiles built into the construction of passenger cars was, on average, 21 kg. Now the use of textiles is increasing, and by the end of 2020 textile-based materials are expected to weigh 35 kg [8].

The most common materials used in cars are closed-cell foam formed sound absorbing materials or fibre structure materials with open-cell air pockets. The latter includes non-wovens (NWM). In accordance with the EU regulation, the use of fibre-based materials in the automotive industry, including NWM, continues to increase.

The air trapped in the structure of NWM makes it an effective soundproofing and sound absorption material. The sound propagation speed through air is 331 m/s (at 0 °C), which is low compared to other media. The void volume in the structure of the material influences its geometrical form and is related to the fibre surface area. NWM total fibre surface area [9] depends on the denier and cross-sectional shape of fibres constituting the material. Finer fibres have to be arranged more densely and the surface area they form is larger. Apart from fibre denier, the surface area is influenced by the fibre cross-section. Comparing thermally bonded non-wovens manufactured from the same fibre denier, but three different cross-sectional shapes (round fibre, trilobal fibreangular and octalobal fibre), the materials from octalobal fibres have the largest surface area, which is up to three times the area of the round fibre NW. Non-wovens made from round fibres have the smallest surface area, if 3 denier and coarser fibres are used [9].

In addition to NWM, the automotive industry also uses woven and knitted textiles, laminated fabrics and surfaces, which are obtained by an electro-static flocking method [10].

Using a mechanical needle-punching method for manufacturing NWM polyester (PES), polyamide (PA) and polypropylene (PP) fibres are most commonly used [11].

In order to obtain a material with the highest possible absorption capacity and high transmission losses, a material with a multilayered structure where each layer has a specific task can be created.

2. EXPERIMENTAL PART

2.1. Materials

The samples of non-woven material with a multilayer structure are made from 6.5 ± 0.5 den fine and 64 ± 4 mm long polyactide (PLA) fibres (60 wt%) (fibre type SLN 2660D delivered from the company Ingeo) and hemp (40 wt%) technical fibres

(Vliesfähige Faser VF6 with fibre diameter between 16 and 50 μm, and average fibre length 50–80 mm delivered from the company BaFa Badische Naturfaseraufbereitung GmbH).

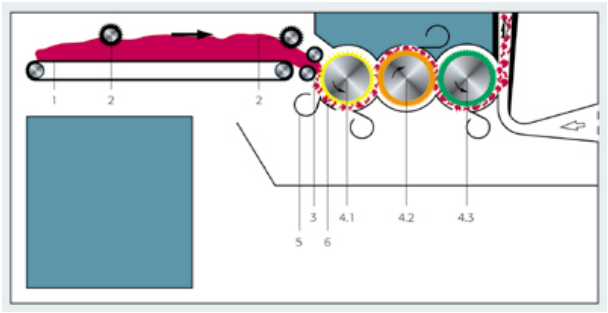

Fig. 2. Cleanomat Cleaner CVT3 by Trutzschler. 1 – Feed Lattice, 2 – Pressure Rollers, 3 – Feed Rolls. 4.1 – Fully-Spiked Rollers, 4.2 – Coarse Saw-Toothed Roller, 4.3 – Medium Saw-Toothed Roller, 5 – Mote Knives, 6 – Carding Segment [13].

Before incorporation into the non-woven material, the necessary amount of fibres is weighed and loosened. For each sample from the prepared fibres five web layers are formed initially: Layer 1 – PLA fibres, Layers 2, 3 and 4 – PLA fibres mixed with hemp technical fibres, Layer 5 – PLA fibres. Loosing of the fibres, mixing of the fibre types and preparation of the fibre web layers with the air-laid method [12] are performed on TRÜTZSCHLER CVT3 1200 (Fig. 2).

Bonding of the web layers, transformation of the five fibre web layers into three layers, and bonding of the three fibre web layers were performed by mechanical needle punching [14] using DILO LBM 6 laboratory type needle-punching equipment (see Fig. 3). DILO LBM 6 is equipped with the company GROZ-BECKERT needles produced for flax processing 15X18X25X3 ½ R333 G 3007.

Fig. 3. Laboratory needle loom with one needle board down stroke DILO LBM 6 (600 mm working width, 2000–3000 needles/m., 3000 strokes/min) [15], [16].

Fig. 4. GROZ-BECKERT punching needle (picture taken by the authors).

The NWM samples developed within the framework of the project were marked with the letters A, B, C, D and E. In the present article, Sample A, B and D characteristics were analysed. Samples for testing were taken from the two places of

material – one piece was tested in the frequency up to 500 Hz, the second piece was tested in the frequency range from 500 to 5000 Hz.

The sample thickness was measured by textile thickness gauge SDL Atlas J100. To attain a higher insulation performance, the material was placed in two layers positioning the PLA fibre web layers on its outer sides, as they were needle punched more densely in the process being situated just above the needle board. Thus, the acoustic parameters were determined by placing the NWM in two layers.

2.2. Acoustic Testing

To determine the sound absorption of the materials, two test methods are most commonly used [9]: the Impedance Tube Method [17] and the Reverberation Room Test Method [18]. The dimensions of automotive textiles compared to the materials for soundproofing in buildings and premises are small. Due to this reason, it is more convenient to use the impedance tube method for testing the acoustic properties of the material. In this project, the absorption of all samples was tested by the impedance tube method. The main components of the impedance tube are speakers, tubes, two microphones and a material sample holder. The task of the loudspeaker is to generate a special sound called white noise. The white noise is composed of sound contributions from all frequency bands in the audible range. The sound moves straight down the tube and strikes the test material. Depending of the material, some of the sound is absorbed and some is reflected back. The two microphones measure the reflected sound and from the two microphone signals, the sound absorption can be calculated [19].

The sound insulation capacity of the experimental hemp and PLA NWM samples was evaluated by the sound absorption coefficient α, and transmission loss measurements in the impedance tube according to the standard [20]. The measured parameters: r – normal angle of incidence sound refractive index over the linear frequency scale; α_{linear} – normal angle of incidence sound absorption coefficient over the linear frequency scale; STL_{linear} – sound transmission loss over the linear frequency scale. The parameters to be calculated: α – normal angle of incidence sound absorption t 1/3 octave bands; STL – sound transmission loss at 1/3 octave bands.

Five samples were prepared for testing, of which three samples A, B and C were selected for testing acoustic properties. From these samples, three sample strips were cut with Ø99.5 mm (large samples) and three samples with Ø30 mm (small samples). The small sample strips were tested at frequencies over 1600 Hz, the large sample strips – at frequencies up to 1600 Hz.

3. RESULTS AND DISCUSSION

As seen in Figs. 4 and 5, although the thickness of NMW samples A and B is equal, the difference between their structures is meaningful as surface density of NWM variant B exceeds the surface density of Sample A by 1.22 times and 1.15 times that of Sample D.

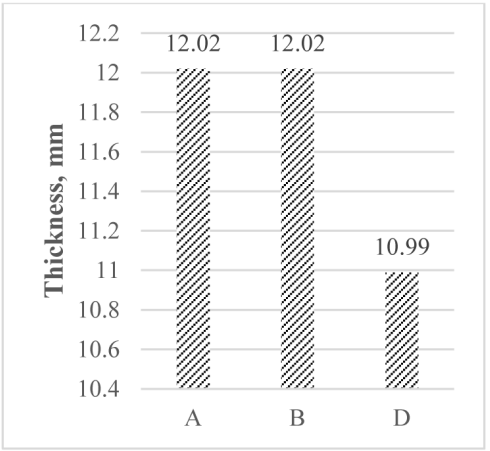

Fig. 5. Thickness of non-woven variants.

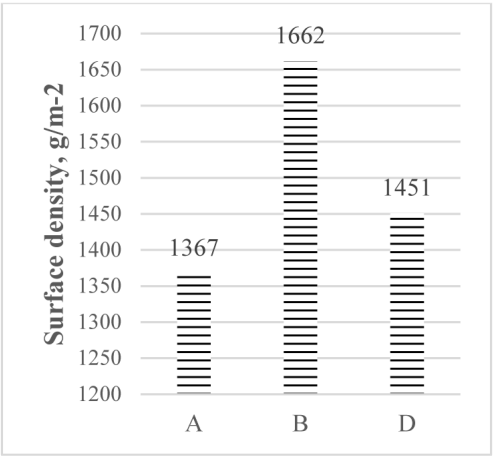

Fig. 6. Surface density of non-woven variants.

Within the present study, NWM samples A, B and D were tested in the frequency range from 50 to 5000 Hz. As mentioned above, an important factor for cars is the noise absorption at low frequencies up to 500 Hz related to the sound radiation of the engine, intake and exhaust system. The other common noise frequency band is from 500 Hz to 2000 Hz with a peak at 1000 Hz caused by tyre/road noise. The absorption coefficient value of NWM sample A exceeds the corresponding values of samples B and D for the entire low frequencies range, and at frequency 63 Hz corresponds to the sound absorption class E (Fig. 6, Table 1). At the same time, samples of variants B and D through almost the entire range of low frequencies demonstrate sound absorption coefficients below limits corresponding to class E.

NWM of variant in the sound frequency range from 500 to 1000 Hz A will absorb more efficiently since throughout the entire frequency range **α** corresponds to the class E (Fig. 7, Table 1). Sound absorption coefficients of the B and D NWM samples for this frequency band only partly correspond to the class E. In the frequency band from 1250 to 2500 Hz, the sound absorption capacity of the sample A

improves, over the entire frequency range **α** corresponds to the class D and at the frequency of 3150 Hz even to the class C. The absorption capacity of variants B and D is slightly worse.

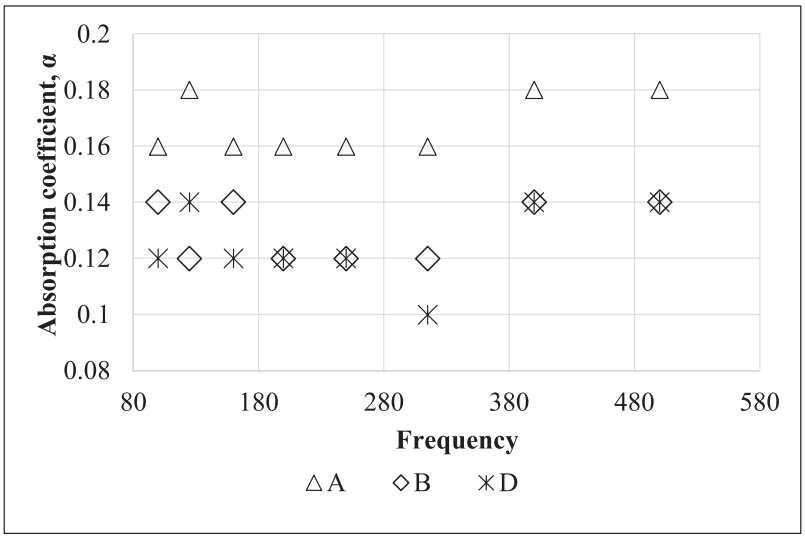

Fig. 7. Absorption coefficients corresponding to the range of low frequencies.

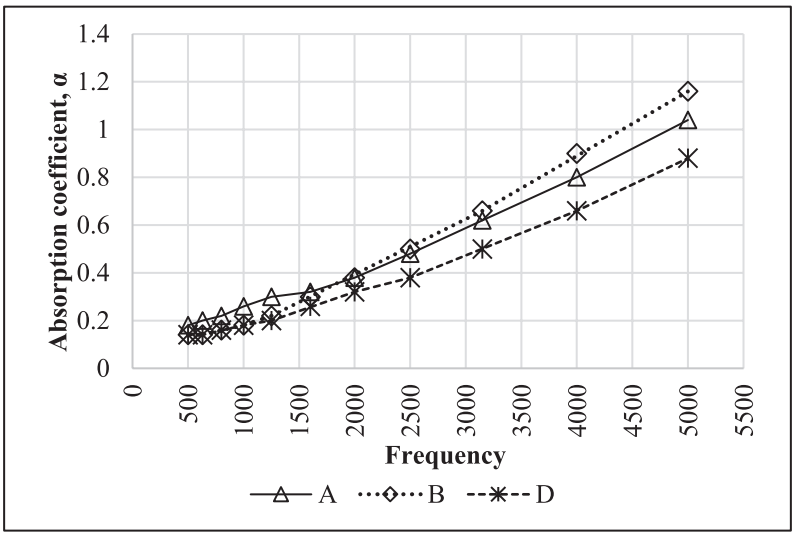

Fig. 8. Absorption coefficients corresponding to the range of middle frequencies.

Absorption coefficient values summarised in Table 1 show that all the test samples depending on frequency correspond to sound absorption classes C, D and E. The material demonstrates the trend that absorption class becomes higher with an increase in the sound frequency.

Table 1

Values of Absorption Coefficients and Sound Transmission Loss

Variant	A		B		D	
Frequencies, Hz α	α	STL [dB]	α	STL [dB]	α	STL [dB]
50	0.14	1.20	0.14	1.90	0.14	0.79
63	0.18	1.20	0.18	2.00	0.10	0.76
80	0.22	1.30	0.18	2.10	0.12	0.84
100	0.16	1.40	0.14	2.20	0.12	0.96
125	0.18	1.40	0.12	2.30	0.14	1.10
160	0.16	1.50	0.14	2.40	0.12	1.15
200	0.16	1.50	0.12	2.50	0.12	1.18
250	0.16	1.50	0.12	2.50	0.12	1.25
315	0.16	1.50	0.12	2.50	0.10	1.31
400	0.18	1.60	0.14	2.60	0.14	1.36
500	0.18	1.70	0.14	2.60	0.14	1.43
630	0.20	1.70	0.14	2.70	0.14	1.51
800	0.22	1.80	0.16	2.80	0.16	1.57
1000	0.26	1.70	0.18	2.80	0.18	1.58
1250	0.30	1.80	0.22	2.80	0.20	1.63
1600	0.32	2.00	0.30	2.90	0.26	1.75
2000	0.38	2.10	0.38	3.10	0.32	1.86
2500	0.48	2.20	0.50	3.20	0.38	1.97
3150	0.62	2.40	0.66	3.30	0.50	2.10
4000	0.80	2.50	0.90	3.50	0.66	2.25
5000	1.04	2.80	1.16	3.90	0.88	2.52

Absorption Class α-value

A 0.90; 0.95; 1.00

B 0.80; 0.85

C 0.60; 0.65; 0.70; 0.75

D 0.30; 0.35; 0.40; 0.45; 0.50; 0.55

E 0.15; 0.20; 0.25

not classified 0.00; 0.05; 0.10

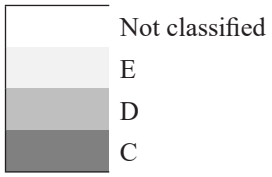

The American standard ASTM 423 provides similar test criteria to EN ISO 354 as well as provides a method for calculating Noise Reduction Coefficient (NRC) using the following equation that gives a single figure result:

$$NRC = (\alpha_{250} + \alpha_{500} + \alpha_{1000} + \alpha_{2000})/4 \quad (2)$$

Table 2

Values of Noise Reduction Coefficient of Non-woven Variants

	α_{250}	α_{500}	α_{1000}	α_{2000}	NRC
A	0.16	0.18	0.26	0.38	**0.25**
B	0.12	0.14	0.18	0.38	**0.21**
D	0.12	0.14	0.18	0.32	

According to the estimated NRC values in Table 2, the Sample A demonstrates the best sound absorption of all the three samples in the frequency range from 250 to 2000 Hz. The sound absorption performance can be increased by increasing the structure thickness of sample A.

Sound transmission loss characterises the material capacity to reduce undesirable sound penetration – the higher the STL, the better a material reduces sound. In the frequency range from 50 to 5000 Hz, STL varies from 0.76 (Sample D at 63 Hz) to 3.90 (Sample B at 5000 Hz) dB (see Table 1). Figure 8 shows a tendency of STL to increase with an increase in sound frequency for all samples. STL Sample B has the highest values, which could be expected considering greater surface density of the sample. In order to additionally increase the STL in the range of low frequencies, the surface density of the material has to be increased. The porous structure of hemp PLA non-wovens is suitable for sound absorption and upon laminating the PLA located at the outer sides of the material both the STL and dimensional stability of the material would increase.

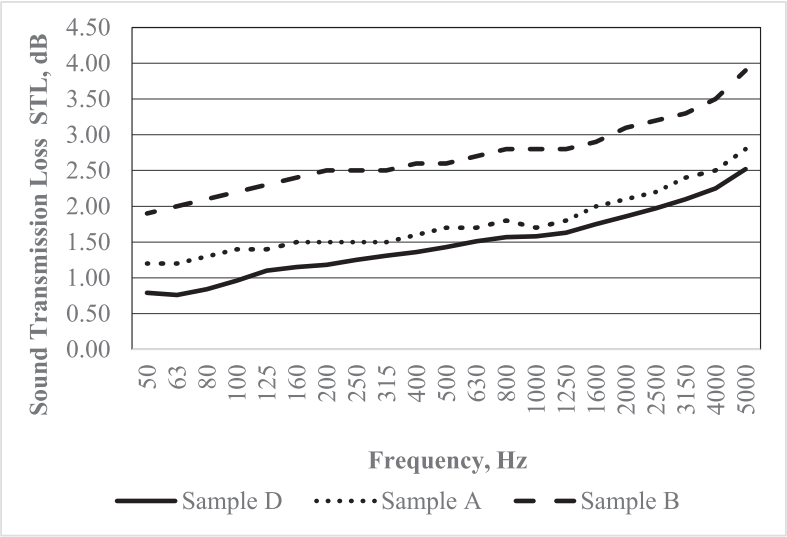

Fig. 9. Sound transmission loss corresponding to the tested range of frequencies.

4. CONCLUSIONS

The multilayer structure of the material contributes to sound wave propagation attenuation in the material. The mechanical needle-punching method used in the

manufacture of the non-woven material provides air pockets in the material structure acting as a contributing factor to the soundproofing capacity of the material.

Upon determining the acoustic properties of hemp PLA non-woven material when comparing the frequency ranges where the material demonstrates the best performance of the measured and calculated parameters, 50–2000 Hz has been found to be the frequency range that best characterises the NWM acoustic performance. According to the obtained data, the sample A demonstrates the greatest porosity because it has the highest sound absorption coefficient in the range of low frequencies, the second highest absorption coefficient is in the remaining range of test frequencies. Low frequency sounds have long wave lengths. Because of wave length, low frequency sounds pass through material much easier than high frequency sounds. To improve better sound absorption of material at low frequencies without increasing the thickness of the material, film (from aluminium polyester or analogue material) layer of one side of the material is considered. Placing a film layer to the direction of sound, the film will act as a spring-mass resonator for the low frequency peak. It should be taken into account that increasing the sound absorption of the material by the film layer, absorption decreases at high frequencies. In order to increase STL in the range of low frequencies and in general, either the outer sides of the material should be additionally reinforced or the existing PLA webs should be processed thermally.

The hemp PLA non-woven material tested during the research, according to its sound absorption coefficient range in 1/3 octave frequency band, is close to such materials used in building construction as a cut pile carpet (fringe length from 3.13 to 6.25 mm) and a carpet with a combined cut pile (fringe length 4.69 mm) – foam structure [21].

The fibres used in the manufacture of the non-woven material are obtained from renewable resources. The results obtained for the acoustic properties of the hemp/PLA non-woven material justify the use of the fibres and the method of manufacture of the material.

ACKNOWLEDGEMENTS

Support for the present research has been provided by Riga Technical University through the Scientific Research Project Competition for Young Researchers No. ZP-2016/31.

REFERENCES

1. Cherng, J.G. (2005). *Smart acoustic material for automotive applications*. Center for Engineering Education and Practice. Annual Progress Report. Project #2005/3.
2. Lamancusa, J.S. (2001). *Lecture material of engineering noise control*. Retrieved 28 February 2017, from http://www.mne.psu.edu/lamancusa/me458/
3. Regulation (EU) No 540/2014 of the European Parliament and of the Council of 16 April 2014 on the sound level of motor vehicles and of replacement silencing systems. Official Journal of the European Union, L 158/131. Available at http://eur-lex.europa.eu/legal-content/EN/TXT/?uri=OJ%3AJOL_2014_158_R_0005

4. Brauna, M.E., Walsha, S.J., Hornera, J.L., & Chuterb, R. (2013). Noise source characteristics in the ISO 362 vehicle pass-by noise test: Literature review. *Applied Acoustics*, *74*(11), 1124–1265. DOI: 10.1016/j.apacoust.2013.04.005
5. Bosch (Robert Bosch GmbH). (2004). *Kraftfahrtechnisches Taschenbuch* (Bosch – Automotive Handbook). (25th ed.) Wiesbaden, GER: Vieweg + Teubner.
6. Wang, X. (2010). Vehicle noise measurement and analysis. In X. Wang (ed.), *Vehicle Noise and Vibration Refinement* (pp. 68–92). Woodhead Publishing Limited.
7. Harrison, M. (2004). *Vehicle Refinement – Controlling Noise and Vibration in Road Vehicles: Exterior Noise: Assessment and Control.* SAE International. Elsevier Butterworth – Heinemann.
8. Normand, X. (2008). Recycling of automotive textiles. In R. Shishoo (ed.), *Textile Advances in the Automotive Industry* (pp. 86–112). Woodhead Publishing Limited.
9. Tascan, M., Vaughn, E.A., Stevens, K.A., & Brown, P.J. (2011). Effects of total surface area and fabric density on the acoustical behavior of traditional thermal-bonded highloft nonwoven fabrics. *The Journal of the Textile Institute, 102*(9), 746–751. DOI: 10.1080/00405000.2010.515731
10. Söderbaum, E. (2008). Requirements for automotive textiles – A car producer's view. In R. Shishoo (ed.), *Textile Advances in the Automotive Industry* (pp. 13–16). Woodhead Publishing Limited.
11. Graupner, N., & J. Müssig. (2010). Technical applications of natural fibres: An overview. In J. Müssig (ed.), *Industrial Applications of Natural Fibres* (pp. 63–72). A John Wiley and Sons.
12. Pourmohammadi, A. (2007). Dry-laid web formation. In S.J. Russell (ed.), *Handbook of Nanwovens* (pp. 76–80). Woodhead Publishing Limited.
13. Sheikh, H.R. (2003). Modernisation option for conventional Blow Rooms. *Pakistan Textile Journal.* Retrieved 19 March 2017, from http://ptj.com.pk/Web%202003/9-2003/art-sheikh.htm
14. Swarbrick, G. (2007). Mechanical bonding: Needlepunching: Introduction. In S.J. Russell (ed.), *Handbook of Nanwovens* (pp. 240–251). Woodhead Publishing Limited.
15. Tornado (Tornado Textilmaschinen GmbH). (n.d.). *Second-hand nonwoven and textile machines.* Retrieved 19 March 2016, from http://www.tornado-tex.de/textile-machines-second-hand/needle-looms-laboratory.htm
16. Allstates Textile (Allstates Textile Machinery Inc.). (n.d.). *Used textile equipment*. Retrieved 24 October 2016, from www.allstatestextile.com/
17. ASTM International. (1998). ASTM C384-98 – Standard Test Method for Impedance and Absorption of Acoustical Materials by the Impedance Tube Method. West Conshohocken, PA.
18. ASTM International (2008). ASTM C423-08 – Standard Test Method for Sound Absorption and Sound Absorption Coefficients by the Reverberation Room Method. West Conshohocken, PA.
19. Deshpande, S.P., & Rao, M.D. (2014). Development of a low-cost impedance tube to measure acoustic absorption and transmission loss of materials. *121st ASEE Annual Conference & Exposition*. Paper ID #8776.
20. LVS EN ISO 10534-2:2002. (2002). Acoustics – Determination of sound absorption coefficient and impedance in impedance tubes – Part 2: Transfer-function method. Standardisation division, Latvian standard.
21. CertainTeed. (n.d.). *Noise control for buildings. Guidelines for acoustical problem solving*. Retrieved 13 November 2016, from http://www.certainteed.com/resources/NoiseControl%20Brochure%2030-29-121.pdf

NEAUSTIE SKAŅAS IZOLĀCIJAS MATERIĀLI

D. Belakova, A. Seile, S. Kukle, T. Plamus

K o p s a v i l k u m s

Pētījumā analizēta kaņepju (40 wt%) un polilaktīda (60 wt%) neaustā materiāla virsmas blīvuma, biezuma un šķiedru klājuma kārtu skaita ietekme uz skaņas absorbcijas koeficientu un skaņas pārvades zudumiem frekvenču amplitūdā no 50 – 5000 Hz. Noteiktas eksperimentālo paraugu skaņas izolācijas īpašības, salīdzinātas ar praksē lietotajām, definēts iespējamais materiālu lietojums. Neaustie materiāli ir ideāli piemēroti lietošanai akustiskās izolācijas produktos, jo šķiedru kārtojums rada porainu materiāla struktūru, kas rada lielāku mijiedarbību starp skaņas vilni un šķiedru struktūru. Lielāks virsmas blīvums nodrošina lielāku skaņas izolāciju. No visiem pārbaudītajiem paraugiem (A, B un D), visaugstākais virsmas blīvums ir paraugam B un ir 1.22 reizes lielāks par parauga A un 1.15 reizes par parauga D virsmas blīvumu. Saliekot neausto materiālu vienu virs otra 2 kārtās – iespējams palielināt materiāla absorbcijas koeficientu, kas atkarībā no frekvences, atbilst C, D un E akustikas klasēm. No visiem trim neausto materiālu paraugiem, paraugam A ir novērtēta vislabākā skaņas absorbcija frekvenču diapazonā no 250 līdz 2000 Hz. Frekvenču amplitūdā no 50 līdz 5000 Hz skaņas pārvades zudumi variē no 0.76 (paraugs D pie 63 Hz) līdz 3.90 (paraugs B pie 5000 Hz).

08.02.2018.

LATVIAN JOURNAL OF PHYSICS AND TECHNICAL SCIENCES
2018, N 2

DOI: 10.2478/lpts-2018-0015

MEASUREMENT OF LOW CONCENTRATION OF NANOSIZED OBJECTS SUSPENDED IN A LIQUID MEDIUM

D. Merkulovs[1], O. Vilitis[2], V. Kozlovs[3]
[1] Institute of Physical Energetics, 11 Krivu Str., Riga, LV-1006, LATVIA
[2] Institute of Solid State Physics, University of Latvia,
8 Kengaraga Str., Riga, LV-2130, LATVIA
[3] Institute of Microbiology and Virology, Riga Stradins University, Science Hub "Kleisti", 5 Ratsupites Str., Riga, LV-1067, LATVIA
dmitrijs_merkulovs@yahoo.co.uk

The new optical scheme of refractometer with temperature stabilisation 10^{-2} °C is developed, which allows measuring a refractive index of the sample with accuracy not worse than 10^{-5}; dependence of refraction index on concentration of SiO_2 nanoparticles in liquid suspension is obtained within the framework of the research.

Keywords: *concentration measurement, nanoparticles, refractive index, suspension.*

1. INTRODUCTION

Measurement of nanoparticle concentration is a ubiquitous requirement across a diverse range of applications. Methods of dynamic light scattering and atomic force microscopy are the most known methods to measure concentration and sizes of nanoparticles in suspensions [1]. Refractometers, in turn, are widely used to analyse the composition of transparent binary solutions [2].

Earlier we showed that refractometric methods could also be applied to the analysis of liquid suspensions of nanoparticles, though the received results had qualitative character [3]. In the research [4], it is shown how refractometers can also be applied to the quantitative analysis of concentration of nanoparticles in suspensions.

In the present research, the authors continue their studies on an essentially different refractometer [5], [6], [7]. The aim of this article is to simplify the measurement scheme and reduce the sizes of previous constructions [3], [4], without worsening of the resolution of the device.

2. EXPERIMENTAL SETUP

A schematic cross-section of the cylindrical cell (cuvette) showing a simplified route of the beam in the measuring system is shown in Fig. 1. The refractometer measuring system consists of a laser diode (λ=650 nm, power

4 mW), a cylindrical thin-walled cell with its cross-section perpendicular to the axis *O* of the cylinder and a linear image sensor (Hamamatsu CMOS monochromatic linear 1024 pixel image sensor S9226 with the pixel width of 0.0078 mm is used). The cell is filled with distilled water containing nanoparticles. The position ***a*** of the beam is identified using a linear CMOS image sensor. The laser beam axis is lined up with the cell outer wall tangent and perpendicular to the axis of the cylinder. The laser beam after refraction at point 1 crosses the medium of the cell wall and arrives at point 2 on the boundary between the material of the cell inner wall and the liquid.

The experiments demonstrated that in the vicinity of the critical angle the beam intensity of light was the highest [2]. For this reason, to illustrate the trajectory of the coherent light beam in the cylindrical cell, Fig. 1 shows only the path of rays that are close to the critical angle. After being refracted at the boundary point 2, light rays travel through the test liquid and, having crossed it, fall upon the inner wall of the cylinder at point 3, where they are refracted again and reach the point Q_1 through the medium of the cell wall. Points 1, 2, 3, Q_1, 4, Q_2, Q_3, Q_4 and Q_5 are reference points, in which the beam is refracted at the interface between two transparent media with different refractive index (RI).

As the outside surface of the cylinder is coated with a reflective film, the rays falling on this unit area of the boundary surface are reflected and intersect the cell wall and the liquid several times in a similar way.

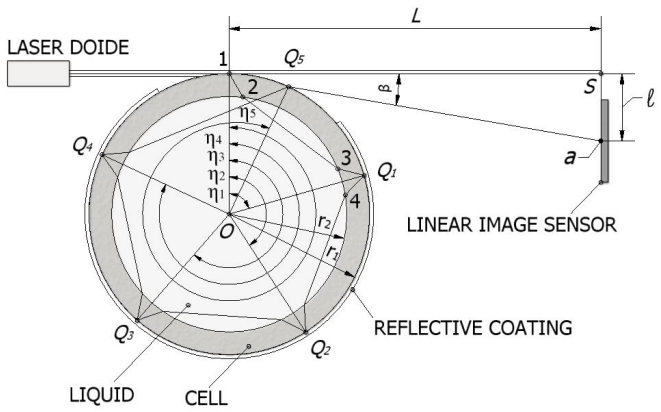

Fig. 1. Schematic cross-section of the cylindrical cell that illustrates a simplified path of the laser beam in the measuring system.

The analytical calculation of the RI of liquids contained in the system described above is given in [8], [9], where applying the laws of light refraction and reflection and using simple trigonometric formulae, the central angle η_m (see Fig. 1 for the case when $m = 5$ – the number of reflections of the laser beam (inside the cuvette) was calculated as follows:

$$\eta_m = 2m[(\pi/2 - \arcsin(k/n_3) + \arcsin(k/n_2) - \arcsin(1/n_2)] \quad \text{rad}, \tag{1}$$

where $k = r_1/r_2$ is the ratio of the outer and inner radii of the cylindrical cell; n_2 and n_3 are the refractive indices of the material of the cell and the liquid, respectively.

Establishing geometric and physical parameters as follows: r_1=5.46 mm; r_2=4.54 mm, L=118 mm, n_2=1.5 (glass), n_3=1.330566...1.330347 (distilled water within 26 °C и 28 °C) [2], it is possible to theoretically calculate the position of the laser beam on a linear image sensor. We obtain l≈17mm.

Traditionally, projected on a linear measuring element (for example, on a CMOS linear image sensor), the beam forms an image area containing a front, namely, a transition region from darkness to light. The position of the front is determined by the critical angle of the optical system comprising the cuvette and the liquid being measured. Since the transition between the dark and light parts of the image is gradual, it is necessary to define the position of the boundary [2]. Such an approach, however, has some disadvantages. The distribution of the light intensity on the front depends on the slope of the light intensity graph, the intensity and stability of the light source and the presence of gaseous or other particles in the measured liquid, such as air bubbles. Consequently, the detection of the front position is difficult and sometimes even impossible.

The refractometer proposed by the authors is free from these unsatisfactory features. Waveform of the images shows that the interference of laser light after it is reflected from different regions in the cuvette generates an interference pattern, as described in more detail in [8], [9]. The image position is determined by the position of the first or any subsequent minimum following the position of the maximum intensity of distribution. This is very clearly seen in Fig. 1. The position of the minimum is given by the ordinal number of the corresponding pixel of the linear sensor. It is determined automatically by the microcontroller using traditional methods of the mathematical analysis. As can be seen in Fig. 1, the minimum position ($p_{\min}$ = 528) is absolutely independent on the exposure time of the laser beam, while the leading front changes position and inclination.

All mentioned elements of the scheme are fixed on the surface of the thermostat the temperature of which can be changed within 20 °C–30 °C (at the stabilisation of temperature within ~ 0.01 °C).

To determine the RI resolution of our device, we explore well-known dependence of RI of water on temperature [2]. Dependence of CCD-sensor photoresponse on temperature of water variations is shown in Fig. 3.

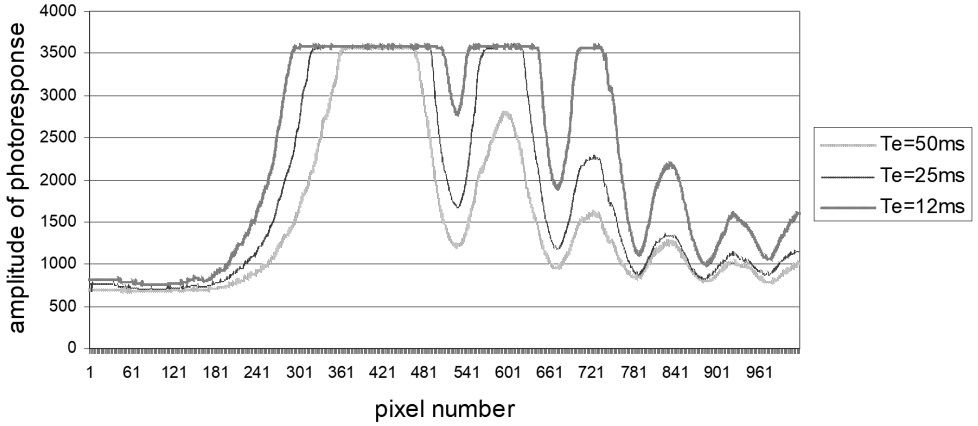

Fig. 2. Dependence of CCD-sensor signals on exposure time T_e of laser illumination.

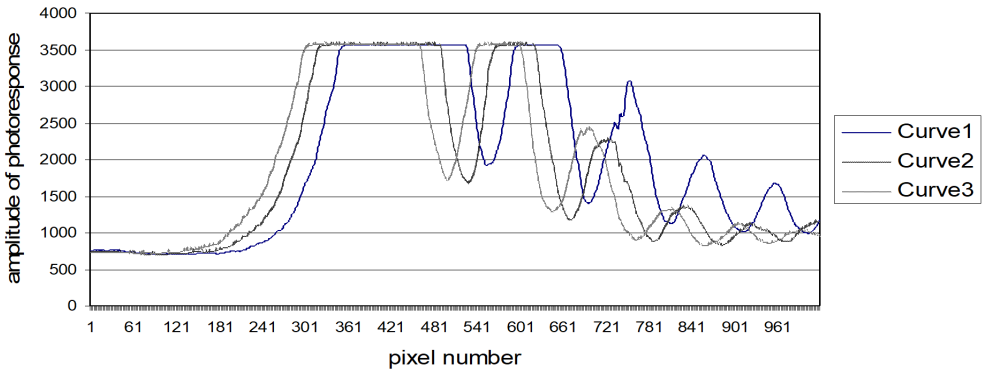

Fig. 3. Temperature dependence of CCD-sensor signal (T_e =25ms):
curve 1 – 26 °C. ($p_{\min} = 559$), curve 2 – 27 °C ($p_{\min} = 528$) and curve 3 – 28 °C ($p_{\min} = 500$).

The temperature dependence of a refractive index of water obtained in such a way is used to estimate resolution of our device: sensor signal shift on 1 pixel corresponds to a change in RI of a sample at a value $\approx 4 \cdot 10^{-6}$

3. RESULTS AND DISCUSSION

For preparation of aqueous suspensions, we used SiO_2 nanoparticles from US Research Nanomaterials, Inc. with a mean size of 70 nm: 36 mg of nanoparticles were mixed up in 100 ml of triple distilled water. Then 0.5 ml of suspension was placed into measuring cuvette.

Measurements were carried at the temperature of 27 °C. We investigated a change in the shape of a signal of sensors at different exposure times. The obtained data are given in Fig. 4.

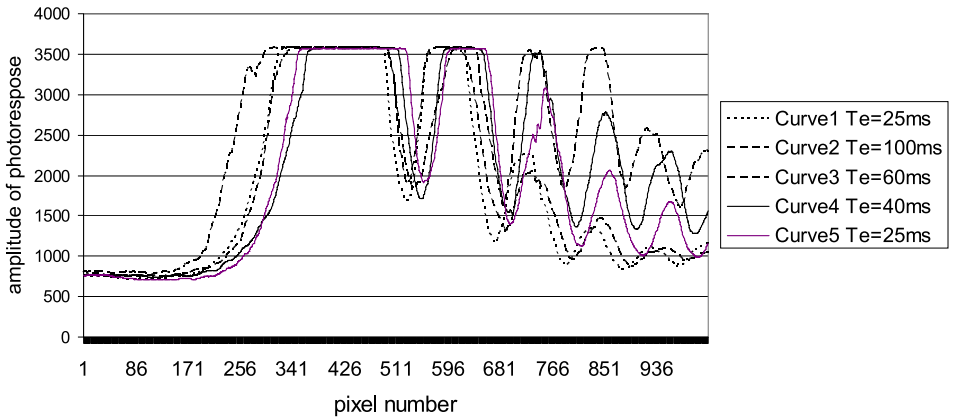

Fig. 4. Dependence of CCD-sensor signals on concentration of SiO_2 nanoparticles in distilled water:
curve 1 – water at 27 °C ($p_{\min} = 528$),
curve 2 – 360mg/l ($p_{\min} = 543$), curve 3 – 180 mg/l ($p_{\min} = 551$),
curve 4 – 90 mg/l ($p_{\min} = 555$), curve 5 – water at 26 °C ($p_{\min} = 559$).

Propagation of light in the turbid media is followed by its scattering and absorption. In our case it leads to a decrease in the amplitude of a signal of sensors. As seen in Fig. 4, with an increase in exposure time duration of impulse of laser radiation – the form of a signal takes a nearby signal form, as in the transparent medium. As seen in Fig. 4, the shape of the leading edge is similar, but differs from one another in slope. When we take the first minimum for the criterion, the readings are made unambiguous. On the basis of the measurements described above, we obtained dependence of concentration of nanoparticles on pixel number of CCD-sensor (Fig. 5).

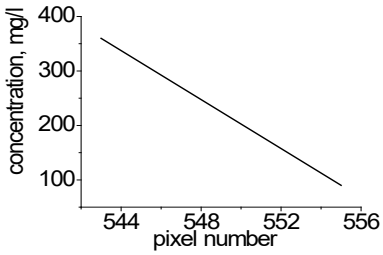

Fig. 5. Dependence of concentration of SiO_2 nanoparticles (mg/l) on the pixel number of CCD- sensor.

The detailed description of propagation of light in the liquids containing nanoparticles has to be described within Mie's theory [11]. By means of this theory, the phase shifts (and the change in refractivity connected with it [10]) arising at light scattering by nanoparticles can be calculated. But in case of suspensions with the small maintenance of SiO_2 nanoparticles as in our case, it is possible to describe light propagation by means of some efficient dielectric constant [12], [13]:

$$\varepsilon_s = \varepsilon_l + c \cdot 3 \cdot (\varepsilon_p - \varepsilon_l) \cdot \varepsilon_l / (\varepsilon_p + 2 \cdot \varepsilon_l), \tag{2}$$

where ε_s, ε_l, ε_p – dielectric constants of suspension, liquid and nanoparticle; c – concentration of nanoparticles in liquid. Since $RI^2 = \varepsilon_s$, at small values of c, as in our case, c must be proportional to RI (see Fig. 5).

4. CONCLUSION

In the present research, we have experimentally confirmed the results of the previous research [4], i.e., the device developed by us – a refractometer – allows measuring concentration of nanoparticles in suspensions up to several mg/l.

It has also been experimentally confirmed that using the unique properties of the new refractometer, especially, where an optical beam refraction and multiple reflections in a cylindrical cell are used and a measurement method, where a minimum place of the detectable beam interference pattern has been used, it is possible to reduce the laser beam motion inside the device by almost 4 times without losing its resolution [4].

REFERENCES

1. Hoo, C. M., Starostin, N., West, P., & Mecartney, M. L. (2008). Comparison of AFM and DLS methods to characterize nanoparticles size distribution. *J. Nanoparticles Res.*, 89–96.
2. Ioffe, B.V. (1974). Refractometric methods in chemistry (2nd ed.). Khimya. (in Russian).
3. Kozlov, V., Merkulov, D., & Merkulova, V. (2016). Determination of concentration of nanoparticles in liquids by laser-diode refractometer. *Book of Abstracts of 19th International Conference on Quantum Electronics "Laser physics and applications"* Sozopol, Bulgaria, 91–92.
4. Vilitis, O., Merkulovs, D., & Kozlovs, V. (2017). Measurement of low concentration of nanosized objects in bioliquids by means of refractometric methods. In *Proceedings of the 13th International Conference on Medical Physics "Medical physics in the Baltic states"*, Kaunas, Lithuania (pp. 132–136).
5. Vilitis, O., Merkulov, D., & Kozlov, V. (2003). *Method and refractometer for measuring refractive index of liquids.* Patent LV13294 B.
6. Vilitis, O., & Merkulov, D. (2006). *Method for detecting optical image of the light beam in refractometer*. Patent LV 13598 B.
7. Vilitis, O., Merkulov, D., & Shipkovs, P. (2007). *Method and sensor for measuring concentration of liquids.* Patent LV 13728B.
8. Vilitis, O., Shipkovs, P., & Merkulov, D. (2008). Determination of refractive index of liquids using a cylindrical cuvette. *Latv.J.Phys.Technol.Sci. 3*, 50–62.
9. Vilitis, O., Shipkovs, P., & Merkulovs, D. (2009). Determining the liquids refractive index by using a cylindrical cuvette. *Measurements Science and Technology*, *20*, 117001, doi:10.1088/0957-0233/20/11/117001.
10. Jackson, J. D. (1998). *Classic electrodynamics* (3rd ed.). New York: John Wiley & Sons.
11. Bohren, G.F., & Huffman, D.R. (1983). *Absorption and scattering of light by small particles.* New York: John Wiley & Sons.
12. Novotny, L., & Hecht, B. (2006). *Principles of nanooptics*. Cambridge: Cambridge University Press.
13. Landau, L., & Lifsitz, E. (1982). *Electrodynamics of continuous media*. Nauka. (in Russian).

ZEMU KONCENTRĀCIJU NOTEIKŠANA NANOIZMĒRU OBJEKTIEM, KAS SUSPENDĒTI ŠĶIDRĀ VIDĒ

D. Merkulovs, O. Vilītis, V. Kozlovs

K o p s a v i l k u m s

Izstrādāta un izveidota refraktometriska mērīšanas sistēma, kas ļauj panākt temperatūras stabilizāciju 10^{-2} °C un nodrošina mēramā parauga laušanas koeficienta mērīšanas precizitāti ne zemāku par 10^{-5}; tādējādi tiek sniegta iespēja novērtēt zemas koncentrācijas nanoizmēra objektu, piemēram SiO_2 nanodaļiņu koncentrāciju ūdenī, nosakot šīs suspensijas laušanas koeficientu.

12.03.2018.